Astronomy & Astrophysics manuscript no. fornax
August 1, 2011
© ESO 2011

arXiv:1007.1007v1 [astro-ph.GA] 6 Jul 2010

A high resolution VLT/FLAMES study of individual stars in the centre of the Fornax dwarf spheroidal galaxy*

Bruno Letarte[1,2,3], V. Hill[4,5], E. Tolstoy[1], P. Jablonka[4,6], M. Shetrone[7], K.A. Venn[8], M. Spite[4], M.J. Irwin[9], G. Battaglia[10], A. Helmi[1], F. Primas[10], P François[4], A. Kaufer[11], T. Szeifert[11], N. Arimoto[12], and K. Sadakane[13]

[1] Kapteyn Astronomical Institute, University of Groningen, PO Box 800, 9700AV Groningen, the Netherlands
[2] California Institute of Technology, 1200E. California Blvd, MC105-24, Pasadena, CA 91125 USA
[3] South African Astronomical Observatory, P.O. Box 9, Observatory 7935, South Africa
[4] GEPI, Observatoire de Paris, CNRS, Université Paris Diderot, F-92125, Meudon, Cedex, France
[5] Université de Nice Sophia-Antipolis, CNRS, Observatoire de Côte d'Azur, Laboratoire Cassiopée, F-06304 Nice Cedex 4, France
[6] Observatoire de Genève, University of Geneva, CH-1290, Sauverny, Switzerland
[7] McDonald Observatory, University of Texas, Fort Davis, TX 79734, USA
[8] Dept. of Physics & Astronomy, University of Victoria, 3800 Finerty Road, Victoria, BC V8P 1A1, Canada
[9] Institute of Astronomy, University of Cambridge, Madingley Road, Cambridge CB3 0HA, UK
[10] European Southern Observatory, Karl-Schwarzschild-str. 2, D-85748, Garching bei München, Germany
[11] European Southern Observatory, Alonso de Cordova 3107, Santiago, Chile
[12] National Astronomical Observatory of Japan, 2-21-1 Osawa, Mitaka, Tokyo 181-8588, Japan
[13] Astronomical Institute, Osaka Kyoiku University, Asahigaoka, Kashiwara, Osaka 582-8582, Japan

Received 6th October 2009 / Accepted 6th July 2010

ABSTRACT

For the first time we show the detailed late-stage chemical evolution history of small nearby dwarf spheroidal galaxy in the Local Group. We present the results of a high resolution (R∼20000) FLAMES/GIRAFFE abundance study at ESO/VLT of 81 photometrically selected red giant branch stars in the central 25′ of the Fornax dwarf spheroidal galaxy. We also carried out a detailed comparison of the effects of recent developments in abundance analysis (e.g., spherical models vs. plane-parallel) and the automation that is required to efficiently deal with such large data sets. We present abundances of α-elements (Mg, Si, Ca and Ti), iron-peak elements (Fe, Ni and Cr) and heavy elements (Y, Ba, La, Nd and Eu). Our sample was randomly selected, and is clearly dominated by the younger and more metal rich component of Fornax which represents the major fraction of stars in the central region. This means that the majority of our stars are 1−4 Gyr old, and thus represent the end phase of chemical evolution in this system. Our sample of stars has unusually low [α/Fe], [Ni/Fe] and [Na/Fe] compared to the Milky Way stellar populations at the same [Fe/H]. The particularly important role of stellar winds from low metallicity AGB stars in the creation of *s*-process elements is clearly seen from the high [Ba/Y]. Furthermore, we present evidence for an *s*-processorigin of Eu.

Key words. Stars: abundances – Galaxies: dwarf – Galaxies: evolution – Galaxies: formation – Galaxies: stellar content – Galaxies: individual: Fornax dwarf galaxy

1. Introduction

Local Group dwarf spheroidal galaxies (dSph) offer the opportunity to study the star formation history (SFH) and chemical evolution of small systems. They are also believed to provide an insight into the galaxy assembly process. We have undertaken a large observational programme (DART, Dwarf Abundances and Radial velocity Team, Tolstoy et al. 2006) using high resolution spectroscopy to study the detailed nucleosynthesis properties of large samples of individual Red Giant Branch (RGB) stars in 4 nearby dSph galaxies: Fornax, Sculptor, Sextans & Carina. Here we present the analysis of a sample of 81 individual stars in the Fornax dSph.

The Fornax dSph galaxy is a relatively isolated and luminous, dark matter dominated dwarf galaxy with a total mass of $\sim 10^9 \mathcal{M}_\odot$ (e.g., Walker et al. 2007; Battaglia 2007), at a distance of 135 kpc (e.g., Rizzi et al. 2007). It is well resolved into individual stars, and colour-magnitude diagram (CMD) analyses have been made going down to the oldest main sequence turn-offs in the central region (e.g., Stetson et al. 1998; Buonanno et al. 1998; Saviane et al. 2000; Gallart et al. 2005). Fornax also contains a significant carbon star population (e.g., Azzopardi et al. 1999; Aaronson & Mould 1980). Near Infra-Red CMDs have also been made of the RGB stars (Gullieuszik et al. 2007). There have also been extensive variable star searches, resulting in ∼500 RR Lyr variables, 17 anomalous Cepheids, 6 population II Cepheids and 85 short period δ-Scuti and SX Phoenicis stars (Bersier & Wood 2002; Poretti et al. 2008). These works have all shown that Fornax has had a complex

* Based on FLAMES observations collected at the European Southern Observatory, proposal number 171.B-0588

SFH where the majority of stars have formed at intermediate ages 2 − 6 Gyr ago with a peak ∼ 5 Gyr ago. Fornax also contains a young stellar population (few 100 Myr old) as well as an ancient one (>10 Gyr old), as in all dwarf spheroidal galaxies studied to date (provided the observations are deep enough to reach the oldest turnoff).

In common with most other dSph, Fornax has no obvious HI associated to it at present, down to a density limit of 4×10^{18}cm^{-2} in the centre (or 0.037 $M_\odot$pc^{-2}) and 10^{19}cm^{-2} at the tidal radius (Young 1999). Unusually for dwarf galaxies Fornax contains five globular clusters (Hodge 1961). There is evidence that Fornax contains stellar substructure, in shell-like features and hence can be considered evidence of recent merger activity (Coleman et al. 2004; Olszewski et al. 2006; Coleman & Da Costa 2005; Battaglia et al. 2006, (B06)).

Low resolution spectroscopic studies of the Ca II triplet lines have been carried out for increasing numbers of individual RGB stars in Fornax, to determine kinematics and [Fe/H] estimates for samples of ∼30 stars (Tolstoy et al. 2001), ∼100 stars (Pont et al. 2004) and ∼600 stars (B06). There have also been measurements of Fe and Mg features in 2483 individual stars in Fornax (Walker et al. 2009) that have not so far been calibrated to metallicity. These studies have shown that Fornax contains a relatively metal-rich stellar population, and that the metallicity distribution covers a range from −2.8 <[Fe/H]< 0. with a peak at [Fe/H]∼ −0.9. B06 clearly showed that the "metal rich" stars ([Fe/H]> −1.3) have a centrally concentrated spatial distribution, with colder kinematics than the more spatially extended "metal poor" stars ([Fe/H]< −1.3). B06 also showed tentative evidence that the ancient stellar population in the centre of Fornax does not exhibit equilibrium kinematics (apparent as non-gaussian, double peaked velocity distribution). This could be a sign of a relatively recent accretion of external material, such as the gas accretion of the merger with another small stellar system (galaxy or star cluster).

Alpha, iron-peak, and heavy-elements, in individual RGB stars of different ages, can provide detailed information about the evolving conditions of star formation and chemical evolution in a galaxy through-out its history. The most accurate way to determine the elemental abundances of an RGB star is to directly measure the strength of as many individual absorption lines as possible in a spectrum. This typically requires a resolving power of, R ∼ 40000 (which is ∼ 0.125 Å at λ=5000 Å), with a large wavelength coverage (∼ 2000 Å) and has traditionally been carried out one star at a time with slit-spectrographs. The large wavelength coverage is required to obtain a minimum number of individual absorption lines for an accurate abundance analysis of chemical elements of interest. The wavelength range chosen is always a trade off between number of lines available (strong enough to be detected and isolated enough to be of any use) and instrument sensitivity.

Detailed abundance analyses using UVES high resolution spectroscopy have been carried out for 3 individual RGB stars in Fornax (Tolstoy et al. 2003; Shetrone et al. 2003, S03). There have also been high resolution UVES studies of 9 individual stars in 3 of the globular clusters associated with Fornax (Letarte et al. 2006). One of the globular clusters was observed to have a mean metallicity of [Fe/H]=−2.5 and all of them (see also, Strader et al. 2003) have metallicities quite distinctly lower than the majority of the field stellar population, although Fornax field also host a low-level metal-poor tail extending down to −2.8 (B06).

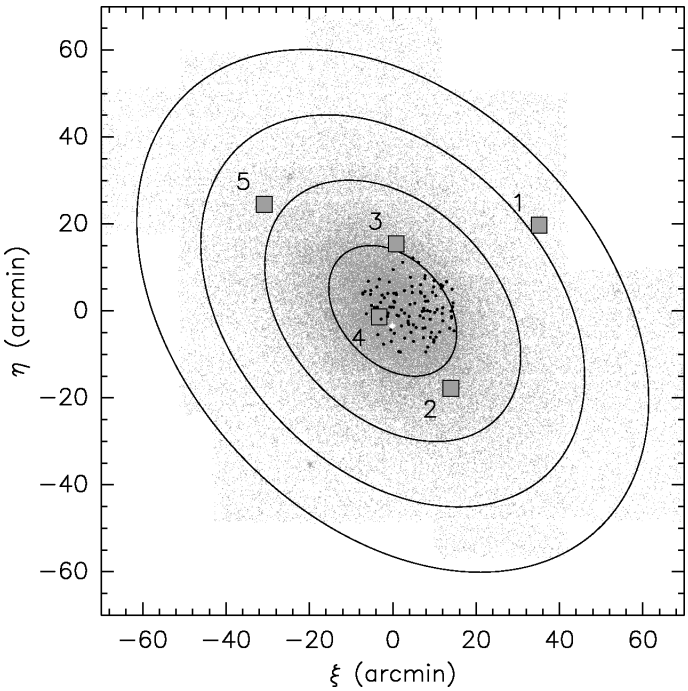

Fig. 1. The spatial distribution of Fornax dSph stars observed at high resolution (centrally concentrated black dots), overlaid on our photometric survey (small grey dots, from B06). The five globular clusters are also shown, as squares. The inner ellipse corresponds to the core radius, and the outer ellipse to the tidal radius.

The FLAMES multi-fibre spectrograph at the VLT has dramatically increased the efficiency with which spectroscopic observations can be made, by allowing more than 100 spectra to be obtained in one shot. However, the observations are of lower resolution (R ∼ 20000) than standard and with much a smaller wavelength coverage (typically a series of ∼300Å wide bands). This trade-off of large samples for lower resolution and less wavelength coverage has required the development of new automated data analysis procedures which will be described in this paper.

In this paper we present detailed chemical abundances for a *large* sample of 81 RGB stars in Fornax (30 times larger than S03), randomly selected on the upper RGB in the center of the galaxy. This allows us to quantify the detailed chemical evolution of this galaxy. Because we selected stars randomly, and in the central parts of the galaxy, we will see that the dominating population in our sample belongs to the peak of its star formation activity. In Sec. 2, we describe the sample selection, observations, reduction and basic measurements, in Sec. 3 we describe the abundance analysis method, in Sec. 4 we discuss the results, and in Sec. 5 we discuss the implications of our results.

2. Observations and data reduction

Figure 1 gives a spatial overview of the Fornax dSph galaxy. We highlight the stars observed in this high resolution FLAMES survey of individual stars in the central 25′ region. The photometric selection of the targets is presented

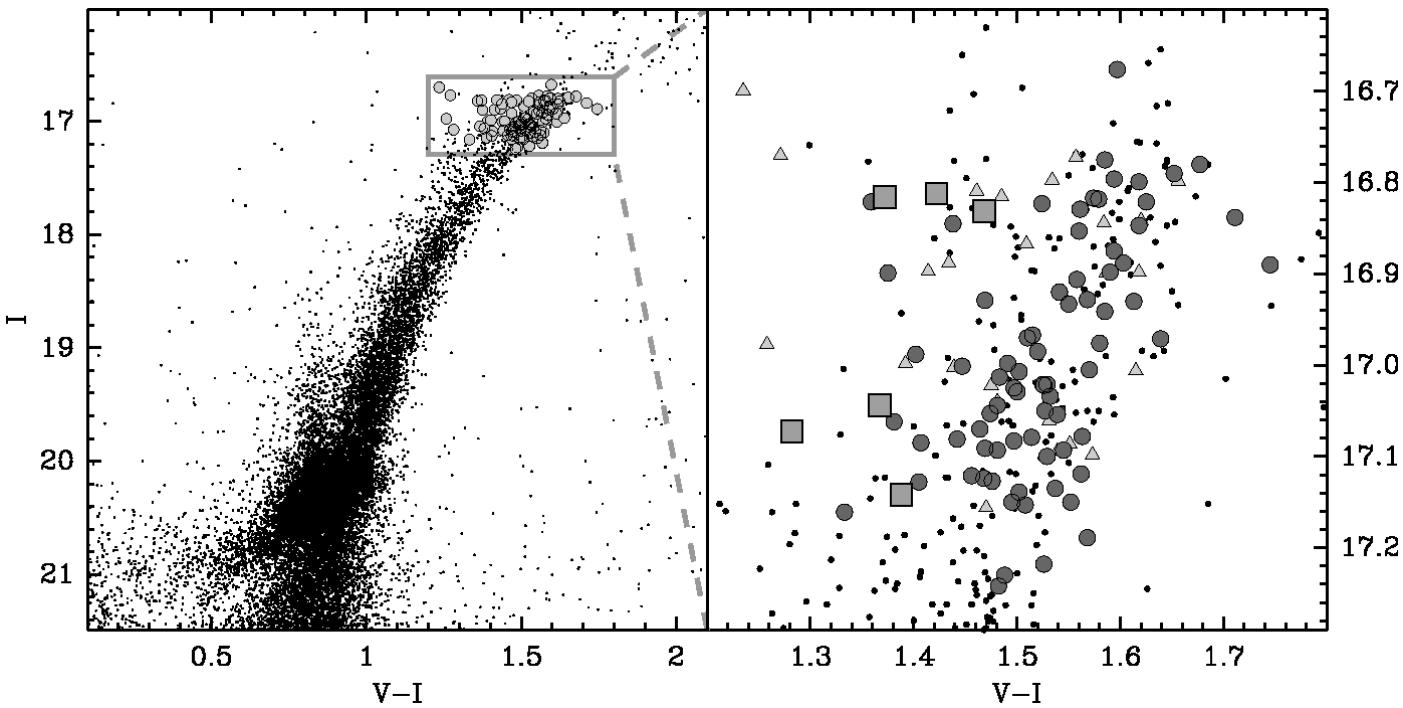

Fig. 2. The I vs $V-I$ color-magnitude diagram of the Fornax centre as derived from our ESO/MPG/2.2m WFI data (B06). It corresponds to the field of view of FLAMES. The spectroscopic targets analyzed in this work are identified with larger grey circles in the box in the left panel. The right panel zooms-in to this region.

in Figure 2. We selected bright RGB stars from the V,I CMD (B06), to include a broad range of colour, and thus the entire age and metallicity range present. We could only select the brightest red giants to keep exposure times down to a reasonable level (see Table 1). In order to minimize the number of AGB stars in our sample, we cross-checked our list of potential targets with known carbon stars (kindly provided by Serge Demers). The low resolution spectroscopic survey of this field with FLAMES with the Ca II triplet setting (as part of B06) also helped to weed out as many as possible obvious foreground stars from our high resolution sample.

2.1. Observations

FLAMES is a fibre-fed, multi-object instrument connected to GIRAFFE, a spectrograph which has a low (R = 6000 − 9000) and a high resolution (R = 17000 − 30 000) grating, covering a total wavelength range $\lambda\lambda 3700 - 9000$ Å broken up into 21 high-resolution (or 8 low-resolution) setups (Pasquini et al. 2002). In its high-resolution mode, each wavelength section (setup) is ~ 300 Å wide. For our purposes we used FLAMES/GIRAFFE with the high resolution setups HR10, HR13 and HR14. Table 1 summarizes the different setups and gives the exposure times. Note that the definition (resolution and wavelength coverage) of HR14 changed after October 10$^{\rm th}$ 2003, when the HR14 grating was up-graded from its engineering to operational version. HR14 was moved from order 9 to order 8 to match the new grating efficiency curve.

We used FLAMES/GIRAFFE in MEDUSA mode, which consists of up to 132 individual 1.2 arc-sec fibres, that can be placed independently on targets in the 25′ diameter FLAMES field of view. We were able to place fibres on 107 stellar targets, and the rest were assigned to blank areas, for an accurate determination of the sky light.

We encountered two technical problems. First, during our first run, at the end of September 2003, one reference star turned out to have a previously unnoticed proper motion. As a consequence, a significant fraction of the flux has been lost due to bad centering of the fiber on the target. Second, GIRAFFE hosts a simultaneous calibration unit that provides 5 fibers evenly spread across the spectrograph entrance slit, that are illuminated by a ThAr lamp. They allow very high radial velocity accuracies. However, during the January 2004 run, these simultaneous calibration fibers have been seriously over-exposed, especially in setup HR14. As a consequence, the bright calibration light leaked on to our stellar spectra. Only a small fraction of our sample was affected. All contaminated lines were simply removed from our abundance analysis.

2.2. Reduction

We used the girBLDRS* (GIRAFFE Base-Line Data Reduction Software) pipeline written at the Observatory of Geneva by A. Blecha and G. Simond, to extract and calibrate our spectra. For the subtraction of the sky emission lines and continuum, we ran our own specially developed software written by M. Irwin (see Battaglia et al. (2008b) for details).

The heliocentric corrected multiple exposures of each setup were combined with the `IRAF`† task `scombine`, using a flux weighted average with median sigma clipping (for

* http://girbldrs.sourceforge.net/
† http://iraf.noao.edu/

Table 1. Exposure Time Log

	HR10	HR13	$HR14_{old}$	$HR14_{new}$
λ_{min}(Å)	5339	6120	6383	6308
λ_{max}(Å)	5619	6406	6626	6701
R	19800	22500	28800	17740
date		Exposure time (s)		
2003-09-29	–	14400	6225	–
2003-09-30	3600	–	14102	–
2003-10-01	10800	–	6900	–
2004-01-14	3600	–	–	–
2004-01-15	–	3600	–	–
2004-01-19	–	7200	–	–
2004-01-20	–	3600	–	–
2004-01-21	–	–	–	7200
2004-01-22	–	–	–	7503
2004-01-23	3600	–	–	3600
2004-01-24	3600	–	–	–
2004-01-26	3600	–	–	–
Total	8h	8h	7h34m	5h05m

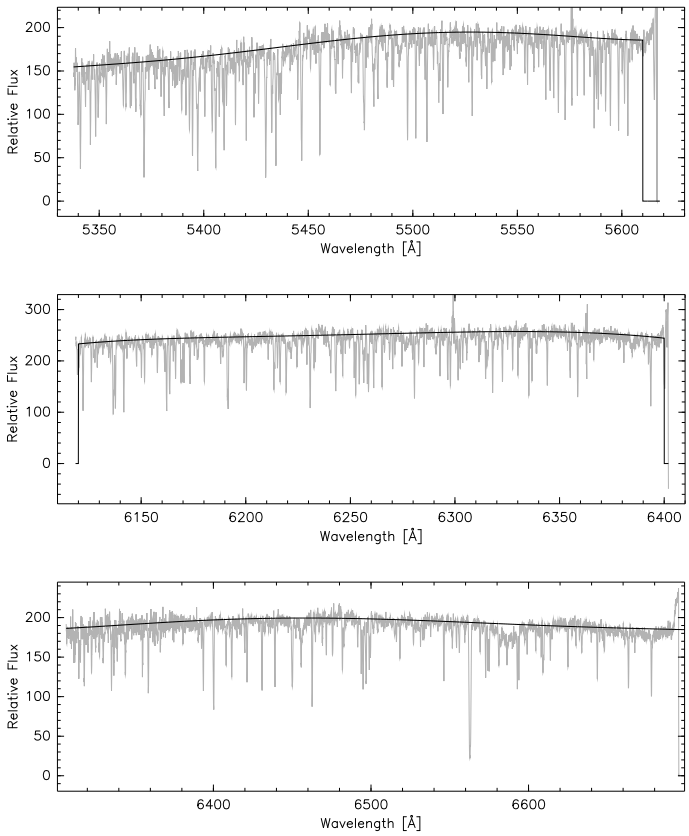

Fig. 3. Reduced spectra of star BL239, in each of the three GIRAFFE setups, HR10, HR13 and HR14, from top to bottom. The continuum fitted by DAOSPEC is also shown.

cosmic ray removal). This was done independently for each period (September and January), due to the change of grating. These two stacked spectra were finally combined in a flux weighted average. For the two HR14 set-ups with different resolution and wavelength coverage, we only used their overlapping section ($\sim$ 6400 – 6600 Å). We convolved the higher resolution (old) HR14 spectra to the lower resolution HR14 one. Figure 3 provides an example of the extracted spectra of BL239 in the three HR setups. BL239, with V = 18.5 mag and S/N of 32 at 5500 Å 37 at 6200Å and 50 at 6500Å is typical of our stellar sample .

2.3. Radial velocity measurements (V_{rad})

In order to verify membership to Fornax, the radial velocity (V_{rad}) of each star has been measured independently in each setup (HR10, HR13 and HR14) and for each observing epoch (September and January), producing six independent measurements. These measurements were made with the girBLDRS routine `giCrossC.py`, cross-correlating the observed spectrum with a mask. We used a G2 spectral-type mask that although hotter than our targets, was found the most robust to yield the velocities of our metal-poor cool giants. Table A.1 lists the final V_{rad}, calculated as the weighted average of the six velocities, with their associated error, corresponding to their standard deviation. We found no systematic difference between setups nor between epochs. However, 8 stars were found to have significantly different velocities between the September and January runs ($>$ 3 km/s difference) and hence they were discarded from any further analysis, as they might be binary stars.

Figure 4 shows the final distribution of V_{rad}, and the central velocity together with the 3σ cut-offs defining stellar membership of Fornax dSph. Our criterion differs only slightly from the 2.5σ chosen in B06. Only one star in our sample is an obvious non member (BL109), with a negative V_{rad} and was excluded from further analysis. The final mean heliocentric velocity (V_{rad}) of the stars identified as probable members is 55.9 km/s with a line of sight velocity dispersion $\sigma = 14.2$. The typical (median) error on the individual velocities measurement is $\simeq 0.55$ km/s (see Table A.1). Our results are very close to the values derived in B06 from a Ca II triplet measurements at lower resolution ($V_{rad} = 54.1 \pm 0.5$ km/s and $\sigma = 11.4 \pm 0.4$ km/s for 2σ selection and $\sigma = 13.7 \pm 0.4$ km/s for a 3σ selection).

Some of our stellar member candidates have been further discarded for various reasons such as noisy spectra or problem with stellar atmosphere model fitting (e.g., too large a dispersion in [Fe/H]).

2.4. Measuring the Equivalent Widths

The equivalent widths (EW) of stellar absorption lines are classically measured individually by hand (e.g., using SPLOT in IRAF). The large data sets that FLAMES produces effectively requires the use of an automatic procedure. This has been developed as DAOSPEC* (Stetson & Pancino 2008), a software tool that has been optimized for GIRAFFE HR spectra. DAOSPEC iteratively detects all lines in the stellar spectrum, fits gaussians of fixed FWHM (in km.s^{-1}) on all detected features, subtracts them from the observed spectrum, fits a continuum over the entire residual spectrum and corrects for it, until the residuals reach a flat minimum. These iterations are meant to converge on the list of detected line, the FWHM of the lines, and the global continuum. Once convergence is achieved, DAOSPEC cross-correlates the list of detected lines with a user provided reference line list to obtain a radial velocity and line identification for its detections.

* http://cadcwww.dao.nrc.ca/stetson/daospec/

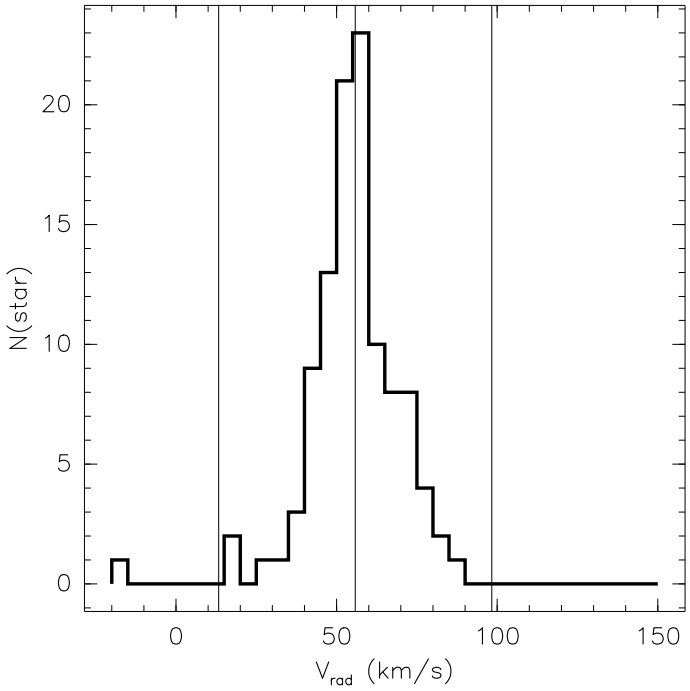

Fig. 4. Histogram of Fornax FLAMES/HR radial velocity measurements, $V_{\rm rad}$. The central value and the $\pm$ 3σ cut-offs are shown with solid vertical lines.

For a thorough description of the algorithm and its performances, see Stetson & Pancino (2008). The use of gaussian approximation of fixed FWHM ((in km.s^{-1}) is fully justified in R=20000 resolution spectra where the instrumental profile dominates over the astrophysical broadening of spectral lines. The placement of the continuum is a critical step, as it influences the measurements of EWs. Since DAOSPEC was run independently on each of the three setups, the continuum levels in each setup were also independently determined. As a consequence, any problem in the continuum level determination would show up as a systematic difference in the abundances deduced from lines of a given element in the different setups. Figure 3 shows an example of the spectra for one star in our sample (BL239) in the 3 setups and together with the continuum placement.

To test for the reliability of DAOSPEC measured EWs, Figure 5 compares, for a given star, the equivalent widths measured on the UVES spectrum with SPLOT by S03 to our DAOSPEC measurements on the same UVES spectrum and, finally, to the EWs measured on the GIRAFFE spectrum. This exercise has been performed for two different stars, that we have in common with S03 (resolution $R \sim$ 43000 and $\Delta\lambda$ = 4800 – 6800 Å). The mean difference between the measurements performed with SPLOT and DAOSPEC on the UVES spectra is minimal and is not increased by decreasing signal-to-noise (SNR), as can be judged from the left column of the figure. Conversely, as expected, the dispersion of the measurements increase with decreasing spectral quality, i.e. with decreasing SNR at the lower resolution of the GIRAFFE spectra. Nevertheless, we find that DAOSPEC can be used with confidence for $EW \lesssim 200$ mÅ.We note that in the comparison of EWs measured from UVES and GIRAFFE spectra, the error is dominated by the GIRAFFE measurement, as expected from the lower SNR per Å of these spectra. For the two stars exemplified in the right column of Figure 5, the corresponding SNR per Å are respectively: (UVES,GIRAFFE)=(231,118),(238,163),(198,119) for BL239-M25 in H10,H13 and H14, and (UVES,GIRAFFE)=(175,103),(161,125),(186,135) for BL278-M21 in H10,H13 and H14.

We did not observe a fast rotating hot star, hence we were unable to directly correct our spectra for telluric absorption. Instead we removed from our abundance analysis the atomic lines that fell within one resolution element of a telluric line.

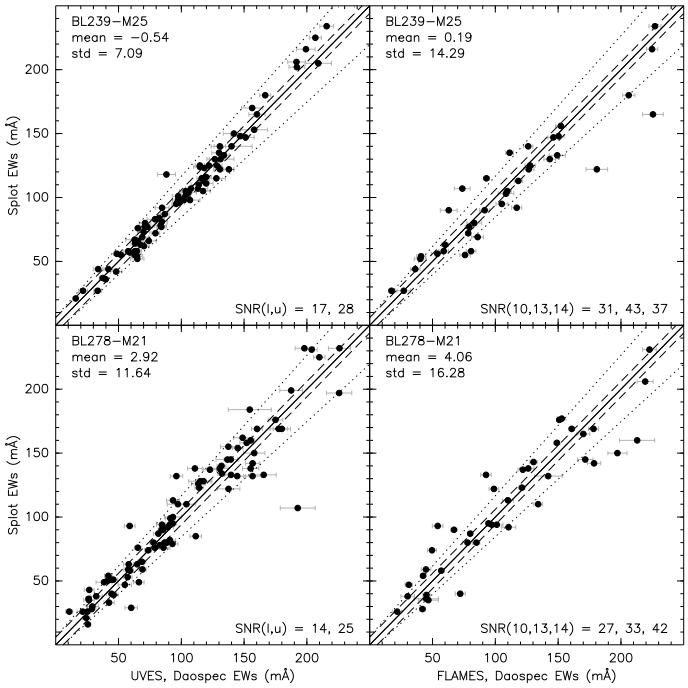

Fig. 5. A comparison of the SPLOT and DAOSPEC EW measurements for GIRAFFE (right-hand side) and UVES (left-hand side) measurements of the same two stars in Fornax dSph, BL239 (top panels) and BL278 (bottom panels). The solid line shows perfect agreement between the two sets of measurements. As in S03, the dashed lines delineate an $\pm$6 mÅ offset from this line, and the dotted lines represent a 10% error convolved with this 6 mÅ error. These lines are representative of the errors on SPLOT-based EWs. We indicate in each panel in the upper left-hand corner the mean difference between the UVES and GIRAFFE measurements (mean) and the standard deviation (std). The signal-to-noise ratios (SNR) as given by DAOSPEC for the UVES lower CCD (l, ∼4800–5800Å), and the upper UVES CCD (u, ∼5800–6800Å) or the three different orders of the GIRAFFE spectra are given in the bottom right-hand corner of each panel.

3. Abundance measurements

3.1. Stellar Models

The release of the spherical MARCS models* represents a major improvement in the modeling of stellar atmospheres (Gustafsson et al. 2003, 2008). Prior to this, most of the abundance analyses of RGB stars were based on the models of Gustafsson et al. (1975), in plane-parallel approximation, meaning that radiative transfer were solved in only one depth variable, neglecting the curvature of the atmosphere. The new MARCS spherical models have been further expanded by B. Plez to cover the extreme range of parameters of our RGB sample, i.e., $T_{\rm eff}<$ 4000 K, [Fe/H] ~ -3.0 dex, and low gravities at all metallicities (B. Plez, private communication).

Due to their relative novelty, spherical models have not yet been widely adopted in the literature (however see Plez et al. (1992) and Plez (1992)). A thorough comparison of the models with spherical and plane-parallel geometries has been conducted by Heiter & Eriksson (2006). One of their main conclusions is that the structure of the spherical models is very different to the plane-parallel ones, and this leads to significantly different stellar abundances. However geometry has much less impact on line formation (spectral synthesis). The discrepancies between the fully spherical (s_s) and fully plane-parallel (p_p) models increase with temperature and decreasing gravity, reaching a maximum around 5000K after which they decrease slightly. More specifically, at $T_{\rm eff} = 5000$K, the difference in FeI abundances can reach 0.15 dex for $\log g = 1.0$, and 0.25 dex for $\log g = 0.5$, for equivalent widths of the order ∼120mÅ as encountered in Fornax. By comparison, at $T_{\rm eff} = 4000$K and $\log g = 1.0$, the difference between (s_s) and (p_p) models does not exceed ∼0.02 dex. Following Heiter & Eriksson (2006), we computed that a spherical model atmosphere combined with a plane-parallel calculation for the line formation (the so-called s_p case) leads to maximum abundance deviation of the order of 0.02–0.03 dex, for temperatures $T_{\rm eff}$ around 4000K and $\log g \sim 0.5$ (typical of our sample). These differences are negligible in view of our measurement errors, therefore we have carried out our abundance analyses in the s_p framework, using the code CALRAI, first developed by Spite (1967) and continuously updated over the years.

3.2. The line list

The choice of a line list is a critical step of the abundance analyses. To be selected, the lines must have reliable *gf*-values and be sufficiently isolated from other lines to be accurately measured at the resolution of the observations. Dealing with cool stars (the mean temperature of our sample is ∼4000K) impose to check for the presence of molecular lines which could contaminate the atomic ones, hence biasing the measurements. The main molecular contaminant in the wavelength domain and stellar parameters covered here is in fact CN, while TiO has been checked to be negligible: the strongest TiO features in our domain are around 6300Å, but although TiO does form in these cool atmospheres, it strongly decrease with both the gravity and metallicity, making it a negligible contaminant to neighboring atomic lines.

We started with the reference line list of S03, which was optimized for UVES and metal poor stars ($-3.0 \leq$ [Fe/H] ≤ -1.5), and adapted it to the higher average metallicity of our Fornax field stars and the smaller wavelength coverage of FLAMES. To do this we selected new lines from Gratton et al. (2003), Hill et al. (2000), and Zoccali et al. (2004) with *gf*-values on the same scale as S03. We checked for possible systematic differences in *gf*-values using a high resolution ($R \approx 120\,000$), high signal-to-noise, UVES spectrum of Arcturus†, from which we derived the abundances from all our lines. Finally, we removed lines with possible blends (molecular or atomic) at the resolution of GIRAFFE (R=20000), using synthetic spectra computed for our range of stellar parameters. The final line list is shown in Table A.4

3.3. Stellar parameters

We started with photometric estimates for $\log g$ and $T_{\rm eff}$, and set [Fe I/H]$=-1.0$ dex and $v_{\rm t} = 2.1$ km/s. We subsequently modified these initial values until a good fit to a model was obtained, as summarized in the following sections.

3.3.1. Photometric effective temperature ($T_{\rm eff}$)

Optical photometry (V, I) was available for the full sample (B06) and was complemented by infrared photometry (J, H, K) from Gullieuszik et al. 2007, for 60% of our sample. We considered four different colours, $V-I$, $V-J$, $V-H$ and $V-K$ to estimate $T_{\rm eff}$, following the calibration of Ramírez & Meléndez (2005), with a reddening law of ($A(V)/E(B-V) = 3.24$) and an extinction $E(B-V) = 0.03$ (Bersier 2000).

The three Fornax stars in common with S03 were used to check the photometric temperature scale against excitation (as constrained from their UVES spectra). Namely, we determined, for these three stars, the spectroscopic effective temperature for which the iron abundance deduced for lines of various excitation potentials ($\chi_{\rm ex}$) was constant and showed no variation with $\chi_{\rm ex}$. The $T_{\rm eff}(V-I)$ were in perfect agreement with the spectroscopic $T_{\rm eff}$, while the temperatures derived from the IR colours, $T_{\rm eff}(V-\{J,H,K\})$, were slightly offset. This could be due to various effects, including a possible zero point on our WFI V and I photometry. Because of the agreement of the $T_{\rm eff}(V-I)$ with the excitation temperature scale, we decided to shift the $T_{\rm eff}(V-\{J,H,K\})$ onto the $T_{\rm eff}(V-I)$ scale by applying constant shifts of 87 K, 109 K and 99 K respectively for $T_{\rm eff}(V-\{J,H,K\})$. This procedure is equivalent to zero-pointing our photometry to make it agree with the excitation temperature scale. For a given star, the different $T_{\rm eff}$ then agree within $\pm$ 50 K.

The colours predicted by the MARCS 2005 atmosphere models at different temperatures, gravities and metallicities were also compared to the temperature calibration of Ramírez & Meléndez (2005), and found to agree well. This is comforting, since it means that the model atmospheres we used to deduce abundances also produce the correct colours for our stars. However we did notice that the $T_{\rm eff}$ derived on the $V-\{I,J\}$ colours are much more sensitive to the grav-

* http://marcs.astro.uu.se/

† http://archive.eso.org/wdb/wdb/eso/uves/form

ity of the model than $V-\{H,K\}$, an effect that is neglected in the calibrations of Ramírez & Meléndez (2005) and may account for some of the systematic differences between temperatures deduced from $V-I$ and infrared colours.

Excitation temperatures were also examined for the whole sample, but found a relatively high uncertainty associated with the slope of measured iron abundance with the line $\chi_{\rm ex}$when using GIRAFFE spectra. The median error associated with the slope measurement for the total sample (0.034 dex.eV-1) corresponds to a $T_{\rm eff}$ uncertainty of $+130/-250$ K. We therefore decided to rely the photometric temperatures for the analysis. The relatively high $T_{\rm eff}$ uncertainty of 200 K quoted in Table 2 reflects a conservative errorbar associated with the color temperature scale and photometric zero-point uncertainties.

The final $T_{\rm eff}$ we used is the average of the four $T_{\rm eff}$, coming from the four photometric colours and they are presented in Table A.2.

3.3.2. Surface gravity ($\log g$)

We used the photometric colours to estimate the surface gravity of the sample stars using the standard relation:

$$\log g_\star = \log g_\odot + \log \frac{\mathcal{M}_\star}{\mathcal{M}_\odot} + 4\times\log\frac{T_{\rm eff\star}}{T_{\rm eff\odot}} + 0.4\times(M_{\rm Bol\star}-M_{\rm Bol\odot})$$

We adopted the distance modulus $(M-m)_V = 20.65$ of (Bersier 2000) and the mass of the RGB stars was assumed to be 1.2 $\mathcal{M}_\odot$, in agreement with the mean young age for are sample, around $\sim 2-5$ Gyrs (Fig.17). Because the sample also contain a small fraction of older stars of lower masses, we iterated the analysis for those stars by modifying the gravity using the corresponding isochrone mass, once the metallicity and age of the star had been determined.

The bolometric corrections were computed for each star using the calibration of Alonso et al. (1999). The gravity had a minor effect on our abundances deduced from neutral ions: lowering $\log g$ by 0.5 dex decreases Fe I by ≈ 0.1 dex and Fe II by ≈ 0.3 dex. We determined that it was preferable to use the same photometric $\log g$ scale for all stars rather than using the ionization balance of Fe, because our Fe II abundances were deduced from too few and too weak lines to warrant a precise ionisation balance determination. This is illustrated in the bottom panels of figure 6 where the distribution of the errors on the mean Fe I and Fe II are reported. Fe II is clearly quite uncertain, with a median error of 0.13 dex, and extending up to 0.2dex or more. The corresponding uncertainty on $\log g$ determined from ionisation balance would be of 0.3 dex or more. The same holds true for Ti, for which the Ti II abundance was too uncertain (derived from 2-3 lines).

3.3.3. Microturbulent velocity ($v_{\rm t}$)

The $v_{\rm t}$ was corrected until the slope measured between [Fe I/H] and EW (slope$_W$) was zero (within its 1σ error). We took advantage of the linearity (and symmetry) of $v_{\rm t}$ on slope$_W$ in order to converge rapidly, applying the linear relation between the slope$_W$ and the $v_{\rm t}$ empirically measured to be $\delta v_{\rm t} = \delta$ slope$_W$/0.0055. The median uncertainty

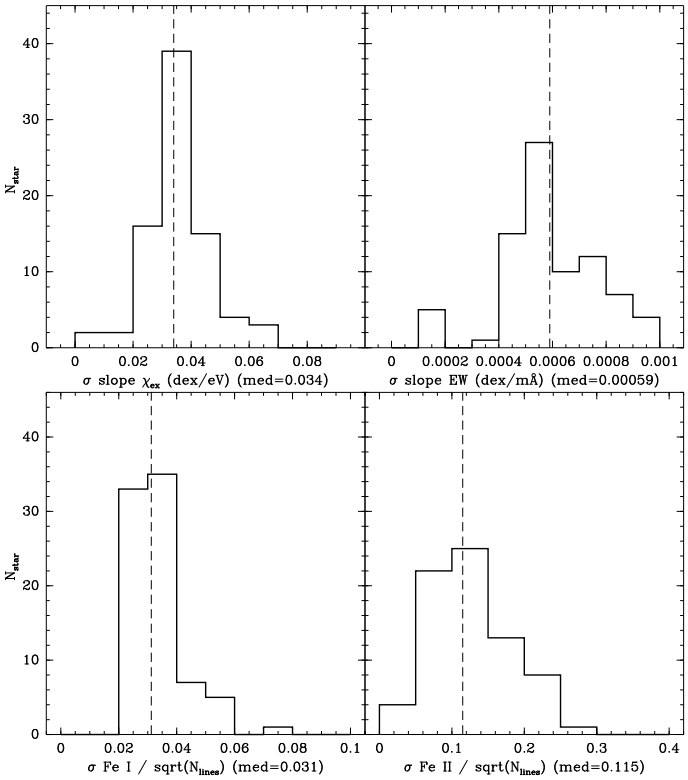

Fig. 6. Distribution of errors of the stellar parameter diagnostics for the total sample. *upper panels:* propagated error on the measurement of the slope of Fe I abundances versus the excitation potential of the line (σ(slope$_\chi$) *left*), and versus the line strength (σ(slope$_W$) *left*). *lower panels:* error on the mean Fe I and Fe II abundances as measured by the dispersion around the mean divided by the square root of the number of lines of each species.

on the determination of slope$_W$ of 0.00059 dex.m Å^{-1} (see Fig. 6) corresponds to 0.11 km.s^{-1}, and the complete sample has formal uncertainties below 0.001 dex.mÅ^{-1}, corresponding to 0.2 km.s^{-1}.

3.4. Precision and error estimates

DAOSPEC provides an error estimate, δEW, for each measured EW (see description of the δEW measurements in Stetson & Pancino 2008). We propagated this EW uncertainty throughout the abundance determination process, thus providing for each line the abundance uncertainty corresponding to $EW \pm \delta EW$. The abundance uncertainty need not be symmetric (and in general it is not), so the largest of the two (upper and lower) uncertainties was adopted as our DAOSPEC abundance error, $\delta_{\rm DAO}$. We also considered the abundance dispersion around the mean $(\frac{\sigma({\rm X})}{\sqrt{(N_{\rm X})}})$ for the element X for which N$_X$ lines could be measured (when N$_X > 3$), which provides an estimate of error including both the EW mesurement and *gf*-values uncertainties. Finally, to avoid biased estimates of the abundance dispersion due to small number statistics, we also considered the dispersion in Fe I abundances as a lower limit for the expected abundance dispersion around the mean of

any element, leading to an error estimate of $\frac{\sigma(\mathrm{Fe\,I})}{\sqrt{(N_{\mathrm{X}})}}$. For the final error on each [X/H], we adopted the maximum of these three values:

$$\delta([\mathrm{X/H}]) = \mathtt{MAX}\left(\delta_{\mathrm{DAO}}, \frac{\sigma(\mathrm{Fe\,I})}{\sqrt{(N_{\mathrm{X}})}}, \frac{\sigma(\mathrm{X})}{\sqrt{(N_{\mathrm{X}})}}\right) \quad (1)$$

The error on the abundance ratios, [X/Fe] was calculated as the quadratic sum of the errors on [X/H] and [Fe/H]. This conservative estimate includes all sources of error due to the measurements, and will be used throughout the figures and discussions of Sect. 4 and 5.

The uncertainties caused by our choice of stellar parameters were estimated by varying the stellar parameters of each star by their uncertainties, and comparing the abundances computed with these modified parameters to the nominal abundance. Those errors, averaged over our sample and combined quadratically, are presented in Table 2. Note that combining those errors quadratically explicitely ignores covariances between parameters, and is therefore an upper limit for the total error (see e.g. McWilliam et al. 1995; Johnson 2002).

Table 2. Errors due to uncertainties in stellar parameters.

Element	$\Delta\ T_{\mathrm{eff}}$ = +200 K	$\Delta\ \log g$ = -0.5 dex	$\Delta\ v_{\mathrm{t}}$ = +0.2 km/s	Combined
[Na I/H]	-0.18	0.01	0.01	0.18
[Mg I/H]	-0.06	0.00	0.06	0.08
[Si I/H]	0.14	0.12	0.02	0.19
[Ca I/H]	-0.23	0.04	0.07	0.24
[Ti I/H]	-0.33	0.08	0.04	0.34
[Ti II/H]	0.10	0.21	0.04	0.24
[Cr I/H]	-0.32	0.11	0.09	0.35
[Fe I/H]	-0.04	0.12	0.08	0.15
[Fe II/H]	0.32	0.28	0.04	0.43
[Ni I/H]	-0.03	0.14	0.05	0.15
[Y II/H]	0.06	0.19	0.02	0.20
[Ba II/H]	-0.03	0.15	0.26	0.30
[La II/H]	-0.05	0.23	0.04	0.23
[Nd II/H]	0.00	0.20	0.02	0.20
[Eu II/H]	0.03	0.22	0.04	0.22

3.5. Hyperfine splitting correction

Ignoring the hyperfine structure (HFS) of a line can lead to overestimate the abundance of the element responsible for this line, as HFS acts to desaturate lines that are above the linear part of the curve of growth. Given our large sample size, instead of computing all lines one by one including HFS, we defined a generic *HFS correction* per line to be applied to the abundance deduced without HFS from the EW of each line. We found that, for the range of stellar parameters and abundances of our sample, this correction depends predominantly on the *EW*s, and very little on any other parameter. As an example, Figure 7 displays the HFS correction for Eu (λ = 6645.1 Å). Similar corrections were derived for the La (λ = 6320.4 Å) line and applied to the sample.

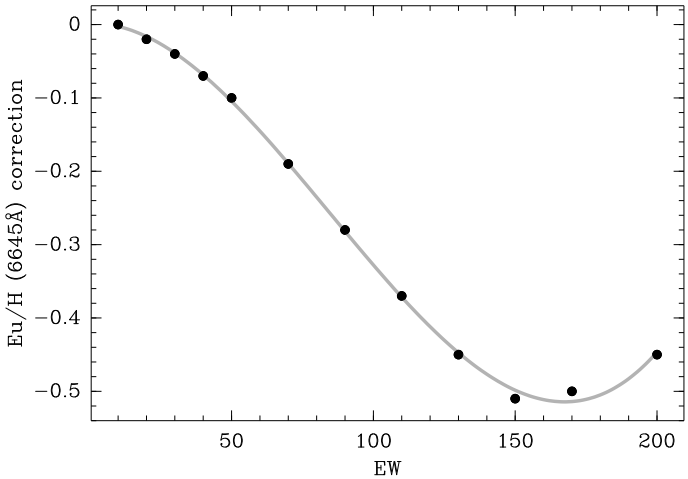

Fig. 7. HFS correction (dex) for the Eu line at 6645.1Å, tested on a plane-parallel model of T_{eff} = 4300, $\log g$ = 0.6, [Fe/H] = -1.5 and v_{t} = 1.7.

3.6. Systematics

Since the present work uses new automatic procedures, new stellar atmosphere models and a new line list adapted to the resolution and wavelength range of GIRAFFE, it is important to estimate possible systematic errors that these changes would trigger.

Our sample includes the 3 stars observed by S03 with UVES that were analyzed in a classical high resolution scheme. We ran checks in 5 steps each tackling a specific ingredient of the analysis presented in this paper. At each step, we re-determined the stellar parameters providing the best fit model. The results are listed in Table 3.

We carried out 5 different analyses, as follows:

- Check 1, basic sanity check: we reproduce the original abundance analysis of S03, starting from the UVES spectra, using the S03 line list, measuring the *EW*s with `splot` and working with the plane-parallel models of Gustafsson et al. (1975).
- Check 2, the influence of the geometry: the same set-up as in Check 1, except the plane-parallel models are replaced by the spherical MARCS models.
- Check 3, the influence of the line list and wavelength coverage: the same set-up as in Check 2, except *(a)* the original line list was replaced by the one used in this work; *(b)* we restricted the analysis to the wavelength coverage of the FLAMES HR 10, 13 and 14 setups.
- Check 4, the influence of the automatic measurement of *EW*s: the same set-up as in Check 3, except the *EW*s are measured automatically with `DAOSPEC` instead of manually with `splot`.
- Check 5, the influence of the spectral resolution: the same set-up as in Check 4, except the *EW*s are now taken from the new GIRAFFE spectra instead of the S03 UVES spectra, and so the spectral resolution is reduced by a factor of two, from $R \simeq 40\,000$ to $R \simeq 20\,000$.

Figure 8 displays the results of these 5 checks and compares the abundances of 13 different elements and/or ionisation states independently determined at each stage. One conspicuous result of our checks is the different [Fe/H] obtained for BL239 in our new analysis compared to S03 (a

Table 3. The results of our investigation into possible systematic errors in our procedures. The names of the three stars common to the present work and to S03 are given as are their coordinates. For each check we give the atmospheric parameters of the best fit models, $T_{\rm eff}$, $\log g$, [Fe/H] and $v_{\rm t}$.

ID	Shetrone	RA(J2000)	DEC(J2000)
BL239	Fnx-M25	02 39 47.09	-34 31 49.8
BL266	Fnx-M12	02 40 10.00	-34 29 58.8
BL278	Fnx-M21	02 40 04.38	-34 27 11.3

Check 1				
Star	$T_{\rm eff}$	$\log g$	[Fe/H]	$v_{\rm t}$
BL239	4100	0.00	-1.30	2.2
BL266	4300	0.00	-1.60	2.0
BL278	4000	0.60	-0.60	1.7
Check 2				
Star	$T_{\rm eff}$	$\log g$	[Fe/H]	$v_{\rm t}$
BL239	4100	0.00	-1.30	2.1
BL266	4200	0.00	-1.50	2.1
BL278	4000	0.60	-0.60	1.7
Check 3				
Star	$T_{\rm eff}$	$\log g$	[Fe/H]	$v_{\rm t}$
BL239	4100	0.60	-1.00	2.0
BL266	4200	0.70	-1.50	1.9
BL278	4000	0.60	-0.70	2.0
Check 4				
Star	$T_{\rm eff}$	$\log g$	[Fe/H]	$v_{\rm t}$
BL239	4100	0.60	-1.00	2.0
BL266	4200	0.70	-1.50	1.9
BL278	4000	0.60	-0.70	2.0
Check 5				
Star	$T_{\rm eff}$	$\log g$	[Fe/H]	$v_{\rm t}$
BL239	4123	0.68	-0.91	2.1
BL266	4212	0.83	-1.44	2.0
BL278	4072	0.64	-0.72	2.3

difference of +0.4 dex). This effect is due to the fact that historically the S03 line list was optimized for metal-poor stars and hence lacks weak lines. This is appropriate for BL266. In the case of BL278, since this star was obviously more metal-rich, S03 were naturally required to add weak lines to their line list. Conversely, BL239 falls between these two regimes and no weak lines were added. This had the effect of driving the micro-turbulence velocities to artificially high values, and thus biasing metallicities towards lower values.

There are several differences between the Gustafsson et al. (1975) and Gustafsson et al. (2008) models. The two most important are the different geometry used (plane-parallel versus spherical) and the physics involved in the opacities. Abundances calculated with these two methods are similar, most of the time within the error bars. As discussed in Sec.3.1, the effect of geometry alone is expected to account for up to ∼0.05 dex and can be partially responsible for the difference in abundance between the triangles and inverted triangles symbols of Figure 8.

The effects of using different line lists can be seen in Figure 8 comparing the triangles and the diamonds. This is usually the largest source of differences, showing the importance of having a common line list for comparing abundance results.

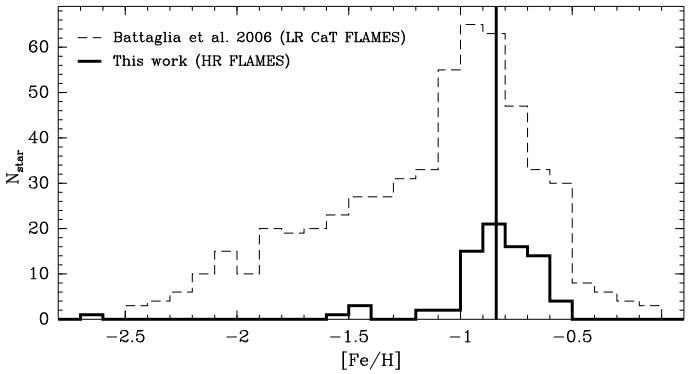

Fig. 9. The [Fe/H] distribution of our FLAMES high resolution abundance analysis (solid line), peaking at [Fe/H] ≈ -0.8. The metallicity distribution obtained from the larger set of Ca II triplet measurements (B06) is shown in dashed line for comparison.

The method used to measure the *EW*s also affects the abundance results but only by a small amount, and in most cases well within the errors. This can be seen by comparing circles and diamonds in Figure 8. This check reinforces our confidence in using the automatic DAOSPEC *EW* measurement code, allowing us to go from hand-measurement to a much faster automated processing.

Finally, comparing UVES and GIRAFFE results shows that even with a loss of a factor two in resolution and a factor three in wavelength coverage, it is possible to determine accurate abundances. By comparing the empty circles to the solid dots in Figure 8, it is clear that not only [Fe/H] but also most of the abundance ratios are identical within the errors.

4. Results

We were able to determine detailed abundances for 81 stars from our original sample of 107 FLAMES spectra. Their atmospheric parameters are presented in Table A.3. The *EW*s are listed in Table A.4. Finally, all abundance ratios are given in Table A.5. In the following, the solar abundances of Anders & Grevesse (1989) are adopted, with the exception of Ti, Fe and La (Grevesse & Sauval 1998).

4.1. Iron abundance

Figure 9 compares our FLAMES HR [Fe/H] distribution to the FLAMES LR [Fe/H] distribution derived by B06, using low resolution ($R = 6500$) Ca II triplet measurements . The overlap between the two samples have allowed (Battaglia et al. 2008a) to verify the Ca II infrared triplet calibration to [Fe/H]. Although B06 have larger uncertainties on their [Fe/H] estimates, they benefited from a much larger sample of 600 stars spread over a much larger area of Fornax than the present work. Our distribution peaks at [Fe/H] $\simeq -0.8$ and is clearly skewed towards more metal rich stars than B06. There are a few outlying stars on the metal poor side, but the centre of Fornax is definitely dominated by stars with [Fe/H] > -1.2. Albeit unevenly, we still sample two orders of magnitude in [Fe/H] ($-2.5 \lesssim$ [Fe/H] $\lesssim -0.5$).

Although our field contains one of the Fornax globular clusters, Cluster 4 (Hodge 1961), we don't seem to have selected any of its stars. Cluster 4 is moderately metal poor, [Fe/H]~ -1.5 (e.g., Strader et al. 2003). Letarte et al. (2006) suggested that the metallicity scale of Strader et al. (2003) tends to over estimate [Fe/H] by 0.3 to 0.5 dex, hence any [Fe/H] ~ -1.8 to -2 dex star in our sample, spatially close to Cluster 4 is a potential cluster member. The closest stars to Cluster 4 all have [Fe/H] ≈ -0.8 dex, and are therefore significantly too metal rich to be members.

The single truly metal-poor star in our sample, BL085 at [Fe/H] $= -2.58$, is not located near Cluster 4 and should thus be representative of the oldest and most metal-poor field population in Fornax. However, the $V_{\rm rad}$ for this star places it at the very edge of our membership boundary, and in the slightly more strict membership criteria of B06 it is considered a non-member. We did not consider this a reason to exclude it from our analysis, but care should be taken in attributing it too definitively to Fornax.

4.2. Alpha Elements

The α elements are predominantly produced by high mass, ($> 8\mathcal{M}_{\odot}$) short lifetime Type II supernovae explosions (SNe II). [α/Fe] is thus a way of tracing the relative contribution of SN II and SN Ia products that were available when the stars formed (e.g., Gilmore & Wyse 1991). Stars forming when the interstellar medium (ISM) has only been enriched by SNe IIs have high [α/Fe], while those forming after the SNe Ia have significantly enriched the ISM in iron have lower [α/Fe].

The individual α-element ratios for our sample of Fornax field stars [Mg/Fe], [Si/Fe], [TiI/Fe] and [Ca/Fe] are shown in Figure 10. For comparison, we also present high resolution abundances of 9 stars in 3 Fornax globular clusters (Letarte et al. 2006), and a compilation of Milky Way halo, thick and thin disk stars (Venn et al. 2004) , as well as eight peculiar halo stars (Nissen & Schuster 1997, hereafter NS97). These eight stars from NS97 have unusual kinematics and orbital parameters, including a large maximum distance from the Galactic centre ($R_{\rm max}$) and a large distance from the Galactic plane ($z_{\rm max}$). They were also found to display low [α/Fe] and [Ni/Fe] (along with other chemical peculiarities) compared to the majority of MW halo stars. These differences have led to the suggestion that these stars might have been accreted by the MW from a dwarf galaxy, and this is why we include them in our figures.

The single metal poor star in our new sample of Fornax field stars, BL085 ([Fe/H] $= -2.58$), has α-element abundances very similar to the Galactic halo stars and also (Fornax) globular cluster stars at similar [Fe/H]. In contrast at higher [Fe/H], the rest of the Fornax field stars are significantly under-abundant in [α/Fe] with respect to the MW. [Mg/Fe] is typically lower than the level of the Galactic stars by between 0.2 and 0.5 dex and the highest values just overlap with NS97 stars. The [Si/Fe] ratios are the highest for the α-elements in Fornax with a mean value close to solar and this corresponds to the same level as the eight peculiar halo stars of NS97. [Ca/Fe] and [Ti/Fe] are typically lower than [Si/Fe] and [Mg/Fe] especially for the 4 stars at [Fe/H] ~ -1.5. In addition, both [TiI/Fe] and [CaI/Fe] are constant in value, contrary to [MgI/Fe] and [SiI/Fe]. This trend was first noticed in dSphs by Shetrone (2004). Venn et al. (2004) hypothesized that it was due to

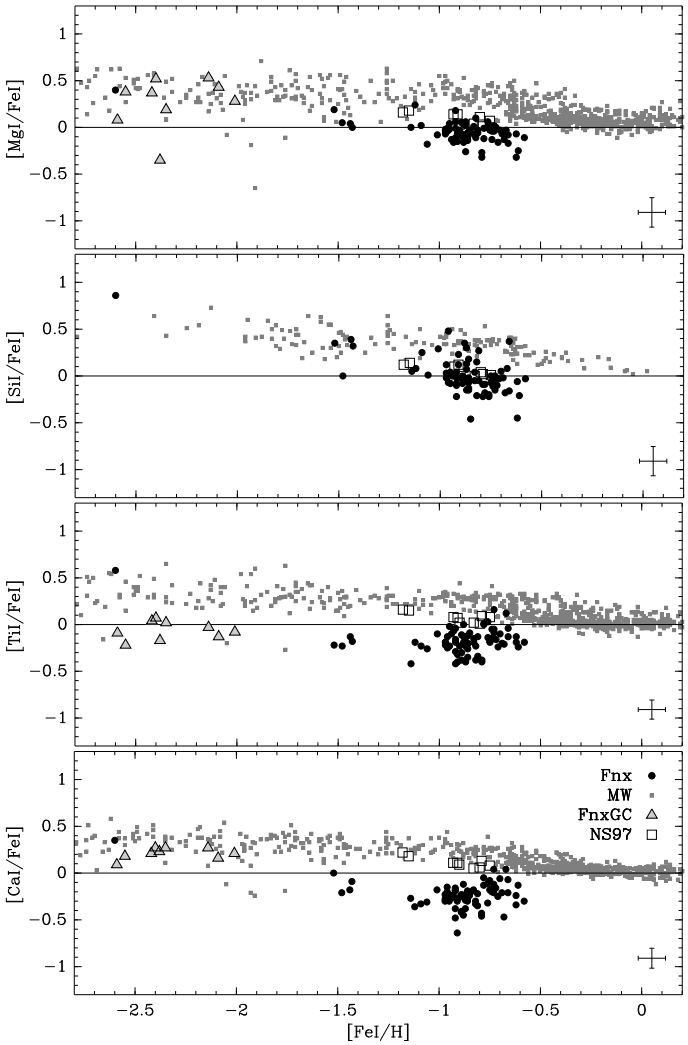

Fig. 10. The abundance ratios [Mg/Fe], [Si/Fe] and [Ca/Fe] versus [Fe/H]. Our observations of Fornax field stars are shown with solid circles. Also plotted for comparison are Galactic stars (original references in Venn et al. 2004) with small grey squares, the Fornax globular clusters (Letarte et al. 2006) with triangles and eight peculiar halo stars (Nissen & Schuster 1997) with empty squares. There is a representative (average) error bar for the Fornax field star abundances in the bottom right corner of each panel. This is the quadratic sum of [X/H] + [Fe/H], (measurement errors) taken from Table A.5.

different nucleosynthetic origins (Mg and Si form through hydrostatic C and O burning in the cores of massive stars, whereas some isotopes of Ca and Ti form in the α-process). Fulbright et al. (2007) have also seen this effect in the galactic bulge, where the evidence for fast chemical enrichment clearly favours massive stars for the main contributors to these elements. Another possibility in Fornax where SNe Ia have clearly have time to contribute strongly the chemical enrichment, is provided by the sensitivity of the SNe Ia ejecta to the metallicity of their progenitors (Timmes et al. 2003; Röpke et al. 2006). As we will see in Section 4.3 it applies to Ni, but it could also affect the intermediate mass elements. SNe Ia are thought to produce little Mg, while they are able to produce significant amounts of Ca and Ti : for example, the ratio of Ca/Fe is only a factor four larger

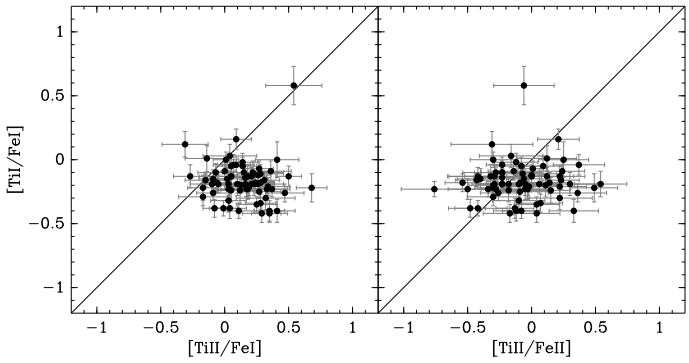

Fig. 11. The two ionisation states for Titanium, Ti I and Ti II are compared to our HR sample of Fornax field stars. On the *left panel,* there is a clear offset of [Ti I/Fe I] versus [Ti II/Fe I], while on the *right panel,* [Ti I/Fe I] and [Ti II/Fe II] are on a more common scale, showing that ionisation balance is probably not very well achieved in these stars.

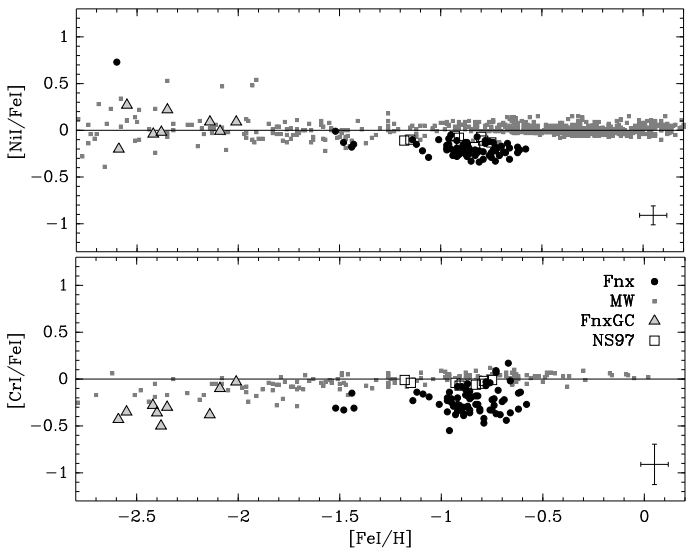

Fig. 12. The Iron peak elements [Ni/Fe] and [Cr/Fe] versus [Fe/H] for the Fornax field stars, the Fornax globular clusters, and MW stars. The references and symbols are the same as in Figure 10.

in a SNe II of $50M_{odot}$ than in a SNe Ia (Tsujimoto et al. 1995), and the total mass of Ca produced is actually larger in the latter. Röpke et al. (2006) show that for a SNe Ia progenitor metallicity $[Z/Z_{\odot}]$ lowered from 0. to -0.5, the production of some Ca and Ti isotopes can diminish by a factor ~ 3. Hence, if a large fraction of Ca and Ti are produced in SNe Ia in Fornax, the low [Ca/Fe] and [Ti/Fe] could then be a consequence of the low metallicity of their progenitors compared to the Milky Way.

These are however still conjectures which require a few words of caution. Figure 11 illustrates that [Ti I/Fe] differs from [Ti II/Fe] and is lower by $\sim$0.4 dex. This *could be a sign of significant non-LTE effects, affecting predominantly Ti* I *though both a departure from ionisation equilibrium and NLTE acting most on the Ti* I *lines that have significantly lower* $\chi_{\rm ex}$ *than Ti* II*However, NLTE may not be the only culprit to blame, as any temperature biais in the* $T_{\rm eff}$ *scale also both shifts ionisation equilibriae and affects more low excitation lines such as those of Ti* I.

We would prefer to determine the Ti abundance using Ti II lines, however the number of available lines ($\sim 2-3$) is small, and smaller than the number of Ti I lines ($\sim 8-9$), as reflected in the larger error bars. Therefore, as [Ti I/Fe] is statistically more reliable, the abundance of titanium is calculated as the average of results from the Ti I lines. This leaves some, quite large, uncertainty as to the true value of [Ti/Fe], although we also point out in Figure 11 that [Ti II/Fe II] agrees reasonably well with [Ti I/Fe I] albeit with a large dispersion, lending strength to a low [Ti/Fe] ratio. CaI could be similarly affected, although we have no way to check.

Of the two O lines available in our wavelength range the most reliable one at 6300 Å is not suitable, as the typical $V_{\rm rad}$ of the Fornax stars means that this matches a telluric absorption line rendering it unusable for most of our stars. The second line is weak at the limit of detection with DAOSPEC at this resolution. The continuum in its immediate vicinity is also not well defined, because it is blended with CN lines and Ca I auto ionisation features. Thus the *EW*s seem to be frequently over estimated by DAOSPEC. For all these reasons, we have decided not to include the O abundances.

4.3. Iron peak elements

According to nucleosynthetic predictions, iron peak elements like Iron (Fe), Chromium (Cr), and Nickel (Ni) are believed to be formed predominantly from explosive nucleosynthesis in SN Ia (Iwamoto et al. 1999; Travaglio et al. 2005). In Figure 12, we present the [Ni/Fe] and [Cr/Fe] abundance ratios for the Fornax stars plotted against [Fe/H]. Both ratios appear to behave in a similar way. [Ni/Fe] has much smaller error bars than [Cr/Fe], due to the larger number of lines available ($\sim$15 versus 1). Hence the additional scatter in [Cr/Fe] compared to [Ni/Fe] is only due to larger error bars.

To test the validity of our [Cr/Fe] and [Ni/Fe] abundance ratios, we carried out tests on a high S/N spectrum of Arcturus, for which we confirmed [Cr/Fe] $\simeq$ [Ni/Fe] $\simeq$ 0.0. Restricting the [Cr/Fe] analysis to the same single line available to our Fornax sample, we obtained [Cr/Fe] $= -0.2$. We performed the same analysis for Ni, using only the Ni lines available for Fornax, and recovered the expected [Ni/Fe] = 0.0. These two results suggest that the Cr line we have access to ($\lambda = 6330.09$Å) has an erroneous log *gf*, leading to a lower abundance. We therefore updated the log *gf* for this Cr transition to reproduce [Cr/Fe] = 0.0 in Arcturus, thereby insuring a proper comparison to the Milky-Way samples in Figure 12.

It is interesting to note that our most metal poor Fornax star, BL085([Fe/H]$=-2.58$), has a significantly higher [Ni/Fe] value than the other Fornax field stars, and is comparable to MW halo stars and Fornax GC stars. However, at this low metallicity, we only detect 4 Ni lines (instead of 15, as for the more metal rich stars), leading to a much larger error bar than the average shown in the bottom right hand corner of the plot (see Table A.5).

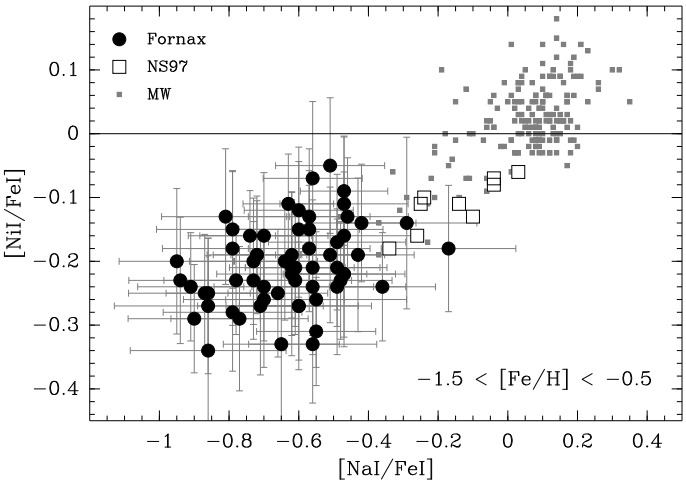

Fig. 13. The relation between Na and Ni. The references and symbols are given in Figure 10.

The underabundance in [Ni/Fe] which we see in Figure 12 for Fornax stars with [Fe/H] > -1.2 has been previously observed in some of the Milky Way halo stars (NS97, Nissen & Schuster 2009) and in the Large Magellanic Cloud (LMC) disk stars (Pompéia et al. 2008). This effect is even stronger in the Sagittarius dSph where the iron-peak elements all exhibit sub-solar ratios for stars with [Fe/H]> -1.5 (Sbordone et al. 2007). Nissen & Schuster (2009) noticed that their low [Ni/Fe] stars also have low [Mg/Fe], similar to what is seen in Fornax.

These low values of [Ni/Fe] and [Cr/Fe] cannot be easily explained with our current understanding of nucleosynthesis. The [Ni/Fe] ratios should be zero and constant for all values of [Fe/H] since both Ni and Fe are believed to be predominantly created by the same production mechanism in SN Ia (Travaglio et al. 2005). The different behaviour seen in Fornax and the NS97 stars from the Galactic trend is an indication that the production factors for each iron-peak element is not the same and depends upon the evolutionary history of the parent population. For example, it is possible that SNe Ia Ni yields are linearly dependent on the original metallicity of the white dwarf progenitor (Timmes et al. 2003; Travaglio et al. 2005).

This under-abundance of Ni (and Cr) was *not* observed by Shetrone et al. 2003, for the three stars we have in common. We attribute this difference to a combination of systematic effects, where the most important one is the use of a different line list. See section 3.6 and Figure 8 for more details on systematic effects in abundance determinations.

4.4. The Na-Ni relationship

As mentioned in section 4.3, Ni is assumed to originate predominantly from SNe Ia. However, the production of Ni might also be linked to the production of Na in SNe II (Thielemann et al. 1990; Timmes et al. 1995). The amount of Na produced is controlled by the neutron excess, where ^{23}Na is the only stable neutron-rich isotope produced in significant quantity during the C and O burning stage. During the SNe II explosions, the elements are photo-dissociated into protons and neutrons, further recombining to form ^{56}Ni, which in turn β decays into ^{56}Fe, the dominant isotope of iron. ^{54}Fe and/or ^{58}Ni can also be produced at this stage, depending on the abundance of neutron-rich elements (e.g. ^{23}Na). The amount of ^{54}Fe made is small compared to the total yield of iron (which is dominated by ^{56}Fe production), but this is the main source of ^{58}Ni, the stable isotope of nickel (Clayton 1983).

In summary, the production of Ni depends on the neutron excess and the neutron excess will depend primarily on the amount of ^{23}Na previously produced. Hence, a Na-Ni correlation is expected when the chemical enrichment is dominated by SNe II. The advent of the SNe Ia explosions can break (or flatten) this relationship, as Ni is produced without Na in the standard model of SNe Ia (e.g., Iwamoto et al. 1999).

We have restricted the metallicity range of Figure 13 to $-1.5 <$ [Fe/H] < -0.5, corresponding to the region in which the Na-Ni relation can be seen in Fornax. The region covered by our sample of Fornax stars extend the relation known for the MW to lower [Na/Fe] and [Ni/Fe] values with a similar slope. In SNe II, the dominant source of Ni is independent of the dominant source of Fe. Consequently, low [Ni/Fe] is possible at low metallicities, before the SNe Ia contribute to the ISM chemical patterns. If the first SNe II in Fornax were not neutron rich, then there would be a lack of Na (and therefore also Ni) production. The next generations of stars could carry this signature, even at higher metallicity. The fact that we still see the SNII signature of the correlation between Na and Ni in our sample of Fornax stars, means that the slope of the relation is not diminished due to the subsequent addition of large amounts of Ni. This is consistent with our previous discussion suggesting that low SNe Ia Ni yields are due to lower metallicity progenitors in dSph compared to the Milky Way.

4.5. Heavy elements

Heavy elements (Z > 30) are neutron capture elements. One distinguishes the *s*-process (or slow process) and the *r*-process (rapid process), with respect to the neutron-capture time-scales. The *s*-process is believed to predominantly take place relatively low mass stars ($2 - 4\mathcal{M}_{\odot}$). The *r*-process by contrast requires more extreme conditions, for example the very high temperatures and neutron densities found in SNe II explosions.

4.5.1. Tracing the *s*-process and *r*-process contribution

Figures 14 and 15 display our results for [Ba/Fe], [Y/Fe], [La/Fe], [Nd/Fe] and [Eu/Fe], in decreasing order of *s*-process contribution in the Sun. [Ba/Fe] and [La/Fe] display significant excesses at [Fe/H] > -1. Both [Ba/Fe] and [La/Fe] rise steeply with increasing [Fe/H], however [Ba/Fe] reaches much higher levels than in the Milky Way. Conversely, [YII/Fe] is stable, with a large dispersion, ranging from the solar values, like in MW stars, down to ~ -0.7. [Eu/Fe] and [Nd/Fe] are constant in our sample at the same levels observed in the MW for the same [Fe/H]. In summary, the *r*-process elements are overabundant by $\sim$0.5 dex compared to iron and stay constant. The *s*-process elements are also overabundant but this increases with increasing [Fe/H]. The *s*-process origin of Ba (and hence La), over the full [Fe/H] range of our sample is shown in Figure 16, where Ba is compared to Eu, a 97% *r*-process dominated element in the sun (Kappeler et al. 1989; Travaglio et al. 1999).

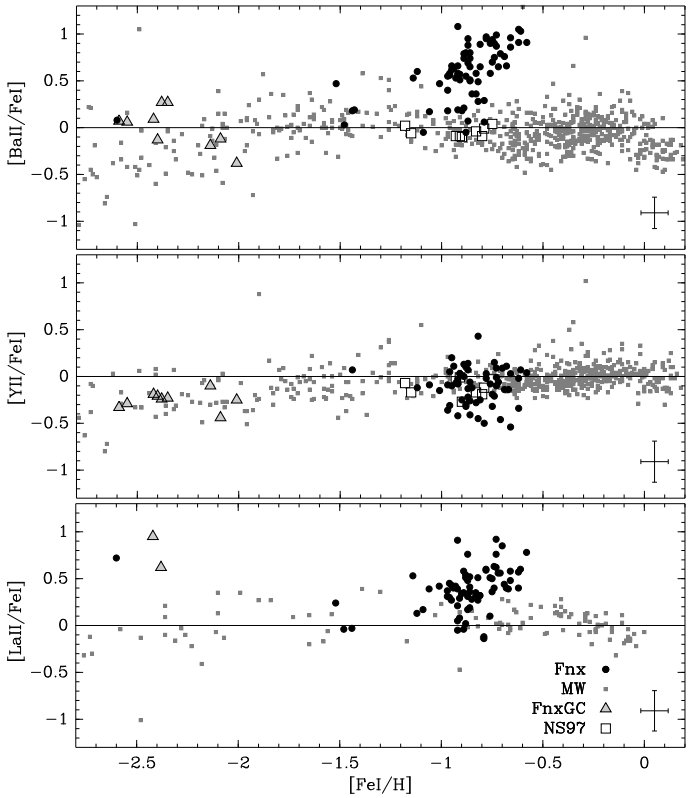

Fig. 14. The *s*-process elements [Ba/Fe], [Y/Fe] and [La/Fe] plotted against [Fe/H] for the Fornax field stars, the Fornax globular clusters, the MW compilation and the stars from NS97. The references and symbols are the same as given in Fig 9, and in addition we use data from Johnson (2002) and Simmerer et al. (2004) for [La/Fe].

The exception to the rule of the dichotomy between *r*-process and *s*-process elements in Fornax is [Y/Fe], which has a flat distribution, and falls on the locus of the MW observations, at same [Fe/H]. In order to shed light on this matter, Figure 16 also presents [Ba/Y] as a function of [Fe/H]. Ba is clearly more abundant than Y and well above the level of the MW at same [Fe/H].

There are three s-peaks of very small neutron capture cross sections resulting in large *s*-process abundances. The first one corresponds to Sr, Y, Zr, the second one corresponds to Ba, La, Ce, Pr, Nd and the third one terminates the *s*-process involving Pb (Clayton et al. 1961; Seeger et al. 1965). Travaglio et al. 2004 have shown that the *s*-process production in AGB stars is strongly dependent on [Fe/H]. At solar metallicity, AGB stars produce large amounts of *s*-process elements from the first peak. At lower [Fe/H], more neutrons per Fe seed are available, thus bypassing the first peak and progressively feeding elements in the second neutron magic number peak.

As a consequence, the high [Ba/Y] could be explained if Fornax has a larger contribution from metal poor AGB stars compared to the MW, favouring the creation of heavier *s*-process elements.

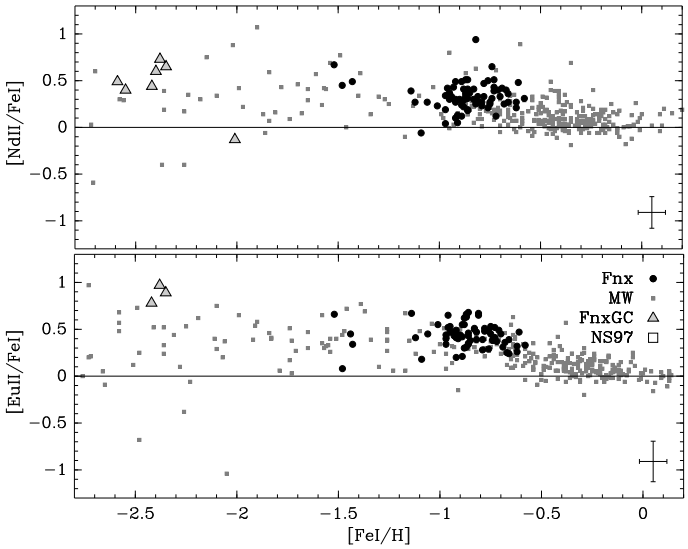

Fig. 15. The *r*-process elements [Nd/Fe] and [Eu/Fe] plotted against [Fe/H] for the Fornax field stars, the Fornax globular clusters, and the MW. The references and symbols are those of Fig. 9. In addition the [Nd/Fe] values for the Milky Way stars are taken from Burris et al. (2000) and Reddy et al. (2003, 2006).

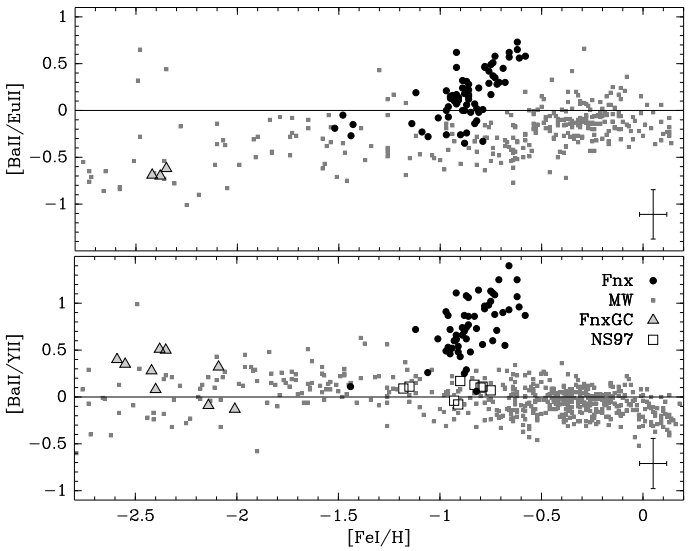

Fig. 16. [Ba/Eu] and [Ba/Y] as a function of [Fe/H] for the Fornax field stars as well as Fornax globulars and MW compilation. The references are given in Figure 10.

5. Discussion

5.1. Ages

Having measured the abundances for our sample of 81 Fornax RGB stars we can now use isochrones of the appropriate metallicities and α-element content to determine their ages. Following B06, we base our analysis on our ESO/MPG/2.2m WFI V and I photometry and on the isochrones of Yi et al. (2001) and Kim et al. (2002).

In Figure 17, we combine the results of this work with Ca II triplet measurements (B06) of a larger data set to derive a global age-metallicity relation for the Fornax dSph. There is a very nice match between B06 and the present

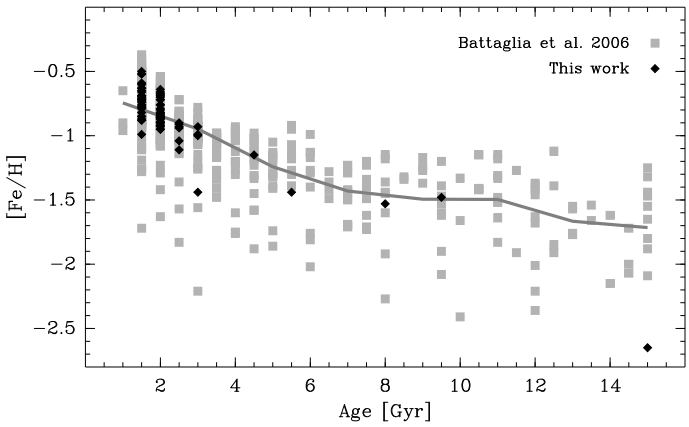

Fig. 17. The age-metallicity relation for the Fornax dSph, as derived from the 81 stars from the HR sample (black diamonds) and the LR sample of B06 (grey shaded squares). The central line follows the average [Fe/H] value of each age bin.

work. It also stands out clearly that the majority of the stars we observed here at high spectroscopic resolution in the center of Fornax have ages between 1.5 and 2 ($\pm$1) Gyr old. We note however, all these ages have been derived from solar-scaled chemical composition isochrones. The inclusion of alpha-enhancement effects has been shown to reduce stellar ages by $\sim$ 1 - 1.5 Gyr if one takes [α/Fe]=0.3 instead of [α/Fe]=0.0 (Kim et al. 2002). If this behaviour extrapolates to low [α/Fe], the true ages of our sample stars might be slightly higher, between 1 and 4 Gyr old. In any case, it can be appreciated that this central sample of stars mostly probes the population born in the most recent and most intense star formation episode in the history of Fornax, although it also bears the imprints of the full chemical evolution of the galaxy.

Coleman & de Jong (2008) present deep photometry over the full surface of Fornax and provide age-metallicty relations at different galactocentric distances. The results of this study agree qualitatively with our results: the youngest stellar population is the most centrally concentrated and the most metal-rich. However, going into finer details, our spread in metallicity is nearly twice as large as in Coleman & de Jong (2008), which also seems to suffer from a systematic shift in [Fe/H] of $\sim$0.5 dex. These discrepancies can be attributed to the different techniques of analyses. In particular, Coleman & de Jong (2008) use the solar-scaled isochrones of Girardi et al. (2002). It is not clear how under solar α-element abundances, as revealed in the present study, would affect the colors of the isochrones. If we extrapolate the effects of passing from α over-abundance to solar-scaled models, for which the colors get redder due to higher mean opacity, Coleman & de Jong (2008) might have compensated for the effect of α-element under-abundance by increasing their overall metallicity.

5.2. Chemical Evolution

Figure 18 compares the α-element, [Mg/Fe], distribution in the central region of Fornax dSph, with the results of a similar FLAMES study of the Sculptor dSph (89 stars, Hill et al., in prep, Tolstoy et al. 2009), the Milky Way (Venn et al. 2004), the Sgr dSph (Sbordone et al. 2007; Monaco et al. 2005; Bonifacio et al. 2004) and Carina (Koch et al. 2008)

Sculptor is to date the only dSph galaxy with a statistically significant number of stars observed with high [Mg/Fe], matching the locus of the Milky Way halo and thick disk stars. Nevertheless the few stars gathered at [Fe/H] $\leq$ -2.5 in Carina and Fornax, and also the Sagittarius and Draco (Cohen & Huang 2009) stars with [Fe/H] $\sim$ -1.5 suggest that it is very likely that all Local Group dSphs possess α-overabundant old stellar populations (see also Shetrone et al. (2009) for the LeoII dSph from lower resolution spectroscopy). The metallicity at which [Mg/Fe] starts to decrease (sometimes called "the knee"), as a consequence of the onset of the SNe Ia explosions, depends on the specific star formation history of each galaxy, and in particular on its efficiency (e.g., Tinsley 1979). The Sculptor dSph is currently the only system for which we can identify this point ([Fe/H]=-1.8) with any accuracy. Intriguingly this is roughly the same metallicity which defines the break between two distinct kinematic and spatial components in Sculptor (Tolstoy et al. 2004; Battaglia et al. 2008a).

All four dSphs in Figure 18 clearly have lower star formation efficiency than the Milky Way, because SNe Ia start to explode at [Fe/H] $<<$ -0.8, which is at much lower values than the "knee" of the MW. It is interesting to see how Sculptor, Fornax and Sagittarius form a sequence increasing "knee" metallicity position, reflecting increasing strength and duration of star formation periods that also lead to higher mean metallicities. This is also reflected in the metallicity luminosity relation observed for dSph galaxies (e.g. Mateo 1998; Kirby et al. 2008). The "knee" position in the low luminosity Draco may be as low as ([Fe/H]$\leq$ -2.5) (Cohen & Huang 2009).

The [Mg/Fe] values for all dSph also reach lower values than in the Milky Way, as predicted by chemical evolution models (Lanfranchi & Matteucci 2004; Revaz et al. 2009). This is a consequence of the absence of a balance between SNe Ia ejecta and on-going star formation.

These three galaxies also exhibit a very small dispersion in [Mg/Fe] at a given [Fe/H], and what there is comes mostly, if not all, from the measurement errors. Conversely, Carina seems to shows hints of a larger dispersion in [Mg/Fe] (Koch et al. 2008), which is presumably the result of an highly episodic star formation history (Smecker-Hane et al. 1996; Hurley-Keller et al. 1998). Long periods of quiescence between the star formation events can translate into scattered abundance ratios (Matteucci & Brocato 1990; Gilmore & Wyse 1991). Revaz et al. (2009) predict that low mass systems (initial baryonic + dark matter mass $< 3\times10^8$ $\mathcal{M}_\odot$, such as Carina, can have episodic bursts of star formation, as a consequence of their long gas cooling time. Also additional factors may play a role in shaping the star formation history of galaxies of similar masses, such as the environment (galaxy orbit around the Milky-Way for example).

5.3. Nucleosynthesis

Figure 19 extends the comparison of Fornax with other dSph galaxies to the case of the neutron capture elements. It supports different sites and relative contributions for the production of α- and r-process elements. If Eu and α-elements were synthesized in the same sites, the ratio of

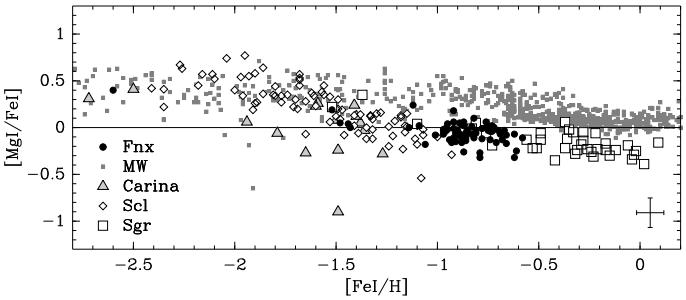

Fig. 18. The relation between [Mg/Fe] and [Fe/H] for our sample of RGB stars observed in Fornax, for the Milky Way halo and disk population (original references in Venn et al. 2004), the Sculptor dSph (DART, Hill et al. in prep.), the Sgr dSph (Sbordone et al. 2007; Monaco et al. 2005; Bonifacio et al. 2004) and Carina (Koch et al. 2008)

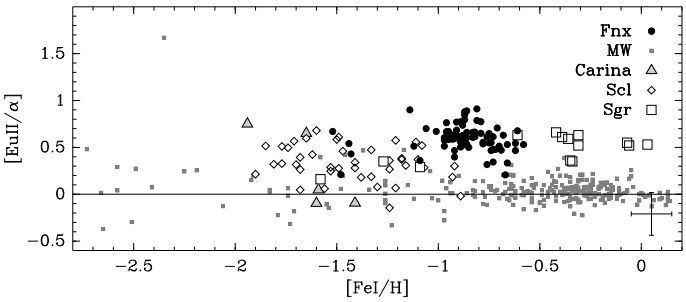

Fig. 19. The relation between [Eu/Mg] and [Fe/H] in our Fornax star sample as compared to the Milky Way (original references in Venn et al. 2004), and three other dSph galaxies: Sagittarius (McWilliam & Smecker-Hane 2005, private communication), Sculptor (DART sample, Hill et al., in preparation) and Carina (Shetrone et al. 2003).

[Eu/α] would stay constant and identical in all galaxies, which it clearly does not.

This is not the first evidence for a decoupling of the production of α and r-process elements : it is already well known among the very metal-poor stars of the Milky Way. Sneden et al. (2008) compiled different analyses of Milky Way halo metal-poor stars demonstrating that, while there is very little dispersion in [Mg/Fe] (taken as representative of the α elements), [Eu/Fe] exhibits a very large scatter at metallicities around [Fe/H]~ -3.0 (e.g., McWilliam et al. 1995; Fulbright 2002; Cayrel et al. 2004; Cohen et al. 2004; Barklem et al. 2005; François et al. 2007). Not only does this indicate that the production of r-process elements was rare while there was profusion of α-elements in the Milky Way at early times, but this also points towards a different mass range of progenitor.

Several scenarios have been proposed for the origin of the r-process elements, including high entropy neutrino winds (e.g. Woosley et al. 1994; Farouqi et al. 2009) and prompt supernova explosions of 8-10$\mathcal{M}_{\odot}$progenitors (e.g. Wanajo et al. 2003). This latter scenario is characterized by a lack of α elements and only a small amount of iron-peak nuclei. Whilst the exact low mass boundaries vary, the origin of α and r-process elements in respectively massive and light SNeII reach broad agreement in reproducing Milky Way halo metal-poor stars (e.g., Mathews et al. 1992; Travaglio et al. 1999; Cescutti et al. 2006; Qian & Wasserburg 2007), including the downturn in the second-peak r-process at the very lowest metallicities (François et al. 2007; Andrievsky et al. 2009).

The dSph galaxies assembled here provide another perspective on the origin of Eu. Indeed, it is noteworthy that the two galaxies which have distinctively high [Eu/α], overabundant by +0.7 and +0.5 dex compared to the Milky Way, also reveal a significant influence of AGB winds in their chemical evolution. [Ba/Fe] is in general extremely high in most of our sample of Fornax stars, and this is also true for Sgr as well as the LMC (Pompéia et al. 2008). Interestingly, Sgr and Fnx dSphs are also the most massive dSphs in the Local Group, reaching the highest metallicities of their family of galactic systems and are the only ones to possess globular clusters, implying that higher mass galaxies in the vicinity of the Milky Way are better able to hold on to their gas, allowing them to reach this evolutionary stage where AGB contribute significantly to the enrichment. Given this strong influence of the s-process in Fornax, one may question whether the s-process can participate a significant fraction of the Eu production in this galaxy.

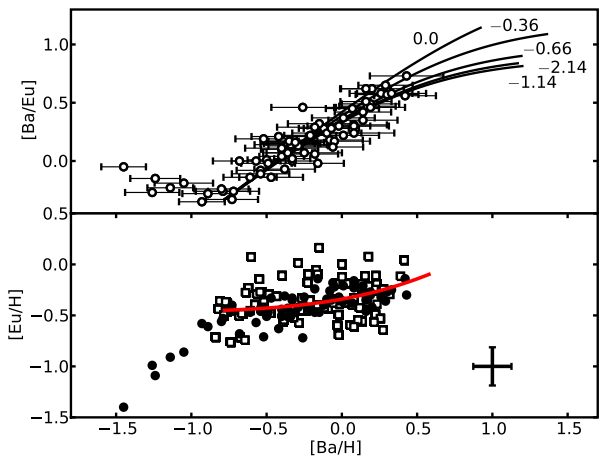

Fig. 20. [Eu/H] and [Ba/Eu] versus [Ba/H]. *Upper panel :* The expected evolution of [Ba/Eu] as a function of [Ba/H] when the evolution of Ba and Eu are triggered by AGB winds only, starting at [Ba/H]=−0.78 and [Ba/Eu]=−0.33. The five solid lines follow the chemical evolution induced by the AGB models of Cristallo et al. (2009) at different metallicities ([Z/Z$_{\odot}$]), which values are indicated close to the upper edges of the model lines. The Fornax sample stars from this work are shown in open circles, together with the individual error bars in [Ba/H]. *Lower panel :* The black points show the observations of Fornax stars from this work. The solid line traces the locus of the evolution in Eu and Ba induced by the yields of [Z/Z$_{\odot}$]=−2.14 AGBs (Cristallo et al. 2009), starting at [Ba/H]=−0.78 and [Ba/Eu]=−0.33. The black open squares are 85 random trials taking into account the mean observational errors, 0.15 dex in [Ba/H] and 0.19 dex in [Eu/H] indicated at the bottom right of the frame. They show the scattering of the single model line induced by the observational uncertainties only.

Aoki et al. (2003) have demonstrated the s-process origin of Eu in two Milky Way halo stars strongly enriched in s-process elements. This is thus a good starting point

for the investigation of Fornax at [Fe/H]≥ -1 where the s-process begins to dominate. The effective s-process component integrates successive generations of AGB stars according to the chemical evolution of the galactic system which is considered, hence mixing the products of different AGB yields, themselves functions of the initial metallicity, stellar mass, 13C pocket efficiency, and other physical properties (Travaglio et al. 2004). At [Fe/H]$=-1$, where [Ba/Fe] rises strongly, Fornax is already a chemically complex system with signatures of SNe Ia and AGB products. We will try to reproduce the behavior of Ba and Eu from there on.

Figure 20 presents the variation of [Eu/H] and [Ba/Eu] as a function of [Ba/H] for our sample of Fornax stars. Analogous to McWilliam & Smecker-Hane (2005) in the case of the Sgr dSph, we find that a continuous enrichment by 90% s-process and 10% r-process as defined in the solar neighborhood (Simmerer et al. 2004) and starting at [Ba/H]~ -0.8 and [Ba/Eu]~ -0.3 reproduces the observed trend between Ba and Eu. This is equivalent to considering that, from [Fe/H]$=-1$ on, the nucleosynthesis in AGBs is responsible for 90% of the neutron-capture elements via the s-process and only 10% is contributed by the r-process. Still, the exact r-process and s-process fractions depend on the prescriptions for AGB yields which are considered. Recently, Cristallo et al. (2009) calculated that not only the yields of Ba and Eu of a $2\mathcal{M}_{\odot}$AGB vary with [Fe/H], but also their ratio, leading to an increased fraction of Eu relative to Ba with decreasing metallicity. In the upper panel of Figure 20, the evolution in [Ba/Eu] as a function of [Ba/H], induced by each of the 5 different metallicities ([Z/Z$_{\odot}$]) of Cristallo et al. (2009), are overplotted on the measurements of our sample of Fornax stars. The [Z/Z$_{\odot}$]=0.0 and -0.36 AGBs tend to produce too high [Ba/Eu], and so does the -0.66 model, albeit marginally. It is nearly impossible to distinguish between the -1.14 and -2.14 models, both passing satisfactorily through the data points. In the lower panel of Figure 20, we now consider [Z/Z$_{\odot}$]$= -2.14$ AGBs only. This single model is then convolved with the mean observed errors in [Ba/H] (0.15 dex) and [Eu/H] (0.19 dex) resulting in the scattered squares which convincingly match the observations. In conclusion, whilst the high [Eu/α] of the 1 to 4 Gyr Fornax stars is primarily due to their low [α/Fe] content, the strong influence of the AGB nucleosynthesis increases their Eu abundance and accentuates this feature of their abundance ratio. This provides an explanation for the observed plateau in [Eu/Fe] at [Fe/H]> -1 seen in Fornax, while it decreases in the Milky Way after the onset the SNe Ia explosions. An additional r-process is required only if too high metallicity AGBs are considered, such as the solar neighborhood standard model one. A refined and more detailed chemical evolution modeling is mandatory to evaluate whether a range in AGB metallicities (rather than a single one as investigated here) is necessary to reproduce Fornax properties.

6. Conclusions

Thanks to the multi-fibre capability of FLAMES we have been able to make detailed abundance measurements of 14 elements for a sample of 81 individual RGB stars in the central 25′ of Fornax. This is a significant, even dramatic, improvement on the previous UVES sample of 3 individual field stars Shetrone et al. (2003). We use new automatic procedures to measure absorption line equivalent widths, new spherical stellar atmosphere models and new line list, all adapted to the resolution and wavelength coverage of GIRAFFE. Our thorough investigation of the potential systematic errors firmly demonstrate that our abundances are accurate. We summarize below the most important results of this work:

- Although our sample was randomly chosen from the entire breadth of the RGB (see Figure 2), it is dominated by a relatively young (1 to 4 Gyr) and metal rich ($-1.5 <$[Fe/H] < -0.5) stars .
- These stars are significantly underabundant in [α/Fe] with respect to the Milky-Way. We observe a slightly different behaviour among the α-elements such that the underabundance of Ti and Ca is more pronounced than that of Mg and Si. Either these two groups of elements have different nucleosynthetis, or a large fraction of both Ca and Ti is produced in low metallicity SNIa. However, we cannot discard the possiblity that non-LTE effects have caused these differential trends.
- The dispersion in [α/Fe], and also other abundance ratios, is found to be very small, essentially within the measurement errors, which is similar to what is seen in Sculptor and Sagittarius dSph and also the Milky Way halo.
- Our sample includes one star, at [Fe/H]$=-2.5$, which contains above solar values of α-elements, equivalent to a Galactic halo star at the same [Fe/H]. This and a few similar stars already found in Sculptor, Carina, and Sagittarius dSph galaxies suggest that an old stellar population with above solar α-element abundances is a common feature in all galaxies.
- [Ni/Fe] and [Cr/Fe] are typically sub-solar in our sample. The different behaviour seen in Fornax stars compared to the Galactic trend suggests that the iron-peak elements are sensitive to the evolutionary history of the parent galaxy and in particular the low SNe Ia yields are due to the excess of low metallicity progenitors in dSph galaxies. This hypothesis is also supported by the Na-Ni relationship in Fornax, which extends the relation found in the Milky Way to lower [Na/Fe] and [Ni/Fe].
- [Ba/Fe] and [La/Fe] values rise steeply with increasing metallicity, with [Ba/Fe] reaching much higher levels than in our Galaxy. Conversely, [Y/Fe] remains constant. The high [Ba/Y] can be explained by a attriburing an important contribution to low metallicity AGBs. This also implies that the high [Eu/α] is not only a consequence of the low abundance in α elements but is also linked to the strong influence of AGBs at [Fe/H]<-1, which increases the abundance of Eu.

Acknowledgements. This work was made possible by a grant from NWO (614.031.018). BL and ET thank Paris Observatory for hospitality and the Programme National Galaxies financial support. We thank Marco Gullieuszik and Enrico Held for sending us in advance of publication their IR photometry for stars in our sample. MS thanks the National Science Foundation for support under AST-0306884. E.T. gratefully acknowledges support from an NWO-VICI grant.

References

Aaronson, M. & Mould, J. 1980, ApJ, 240, 804
Alonso, A., Arribas, S., & Martínez-Roger, C. 1999, A&AS, 139, 335
Anders, E. & Grevesse, N. 1989, Geochim. Cosmochim. Acta, 53, 197
Andrievsky, S. M., Spite, M., Korotin, S. A., et al. 2009, A&A, 494, 1083
Aoki, W., Ryan, S. G., Iwamoto, N., et al. 2003, ApJ, 592, L67

Azzopardi, M., Muratorio, G., Breysacher, J., & Westerlund, B. E. 1999, in IAU Symposium, Vol. 192, The Stellar Content of Local Group Galaxies, ed. P. Whitelock & R. Cannon, 144–+
Barklem, P. S., Christlieb, N., Beers, T. C., et al. 2005, A&A, 439, 129
Battaglia, G. 2007, PhD thesis, University of Groningen
Battaglia, G., Helmi, A., Tolstoy, E., et al. 2008a, ApJ, 681, L13
Battaglia, G., Irwin, M., Tolstoy, E., et al. 2008b, MNRAS, 383, 183
Battaglia, G., Tolstoy, E., Helmi, A., et al. 2006, A&A, 459, 423 (B06)
Bersier, D. 2000, ApJ, 543, L23
Bersier, D. & Wood, P. R. 2002, AJ, 123, 840
Bonifacio, P., Sbordone, L., Marconi, G., Pasquini, L., & Hill, V. 2004, A&A, 414, 503
Buonanno, R., Corsi, C. E., Zinn, R., et al. 1998, ApJ, 501, L33+
Burris, D. L., Pilachowski, C. A., Armandroff, T. E., et al. 2000, ApJ, 544, 302
Cayrel, R., Depagne, E., Spite, M., et al. 2004, A&A, 416, 1117
Cescutti, G., François, P., Matteucci, F., Cayrel, R., & Spite, M. 2006, A&A, 448, 557
Clayton, D. D. 1983, Principles of stellar evolution and nucleosynthesis (Chicago: University of Chicago Press, 1983)
Clayton, D. D., Fowler, W. A., Hull, T. E., & Zimmerman, B. A. 1961, Annals of Physics, 12, 331
Cohen, J. G., Christlieb, N., McWilliam, A., et al. 2004, ApJ, 612, 1107
Cohen, J. G. & Huang, W. 2009, ApJ, 701, 1053
Coleman, M., Da Costa, G. S., Bland-Hawthorn, J., et al. 2004, AJ, 127, 832
Coleman, M. G. & Da Costa, G. S. 2005, Publications of the Astronomical Society of Australia, 22, 162
Coleman, M. G. & de Jong, J. T. A. 2008, ApJ, 685, 933
Cristallo, S., Straniero, O., Gallino, R., et al. 2009, ApJ, 696, 797
Farouqi, K., Kratz, K.-L., Mashonkina, L. I., et al. 2009, ApJ, 694, L49
François, P., Depagne, E., Hill, V., et al. 2007, A&A, 476, 935
Fulbright, J. P. 2002, AJ, 123, 404
Fulbright, J. P., McWilliam, A., & Rich, R. M. 2007, ApJ, 661, 1152
Gallart, C., Aparicio, A., Zinn, R., et al. 2005, in IAU Colloq. 198: Near-fields cosmology with dwarf elliptical galaxies, ed. H. Jerjen & B. Binggeli, 25–29
Gilmore, G. & Wyse, R. F. G. 1991, ApJ, 367, L55
Girardi, L., Bertelli, G., Bressan, A., et al. 2002, A&A, 391, 195
Gratton, R. G., Carretta, E., Claudi, R., Lucatello, S., & Barbieri, M. 2003, A&A, 404, 187
Grevesse, N. & Sauval, A. J. 1998, Space Science Reviews, 85, 161
Gullieuszik, M., Held, E. V., Rizzi, L., et al. 2007, A&A, 467, 1025
Gustafsson, B., Bell, R. A., Eriksson, K., & Nordlund, A. 1975, A&A, 42, 407
Gustafsson, B., Edvardsson, B., Eriksson, K., et al. 2008, A&A, 486, 951
Gustafsson, B., Edvardsson, B., Eriksson, K., et al. 2003, in ASP Conf. Ser. 288: Stellar Atmosphere Modeling, ed. I. Hubeny, D. Mihalas, & K. Werner, 331–+
Heiter, U. & Eriksson, K. 2006, A&A, 452, 1039
Hill, V., François, P., Spite, M., Primas, F., & Spite, F. 2000, A&A, 364, L19
Hodge, P. W. 1961, AJ, 66, 83
Hurley-Keller, D., Mateo, M., & Nemec, J. 1998, AJ, 115, 1840
Iwamoto, K., Brachwitz, F., Nomoto, K., et al. 1999, ApJS, 125, 439
Johnson, J. A. 2002, ApJS, 139, 219
Kappeler, F., Beer, H., & Wisshak, K. 1989, Reports of Progress in Physics, 52, 945
Kim, Y.-C., Demarque, P., Yi, S. K., & Alexander, D. R. 2002, ApJS, 143, 499
Kirby, E. N., Simon, J. D., Geha, M., Guhathakurta, P., & Frebel, A. 2008, ApJ, 685, L43
Koch, A., Grebel, E. K., Gilmore, G. F., et al. 2008, AJ, 135, 1580
Lanfranchi, G. A. & Matteucci, F. 2004, MNRAS, 351, 1338
Letarte, B., Hill, V., Jablonka, P., et al. 2006, A&A, 453, 547
Mateo, M. L. 1998, ARA&A, 36, 435
Mathews, G. J., Bazan, G., & Cowan, J. J. 1992, ApJ, 391, 719
Matteucci, F. & Brocato, E. 1990, ApJ, 365, 539
McWilliam, A., Preston, G. W., Sneden, C., & Searle, L. 1995, AJ, 109, 2757
McWilliam, A. & Smecker-Hane, T. A. 2005, in Astronomical Society of the Pacific Conference Series, Vol. 336, Cosmic Abundances as Records of Stellar Evolution and Nucleosynthesis, ed. T. G. Barnes, III & F. N. Bash, 221–+
Monaco, L., Bellazzini, M., Bonifacio, P., et al. 2005, A&A, 441, 141
Nissen, P. E. & Schuster, W. J. 1997, A&A, 326, 751 (NS97)
Nissen, P. E. & Schuster, W. J. 2009, in IAU Symposium, Vol. 254, IAU Symposium, ed. J. Andersen, J. Bland-Hawthorn, & B. Nordström, 103–108
Olszewski, E. W., Mateo, M., Harris, J., et al. 2006, AJ, 131, 912
Pasquini, L., Avila, G., Blecha, A., et al. 2002, The Messenger, 110, 1
Plez, B. 1992, A&AS, 94, 527
Plez, B., Brett, J. M., & Nordlund, A. 1992, A&A, 256, 551
Pompéia, L., Hill, V., Spite, M., et al. 2008, A&A, 480, 379
Pont, F., Zinn, R., Gallart, C., Hardy, E., & Winnick, R. 2004, AJ, 127, 840
Poretti, E., Clementini, G., Held, E. V., et al. 2008, ApJ, 685, 947
Qian, Y.-Z. & Wasserburg, G. J. 2007, Phys. Rep., 442, 237
Ramírez, I. & Meléndez, J. 2005, ApJ, 626, 465
Reddy, B. E., Lambert, D. L., & Allende Prieto, C. 2006, MNRAS, 367, 1329
Reddy, B. E., Tomkin, J., Lambert, D. L., & Allende Prieto, C. 2003, MNRAS, 340, 304
Revaz, Y., Jablonka, P., Sawala, T., et al. 2009, A&A, 501, 189
Rizzi, L., Held, E. V., Saviane, I., Tully, R. B., & Gullieuszik, M. 2007, MNRAS, 380, 1255
Röpke, F. K., Gieseler, M., Reinecke, M., Travaglio, C., & Hillebrandt, W. 2006, A&A, 453, 203
Saviane, I., Held, E. V., & Bertelli, G. 2000, A&A, 355, 56
Sbordone, L., Bonifacio, P., Buonanno, R., et al. 2007, A&A, 465, 815
Seeger, P. A., Fowler, W. A., & Clayton, D. D. 1965, ApJS, 11, 121
Shetrone, M., Venn, K. A., Tolstoy, E., et al. 2003, AJ, 125, 684 (S03)
Shetrone, M. D. 2004, in Origin and Evolution of the Elements, ed. A. McWilliam & M. Rauch, 218–+
Shetrone, M. D., Siegel, M. H., Cook, D. O., & Bosler, T. 2009, AJ, 137, 62
Simmerer, J., Sneden, C., Cowan, J. J., et al. 2004, ApJ, 617, 1091
Smecker-Hane, T. A., Stetson, P. B., Hesser, J. E., & Vandenberg, D. A. 1996, in Astronomical Society of the Pacific Conference Series, Vol. 98, From Stars to Galaxies: the Impact of Stellar Physics on Galaxy Evolution, ed. C. Leitherer, U. Fritze-von-Alvensleben, & J. Huchra, 328–+
Sneden, C., Cowan, J. J., & Gallino, R. 2008, ARA&A, 46, 241
Spite, M. 1967, Annales d'Astrophysique, 30, 211
Stetson, P. B., Hesser, J. E., & Smecker-Hane, T. A. 1998, PASP, 110, 533
Stetson, P. B. & Pancino, E. 2008, PASP, 120, 1332
Strader, J., Brodie, J. P., Forbes, D. A., Beasley, M. A., & Huchra, J. P. 2003, AJ, 125, 1291
Thielemann, F.-K., Hashimoto, M.-A., & Nomoto, K. 1990, ApJ, 349, 222
Timmes, F. X., Brown, E. F., & Truran, J. W. 2003, ApJ, 590, L83
Timmes, F. X., Woosley, S. E., & Weaver, T. A. 1995, ApJS, 98, 617
Tinsley, B. M. 1979, ApJ, 229, 1046
Tolstoy, E., Hill, V., Irwin, M., et al. 2006, The Messenger, 123, 33
Tolstoy, E., Hill, V., & Tosi, M. 2009, ARA&A, 47, 371
Tolstoy, E., Irwin, M. J., Cole, A. A., et al. 2001, MNRAS, 327, 918
Tolstoy, E., Irwin, M. J., Helmi, A., et al. 2004, ApJ, 617, L119
Tolstoy, E., Venn, K. A., Shetrone, M., et al. 2003, AJ, 125, 707
Travaglio, C., Galli, D., Gallino, R., et al. 1999, ApJ, 521, 691
Travaglio, C., Gallino, R., Arnone, E., et al. 2004, ApJ, 601, 864
Travaglio, C., Hillebrandt, W., & Reinecke, M. 2005, A&A, 443, 1007
Tsujimoto, T., Nomoto, K., Yoshii, Y., et al. 1995, MNRAS, 277, 945
Venn, K. A., Irwin, M., Shetrone, M. D., et al. 2004, AJ, 128, 1177
Walker, M. G., Mateo, M., & Olszewski, E. W. 2009, AJ, 137, 3100
Walker, M. G., Mateo, M., Olszewski, E. W., et al. 2007, ApJ, 667, L53
Wanajo, S., Tamamura, M., Itoh, N., et al. 2003, ApJ, 593, 968
Woosley, S. E., Wilson, J. R., Mathews, G. J., Hoffman, R. D., & Meyer, B. S. 1994, ApJ, 433, 229
Yi, S., Demarque, P., Kim, Y.-C., et al. 2001, ApJS, 136, 417
Young, L. M. 1999, AJ, 117, 1758
Zoccali, M., Barbuy, B., Hill, V., et al. 2004, A&A, 423, 507

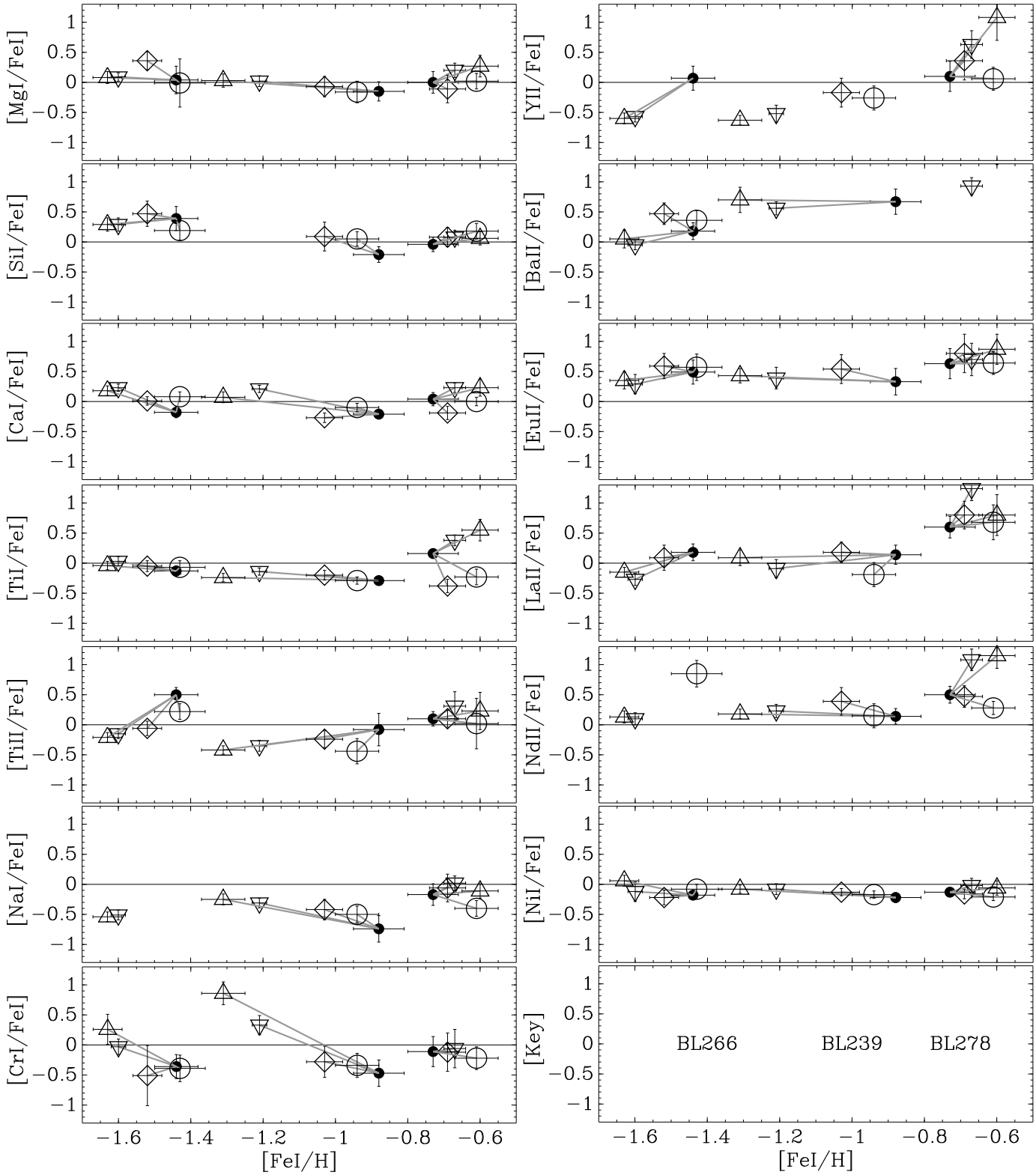

Fig. 8. To check the effect of systmeatics in our analysis the abundance ratios for the 3 stars observed with both UVES (S03) and GIRAFFE (this work) are shown here for the 5 different checks discussed in section 3.7. To see which star is which, see the bottom right-hand panel. The GIRAFFE data points are shown as filled circles with lines joining each different check for the same star. The UVES abundances are shown as open symbols. Check 1 results are shown as inverted triangles; Check 2 as triangles; Check 3 as diamonds; Check 4 as circles and Check 5 as small filled dots.

Table A.1. $V_{\rm rad}$ and associated errors for our Fornax targets. **BOLD** is a probable foreground star, since it falls outside the range of $V_{\rm rad}$ for membership in Fornax (see Figure 4). ~~Struck-out~~ stars have been rejected because their September average velocity was significantly different (>3 km/s) to their January velocity. This suggests the possibility that they are binary stars and they were therefore rejected from further analysis.

Star	$V_{\rm rad}$	Stddev	Star	$V_{\rm rad}$	Stddev	Star	$V_{\rm rad}$	Stddev
BL038	62.86	0.74	BL147	52.39	0.61	BL221	54.25	0.32
BL045	79.54	0.23	BL148	65.48	0.65	BL227	52.15	0.67
BL052	30.32	1.25	BL149	50.70	0.40	BL228	55.00	0.34
BL061	82.38	1.12	BL150	68.70	1.12	BL229	63.09	0.57
BL065	63.86	0.78	BL151	41.41	0.58	BL231	63.28	1.11
~~BL069~~	~~68.85~~	~~2.63~~	BL153	50.68	0.53	BL233	58.91	0.40
~~BL070~~	~~60.43~~	~~2.85~~	BL155	46.18	0.21	BL239	47.47	0.35
BL076	52.83	0.78	BL156	30.63	0.55	BL242	39.48	0.55
BL077	56.23	1.49	BL158	41.26	0.67	BL247	40.40	0.63
BL079	56.31	0.56	BL160	53.50	0.70	BL249	63.30	0.73
BL081	50.58	0.22	BL163	41.29	0.48	BL250	42.06	0.36
BL084	58.92	0.80	BL165	70.01	0.71	BL251	55.14	0.45
BL085	88.97	1.17	BL166	57.36	0.51	BL253	67.48	0.39
BL091	52.79	0.44	BL168	75.50	0.78	BL254	73.05	0.26
BL092	53.99	0.37	BL171	58.27	1.19	BL257	56.51	0.36
BL094	47.45	0.43	BL173	44.93	1.60	BL258	49.41	0.79
BL096	72.90	0.37	BL180	72.51	0.21	BL260	61.11	0.70
BL097	47.47	0.18	~~BL181~~	~~57.46~~	~~1.89~~	BL261	71.35	1.27
BL100	55.92	0.46	BL183	19.09	0.32	BL262	47.72	0.52
BL104	51.36	0.31	BL185	55.32	0.44	BL266	52.47	1.43
BL107	63.97	0.42	BL189	82.78	0.47	BL267	59.04	0.48
BL109	**-15.20**	**0.42**	BL190	57.31	0.24	BL269	45.33	0.30
~~BL112~~	~~53.90~~	~~2.36~~	BL195	39.03	0.46	~~BL273~~	~~63.77~~	~~6.18~~
BL113	59.21	0.31	BL196	79.09	0.25	~~BL274~~	~~41.22~~	~~1.65~~
BL115	70.05	0.30	BL197	46.27	1.02	BL278	52.43	0.56
~~BL119~~	~~56.25~~	~~1.95~~	~~BL198~~	~~45.06~~	~~11.29~~	BL279	67.66	0.73
BL122	65.88	0.75	BL203	56.40	0.92	BL293	56.83	0.99
BL123	73.85	0.71	BL204	59.30	0.81	BL295	42.56	0.37
BL125	58.23	0.77	BL205	59.91	0.27	BL298	62.09	1.43
BL127	46.60	0.67	BL207	48.82	0.42	BL300	69.67	0.41
BL132	40.34	0.48	BL208	54.35	0.53	BL304	71.21	0.26
BL135	45.64	0.57	BL210	51.51	0.32	BL311	50.86	0.23
BL138	56.52	0.33	BL211	50.35	0.20	BL315	53.15	0.85
BL140	46.13	0.69	BL213	71.82	0.45	BL323	52.72	1.15
BL141	76.47	0.35	BL216	66.92	0.26	BL325	18.70	0.80
BL146	50.01	0.61	BL218	63.33	0.46			

Table A.2. Stellar parameters of the model used for our sample of 81 stars, along with the minimum EW used for each star.

Star	$T_{\rm eff}$	$\log g$	[Fe/H]	$v_{\rm t}$	$EW_{\rm min}$	Star	$T_{\rm eff}$	$\log g$	[Fe/H]	$v_{\rm t}$	$EW_{\rm min}$	Star	$T_{\rm eff}$	$\log g$	[Fe/H]	$v_{\rm t}$	$EW_{\rm min}$
BL038	3980	0.69	-0.88	2.2	14.24	BL148	4123	0.72	-0.63	2.2	20.62	BL218	3939	0.67	-0.60	2.0	16.17
BL045	4122	0.85	-1.09	2.1	12.15	BL149	4100	0.88	-0.91	2.2	14.30	BL221	4056	0.81	-0.86	2.1	13.80
BL052	3997	0.72	-1.02	2.4	14.24	BL150	4025	0.80	-0.83	2.2	15.29	BL227	4046	0.84	-0.91	2.0	15.40
BL065	4330	0.97	-1.43	1.9	11.33	BL151	4024	0.81	-0.86	2.1	13.37	BL228	3992	0.71	-0.88	2.3	13.31
BL076	4065	0.83	-0.85	2.2	13.04	BL155	4060	0.90	-0.75	2.3	17.21	BL229	4014	0.80	-0.71	2.3	15.73
BL077	4026	0.80	-0.79	2.2	12.71	BL156	4099	0.89	-1.13	2.2	13.48	BL233	4048	0.83	-0.68	2.2	14.52
BL079	4036	0.76	-0.52	2.1	17.98	BL158	4078	0.87	-0.87	2.0	15.79	BL239	4123	0.68	-0.91	2.1	13.80
BL081	4062	0.82	-0.62	2.1	14.08	BL160	4027	0.66	-0.95	2.2	14.30	BL242	4063	0.58	-1.11	2.1	12.98
BL084	3968	0.60	-0.85	2.1	12.10	BL163	4124	0.73	-0.77	2.3	15.62	BL247	4032	0.85	-0.82	2.3	18.64
BL085	4291	0.73	-2.59	2.2	9.18	BL166	4086	0.84	-0.89	2.3	14.24	BL250	4044	0.65	-0.68	2.2	19.14
BL091	4162	0.86	-0.96	2.1	11.99	BL168	4113	0.83	-0.88	2.1	15.40	BL253	4003	0.58	-0.73	2.3	14.46
BL092	3961	0.74	-0.95	2.0	15.23	BL171	4048	0.87	-0.90	2.4	15.79	BL257	3994	0.78	-0.58	2.3	16.77
BL096	4010	0.75	-0.75	2.1	17.98	BL173	3988	0.57	-0.85	2.3	17.77	BL258	4030	0.68	-0.60	2.2	16.88
BL097	4060	0.82	-0.92	2.3	12.98	BL180	4114	0.77	-0.91	2.2	13.09	BL260	4009	0.75	-0.87	2.4	14.90
BL100	4044	0.84	-0.93	2.1	12.04	BL185	4098	0.69	-0.71	2.1	15.84	BL261	4146	0.57	-0.86	2.0	16.99
BL104	4013	0.77	-0.96	2.2	13.37	BL190	3979	0.82	-0.79	2.3	13.37	BL262	4230	0.84	-0.78	2.1	15.68
BL113	4187	0.83	-0.75	2.2	13.91	BL195	4261	0.91	-0.97	2.1	11.99	BL266	4212	0.83	-1.44	2.0	12.10
BL115	4116	0.63	-1.47	2.0	11.77	BL196	4015	0.59	-1.07	2.4	11.93	BL267	4201	0.80	-0.72	2.1	15.62
BL123	3993	0.71	-0.97	2.3	11.66	BL197	3956	0.68	-0.89	2.2	14.19	BL269	3990	0.75	-0.81	2.0	13.86
BL125	4080	0.79	-0.73	2.1	13.64	BL203	4037	0.79	-0.83	2.1	15.07	BL278	4072	0.64	-0.73	2.3	15.51
BL132	3909	0.52	-0.89	2.1	13.75	BL204	4139	0.97	-1.00	2.4	17.54	BL279	4272	0.95	-1.51	1.6	13.31
BL135	4058	0.83	-0.95	2.2	16.28	BL205	4243	0.96	-0.69	2.2	14.13	BL295	3980	0.70	-0.69	2.3	17.38
BL138	3939	0.71	-1.01	2.3	14.85	BL208	4159	0.89	-0.66	2.1	13.59	BL300	3990	0.71	-0.92	2.2	15.68
BL140	3992	0.75	-0.87	2.1	14.52	BL210	4062	0.81	-0.76	2.2	15.62	BL304	3950	0.46	-0.96	2.3	14.41
BL141	4078	0.84	-0.82	2.1	13.64	BL211	4058	0.69	-0.67	2.1	14.13	BL311	4027	0.79	-0.78	2.2	16.94
BL146	4076	0.84	-0.92	2.3	12.98	BL213	4032	0.53	-0.93	2.2	13.53	BL315	4139	0.86	-0.82	1.8	16.72
BL147	4194	0.94	-1.37	1.8	12.21	BL216	3998	0.55	-0.77	2.2	14.08	BL323	3881	0.53	-0.91	2.3	14.46

Table A.3. Coordinates and photometric temperatures in different colours, shifted on the $T_{\rm eff}(V-I)$ scale. $T_{\rm eff}$ is the average of the four different T_{V-X}, BC_V the bolometric correction and $M_{\rm Bol}$ the bolometric magnitude.

Star	RA (J2000)	DEC (J2000)	T_{V-I}	T_{V-J}	T_{V-H}	T_{V-K}	$T_{\rm eff}$	$\log g$	BC_V	$M_{\rm Bol}$
BL038	02 40 20.45	–34 24 00.1	3984	3976	3996	3964	3980	0.69	–0.93	–3.32
BL045	02 40 07.52	–34 23 31.8	4114	4134	4128	4110	4122	0.85	–0.77	–3.07
BL052	02 40 10.42	–34 25 17.6	4009	3999	3995	3984	3997	0.72	–0.91	–3.27
BL061	02 39 28.59	–34 18 38.0	4316	4341	4335	4333	4331	0.84	–0.60	–3.30
BL065	02 39 22.15	–34 19 40.3	4315	4340	4334	4332	4330	0.97	–0.59	–2.99
BL069	02 39 29.56	–34 25 10.6	4143	3999	4033	3994	4042	0.72	–0.86	–3.29
BL070	02 39 40.46	–34 19 38.8	3939	3928	3931	3935	3933	0.68	–1.00	–3.29
BL076	02 39 31.49	–34 23 05.1	4088	4061	4063	4048	4065	0.83	–0.83	–3.05
BL077	02 39 51.42	–34 21 20.9	4027	4024	4025	4028	4026	0.80	–0.88	–3.08
BL079	02 39 19.60	–34 24 49.3	3986	3903	3922	3934	3936	0.76	–1.01	–3.08
BL081	02 39 56.01	–34 24 10.5	4102	4045	4060	4042	4062	0.82	–0.84	–3.07
BL084	02 38 42.96	–34 25 49.1	3972	3964	3966	3970	3968	0.72	–0.95	–3.23
BL085	02 38 55.53	–34 25 36.3	4277	4299	4294	4293	4291	0.87	–0.63	–3.19
BL091	02 39 04.31	–34 25 18.8	4155	4165	4163	4164	4162	0.86	–0.73	–3.09
BL092	02 38 49.28	–34 24 04.9	3965	3956	3959	3963	3961	0.74	–0.96	–3.16
BL093	02 38 39.87	–34 25 57.1	4068	4070	4070	4072	4070	0.90	–0.82	–2.87
BL094	02 38 53.89	–34 25 06.7	3990	3984	3985	3989	3987	0.72	–0.92	–3.24
BL096	02 39 14.33	–34 22 41.5	4012	4008	4009	4013	4010	0.75	–0.90	–3.19
BL097	02 39 04.07	–34 23 52.7	4058	4059	4059	4062	4060	0.82	–0.84	–3.06
BL100	02 38 56.00	–34 24 44.8	4043	4042	4043	4046	4044	0.84	–0.86	–3.01
BL104	02 39 14.59	–34 23 21.0	4014	4011	4012	4015	4013	0.77	–0.89	–3.15
BL107	02 38 54.37	–34 31 23.5	4366	4396	4389	4387	4384	0.83	–0.56	–3.37
BL109	02 39 04.08	–34 37 58.7	4334	4360	4354	4352	4350	0.93	–0.58	–3.09
BL112	02 38 45.68	–34 34 47.5	4096	4100	4099	4101	4099	0.76	–0.79	–3.27
BL113	02 39 08.16	–34 36 53.3	4179	4191	4188	4189	4187	0.83	–0.72	–3.19
BL115	02 38 43.45	–34 32 05.3	4112	4117	4116	4118	4116	0.79	–0.77	–3.22
BL119	02 38 42.17	–34 29 50.8	3964	3956	3959	3963	3960	0.73	–0.96	–3.19
BL122	02 39 02.91	–34 31 12.0	4051	4051	4052	4054	4052	0.76	–0.84	–3.22
BL123	02 38 53.75	–34 30 06.6	3995	3990	3991	3995	3993	0.71	–0.92	–3.27
BL125	02 39 08.50	–34 30 55.4	4078	4080	4080	4082	4080	0.79	–0.82	–3.17
BL127	02 39 04.00	–34 37 26.1	3963	3955	3957	3961	3959	0.71	–0.96	–3.25
BL132	02 38 53.62	–34 33 04.5	3916	3903	3906	3911	3909	0.65	–1.04	–3.33
BL135	02 39 01.55	–34 36 48.7	4057	4058	4058	4061	4058	0.83	–0.84	–3.06
BL138	02 39 16.20	–34 37 00.2	3989	3906	3924	3937	3939	0.71	–0.99	–3.21
BL140	02 39 11.56	–34 30 44.7	3995	3989	3991	3994	3992	0.75	–0.92	–3.17
BL141	02 39 10.99	–34 28 34.4	4076	4078	4078	4080	4078	0.84	–0.82	–3.04
BL146	02 38 41.76	–34 28 58.4	4074	4076	4076	4078	4076	0.84	–0.82	–3.04
BL147	02 38 44.02	–34 30 51.8	4186	4199	4196	4197	4194	0.94	–0.70	–2.92
BL148	02 39 11.05	–34 39 08.6	3929	3917	3920	3925	3923	0.72	–1.03	–3.16
BL149	02 38 57.19	–34 35 39.8	4097	4101	4100	4102	4100	0.88	–0.80	–2.97
BL150	02 39 13.94	–34 28 36.1	4026	4023	4024	4027	4025	0.80	–0.88	–3.08
BL151	02 39 00.29	–34 30 30.0	4025	4022	4023	4026	4024	0.81	–0.88	–3.06
BL153	02 39 08.35	–34 32 44.8	4035	4033	4034	4037	4035	0.82	–0.86	–3.04
BL155	02 38 40.44	–34 35 25.0	4059	4060	4060	4063	4060	0.90	–0.84	–2.87
BL156	02 39 05.62	–34 26 30.6	4096	4100	4099	4101	4099	0.89	–0.79	–2.95
BL157	02 39 02.44	–34 27 35.4	4073	4075	4075	4077	4075	0.88	–0.82	–2.93
BL158	02 39 06.84	–34 35 45.7	4076	4079	4078	4081	4078	0.87	–0.82	–2.96
BL160	02 39 01.74	–34 27 19.2	4027	4025	4026	4029	4027	0.84	–0.88	–3.00
BL163	02 38 43.54	–34 32 25.4	4025	4022	4023	4026	4024	0.88	–0.88	–2.89
BL165	02 39 13.37	–34 40 15.8	3967	3959	3961	3965	3963	0.77	–0.95	–3.08
BL166	02 39 16.01	–34 30 12.9	4070	4091	4074	4108	4086	0.84	–0.81	–3.06
BL168	02 39 14.78	–34 27 29.8	4014	4011	4012	4015	4013	0.83	–0.89	–3.00
BL171	02 39 15.48	–34 30 46.5	4047	4047	4047	4050	4048	0.87	–0.85	–2.94
BL173	02 39 14.36	–34 34 42.3	3991	3985	3987	3990	3988	0.85	–0.93	–2.92
BL180	02 39 33.38	–34 33 58.4	4115	4102	4107	4134	4114	0.77	–0.78	–3.25
BL181	02 39 16.76	–34 34 49.9	4016	3962	3969	3969	3979	0.80	–0.93	–3.04
BL183	02 39 47.94	–34 26 43.4	4073	4199	4223	4230	4181	0.83	–0.72	–3.16
BL185	02 39 27.67	–34 37 48.5	4026	3980	3999	3988	3998	0.69	–0.92	–3.32
BL189	02 39 38.24	–34 31 20.3	4167	4222	4272	4274	4234	0.91	–0.67	–3.03

Continued on next page

Star	RA (J2000)	DEC (J2000)	T_{V-I}	T_{V-J}	T_{V-H}	T_{V-K}	$T_{\rm eff}$	$\log g$	BC_V	$M_{\rm Bol}$
BL190	02 39 17.80	–34 30 56.8	4004	3954	3967	3990	3979	0.82	–0.94	–2.99
BL195	02 39 20.21	–34 31 57.0	4153	4153	4147	4191	4161	0.91	–0.73	–2.95
BL196	02 39 34.07	–34 33 33.2	4011	4010	4010	4029	4015	0.76	–0.89	–3.17
BL197	02 39 29.33	–34 26 35.5	3958	3953	3963	3948	3956	0.68	–0.97	–3.30
BL198	02 39 19.83	–34 26 27.1	4077	3988	4000	3992	4014	0.78	–0.89	–3.11
BL203	02 39 50.64	–34 26 47.0	4043	4035	4046	4025	4037	0.79	–0.87	–3.13
BL204	02 39 16.23	–34 32 29.9	4076	4184	4161	4134	4139	0.97	–0.75	–2.78
BL205	02 39 38.06	–34 37 06.2	4229	4237	4263	4244	4243	0.96	–0.67	–2.92
BL207	02 39 26.29	–34 29 03.4	3988	3979	3977	3992	3984	0.74	–0.93	–3.19
BL208	02 39 32.94	–34 32 06.2	4140	4166	4161	4170	4159	0.89	–0.74	–3.00
BL210	02 39 47.65	–34 27 05.4	4057	4064	4072	4057	4062	0.81	–0.84	–3.10
BL211	02 39 51.18	–34 29 58.6	3940	3961	3964	3966	3958	0.69	–0.97	–3.28
BL213	02 39 50.18	–34 35 59.3	4039	4045	4017	4025	4032	0.78	–0.87	–3.14
BL216	02 39 41.92	–34 30 35.9	3970	4008	3995	4019	3998	0.75	–0.92	–3.18
BL218	02 39 50.77	–34 28 36.5	3920	3943	3941	3953	3939	0.67	–1.00	–3.31
BL221	02 39 31.85	–34 29 19.9	4051	4051	4057	4064	4056	0.81	–0.84	–3.08
BL227	02 39 45.25	–34 31 57.8	4020	4064	4043	4055	4046	0.84	–0.85	–3.01
BL228	02 39 53.84	–34 29 56.4	3975	3998	3990	4007	3992	0.71	–0.92	–3.28
BL229	02 39 24.80	–34 34 38.1	4022	4008	4012	4013	4014	0.80	–0.90	–3.07
BL231	02 39 18.96	–34 26 43.9	4087	4033	4040	4052	4053	0.86	–0.84	–2.96
BL233	02 39 53.58	–34 37 50.1	4064	4028	4039	4063	4048	0.83	–0.86	–3.03
BL239	02 39 47.09	–34 31 49.8	4083	4145	4127	4137	4123	0.89	–0.77	–2.96
BL242	02 39 28.03	–34 34 01.2	4064	4058	4057	4074	4063	0.85	–0.83	–3.00
BL247	02 39 43.07	–34 40 18.4	4050	4031	4018	4027	4032	0.85	–0.87	–2.98
BL249	02 39 54.24	–34 35 11.2	4032	4034	4009	4019	4024	0.82	–0.88	–3.03
BL250	02 39 45.03	–34 40 11.1	3866	3829	3849	3833	3844	0.65	–1.16	–3.27
BL251	02 39 30.81	–34 35 45.1	3998	3970	3977	3985	3982	0.81	–0.93	–3.00
BL253	02 39 34.08	–34 33 09.6	3989	3995	4006	4022	4003	0.82	–0.91	–3.02
BL254	02 39 41.78	–34 34 16.4	4025	4013	3990	4017	4011	0.83	–0.89	–3.01
BL257	02 39 57.30	–34 31 20.8	3981	3984	3994	4015	3994	0.78	–0.93	–3.10
BL258	02 39 49.68	–34 28 50.4	4008	4045	4026	4039	4030	0.85	–0.88	–2.96
BL260	02 39 55.38	–34 29 54.6	3985	4026	4016	4010	4009	0.79	–0.90	–3.09
BL261	02 39 57.80	–34 26 48.8	4028	4053	4066	4039	4046	0.82	–0.86	–3.06
BL262	02 39 38.42	–34 26 10.3	4054	4021	4027	4018	4030	0.84	–0.88	–2.98
BL266	02 40 10.00	–34 29 58.8	4157	4241	4225	4223	4212	0.83	–0.68	–3.20
BL267	02 40 17.50	–34 26 06.1	4197	4210	4211	4186	4201	0.80	–0.70	–3.27
BL269	02 39 58.20	–34 32 05.3	3965	3992	4008	3997	3990	0.75	–0.92	–3.18
BL273	02 40 09.37	–34 36 17.1	4123	4158	4124	4149	4138	0.81	–0.76	–3.18
BL274	02 40 06.14	–34 28 52.0	4011	4041	4032	4019	4026	0.72	–0.87	–3.29
BL278	02 40 04.38	–34 27 11.3	3964	3967	3977	3980	3972	0.64	–0.95	–3.43
BL279	02 40 02.70	–34 38 29.9	4228	4298	4274	4286	4272	0.95	–0.64	–2.97
BL293	02 40 01.77	–34 27 47.9	4030	4031	4024	4026	4028	0.72	–0.87	–3.29
BL295	02 40 26.72	–34 26 56.8	3994	3976	3975	3975	3980	0.70	–0.94	–3.28
BL298	02 40 13.49	–34 30 02.0	4118	4145	4129	4125	4129	0.85	–0.76	–3.07
BL300	02 40 17.90	–34 27 00.7	3989	3991	4001	3977	3990	0.71	–0.92	–3.27
BL304	02 40 05.49	–34 32 42.7	3959	3936	3941	3965	3950	0.70	–0.97	–3.26
BL311	02 40 22.64	–34 31 31.0	4032	4022	4022	4032	4027	0.79	–0.88	–3.12
BL315	02 40 24.22	–34 26 20.0	4173	4135	4115	4133	4139	0.86	–0.76	–3.06
BL323	02 40 16.76	–34 29 34.4	3897	3859	3881	3887	3881	0.66	–1.08	–3.28
BL325	02 40 27.00	–34 26 44.1	4082	4064	4036	4050	4058	0.81	–0.84	–3.09

Table A.4. List of all the lines, their associated parameters and their measured equivalent width (EWs in mÅ, measured by DAOSPEC) for all our Fornax stars. Part 1/5.

				Equivalent witdh, one star per column, BLxxx															
λ(Å)	elem	χ	gf	038	045	052	065	076	077	079	081	084	085	091	092	096	097	100	104
6154.23	Na I	2.10	-1.56	38.8	...	...	...	23.5	...	35.7	36.3	...	...	25.6	15.5	23.4	19.8	...	...
6160.75	Na I	2.10	-1.26	58.4	...	23.3	...	38.2	38.6	65.5	54.5	...	...	38.5	21.1	47.6	39.7	...	28.5
5528.41	Mg I	4.35	-0.36	221.1	195.6	212.0	165.9	207.0	200.9	253.7	208.8	217.3	112.8	203.8	210.0	220.0	234.8	198.8	219.0
6318.72	Mg I	5.11	-1.97	43.6	...	...	...	34.9	24.6	...	...	...	...	31.1	38.9	52.2	...	17.7	34.0
6319.24	Mg I	5.11	-2.21	...	27.0	26.9	...	...	23.3	36.2	24.9	...	...	...	30.6	42.1	...	31.8	...
6319.49	Mg I	5.11	-2.43	...	...	...	...	...	...	...	...	...	...	...	...	...	...	...	...
6125.03	Si I	5.62	-1.57	25.0	24.7	...	18.3	...	...	...	...	...	...	22.4	...	...	...	...	34.2
6142.48	Si I	5.62	-1.51	...	...	...	...	...	...	...	...	...	...	...	...	...	...	...	...
6145.02	Si I	5.61	-1.37	45.1	...	...	...	16.0	...	...	...	...	...	...	22.0	...	...	...	15.2
6155.14	Si I	5.62	-0.80	42.5	38.5	...	32.4	35.6	39.2	57.8	31.5	27.3	17.0	35.0	25.7	48.1	38.3	23.9	40.1
6237.33	Si I	5.61	-1.02	26.6	...	...	...	...	...	34.7	...	...	...	21.3	25.5	26.1	24.6	...	...
6243.82	Si I	5.61	-1.27	...	...	23.2	...	22.8	24.1	...	...	28.2	...	...	24.1	...	33.2	...	...
6122.23	Ca I	1.89	-0.32	243.6	219.3	218.2	176.0	242.1	237.9	277.5	265.2	239.3	116.5	214.9	...	261.2	...	213.9	236.9
6156.03	Ca I	2.52	-2.39	37.9	...	23.5	...	28.3	19.7	52.0	27.6	17.0	...	...	24.2	36.5	25.5	...	22.9
6161.30	Ca I	2.52	-1.27	144.3	97.1	106.5	44.0	112.7	121.4	167.2	142.5	130.2	17.2	119.5	117.6	141.9	123.9	103.5	131.9
6162.17	Ca I	1.90	-0.32	271.8	248.2	249.9	200.2	266.1	252.9	295.7	293.0	260.4	135.6	243.2	262.4	284.8	267.7	235.3	260.8
6166.44	Ca I	2.52	-1.14	141.2	97.5	107.2	51.6	126.1	114.7	134.7	132.2	122.5	...	105.6	121.1	123.3	119.1	99.9	122.5
6169.04	Ca I	2.52	-0.80	125.4	121.0	120.8	91.9	146.0	143.9	128.0	151.6	144.6	22.7	134.4	130.2	...	146.3	115.4	139.0
6169.56	Ca I	2.52	-0.48	149.8	131.0	135.8	112.8	145.6	164.6	160.8	174.6	158.9	35.6	153.7	156.5	...	161.8	138.9	166.0
6439.08	Ca I	2.52	0.39	234.7	199.4	229.8	167.9	228.2	227.2	258.3	237.6	219.9	105.8	205.8	215.8	...	228.6	201.2	217.9
6455.60	Ca I	2.52	-1.29	146.3	102.4	31.4	117.2	76.1	...	40.6	148.5	134.7	...	123.3	85.0	126.2	154.5	48.1	127.3
6471.67	Ca I	2.52	-0.76	...	...	...	...	...	...	...	...	...	20.7	...	...	...	...	...	...
6493.79	Ca I	2.52	-0.32	217.7	166.2	194.6	143.0	177.2	189.8	239.5	195.4	186.5	78.3	169.0	177.1	181.6	174.1	175.1	179.1
6499.65	Ca I	2.52	-0.82	137.9	101.5	130.4	59.6	142.0	117.8	165.6	136.4	137.1	25.3	118.4	133.8	153.3	118.0	124.2	127.4
6508.84	Ca I	2.52	-2.41	38.6	...	24.6	...	33.7	22.4	67.9	43.1	26.6	...	...	37.0	...	37.3	23.1	38.8
5490.16	Ti I	1.46	-0.93	121.8	83.7	104.4	34.0	109.1	102.3	142.0	125.3	112.4	...	84.4	103.8	109.5	98.8	84.1	116.1
5503.90	Ti I	2.58	-0.19	...	41.0	...	19.8	47.0	47.1	83.9	83.4	55.3	...	43.9	74.4	56.7	71.7	33.9	58.4
6126.22	Ti I	1.07	-1.42	149.2	110.7	119.7	48.9	131.6	130.4	167.1	150.6	142.1	20.0	113.5	107.1	158.2	135.5	113.3	140.1
6220.50	Ti I	2.68	-0.14	78.1	45.9	...	...	...	48.8	79.3	78.6	...	...	...	...	...	58.6	...	...
6258.10	Ti I	1.44	-0.35	208.0	139.2	...	77.3	176.3	159.6	231.6	191.6	195.5	...	143.9	192.0	...	182.0	...	194.3
6303.77	Ti I	1.44	-1.57	...	61.1	66.2	26.0	74.9	72.7	111.6	101.7	84.2	...	50.4	88.8	102.0	80.1	55.4	83.2
6312.24	Ti I	1.46	-1.55	...	...	66.8	...	63.2	66.9	115.9	97.8	79.9	...	51.4	88.8	...	80.6	54.5	88.2
6336.10	Ti I	1.44	-1.74	94.4	48.9	63.7	16.9	74.7	65.8	111.4	84.7	73.2	...	41.0	72.2	90.8	70.4	47.0	71.6
6508.12	Ti I	1.43	-2.05	64.6	27.1	...	...	62.0	40.6	105.0	61.9	50.3	...	28.1	58.9	59.3	37.8	30.2	58.8
6556.08	Ti I	1.46	-1.07	...	104.7	...	...	...	...	...	...	...	...	...	...	164.6	...	...	...
6599.13	Ti I	0.90	-2.09	151.6	81.6	128.0	35.6	141.1	128.7	179.9	146.9	149.8	...	87.8	109.4	141.6	130.8	105.4	120.1
6666.53	Ti I	1.46	-1.62	25.9	...	15.1	...	...	18.7	28.2	25.8	...	...	18.0	...	...	...	...	...
5418.77	Ti II	1.58	-2.11	111.6	107.9	73.6	89.0	94.6	98.7	97.3	91.1	103.5	69.1	96.9	94.9	108.1	108.4	104.0	103.0
6219.94	Ti II	2.06	-2.82	27.2	15.0	...	...	...	...	...	...	...	...	...	...	...	...	...	...
6559.58	Ti II	2.05	-2.02	...	48.3	...	45.2	...	...	...	...	...	16.4	...	...	81.2	...	...	...
6606.95	Ti II	2.06	-2.79	42.2	30.2	...	25.2	42.1	31.9	70.3	36.3	47.5	20.9	44.5	36.2	46.3	43.1	44.9	35.8
6680.13	Ti II	3.09	-1.86	...	...	23.9	18.9	22.7	...	...	19.0	...	16.6	32.6	27.0	...	16.8	...	16.3
6330.09	Cr I	0.94	-2.92	152.6	108.7	130.8	35.1	133.9	128.0	164.9	139.9	134.6	...	115.6	131.3	137.0	122.6	120.7	106.4
5369.96	Fe I	4.37	0.54	146.2	154.2	125.0	...	175.2	177.0	...	180.7	173.9	41.0	159.5	147.4	162.6	145.3	163.9	143.0
5383.37	Fe I	4.31	0.50	165.1	143.0	158.5	126.9	162.0	157.5	154.3	163.4	153.7	68.1	164.4	141.6	166.2	167.7	150.0	158.5
5386.34	Fe I	4.16	-1.74	37.7	62.7	30.2	31.0	...	54.6	...	33.9	66.2	...	32.3	45.6	...	45.1	39.1	...
5393.17	Fe I	3.24	-0.92	191.0	191.9	173.7	149.5	196.3	202.0	210.3	208.5	206.8	77.1	205.9	175.9	189.2	206.5	176.0	195.2
5395.22	Fe I	4.45	-1.73	...	22.3	...	...	...	...	...	41.1	...	...	21.4	...	...	23.4	16.7	...
5405.79	Fe I	0.99	-1.85	...	...	...	268.7	...	...	...	...	...	205.0	...	...	...	...	...	...
5415.19	Fe I	4.39	0.51	115.7	155.6	119.1	137.7	158.7	166.2	148.2	165.9	161.9	71.0	164.8	142.3	149.4	163.3	154.7	145.3
5417.04	Fe I	4.42	-1.42	31.2	27.9	27.6	...	33.1	40.6	31.0	63.1	37.8	24.9	49.4	33.9	28.8	37.1	32.1	46.6
5434.53	Fe I	1.01	-2.12	...	...	...	261.2	...	...	...	...	...	206.0	...	...	...	...	...	...
5436.30	Fe I	4.39	-1.35	...	...	...	...	...	...	...	...	...	...	...	...	...	...	...	...
5464.29	Fe I	4.14	-1.62	74.9	41.2	52.9	...	51.1	57.9	86.4	72.4	73.4	...	48.5	54.0	55.0	59.4	57.9	56.7
5470.09	Fe I	4.45	-1.60	43.2	21.8	26.7	...	29.5	...	34.9	41.2	...	...	18.7	30.8	27.0	25.6	20.8	22.2
5501.48	Fe I	0.96	-3.05	258.9	236.3	239.1	193.2	247.9	269.1	265.1	276.3	273.9	159.8	241.3	254.3	253.3	267.3	243.0	254.7
5506.79	Fe I	0.99	-2.79	...	273.2	294.2	203.6	...	...	...	...	...	158.7	290.6	...	...	...	272.1	...
5539.29	Fe I	3.64	-2.59	47.1	41.0	27.4	31.9	57.1	67.1	62.0	82.3	65.6	...	56.6	42.3	53.9	63.5	54.8	54.8
5586.77	Fe I	3.37	-0.10	194.0	203.2	141.5	175.9	211.2	232.9	175.6	238.8	226.1	108.8	215.9	207.6	214.7	228.6	221.2	229.2
6120.26	Fe I	0.91	-5.94	70.3	67.7	92.1	33.9	87.0	85.8	87.4	106.2	83.2	...	57.9	92.5	94.9	96.2	67.6	91.0
6136.62	Fe I	2.45	-1.50	178.0	...	261.1	209.1	...	...	...	...	...	118.1	...	...	268.1	...	...	...
6137.00	Fe I	2.20	-2.95	...	...	181.4	...	...	...	...	...	...	...	...	...	165.2	...	...	...
6151.62	Fe I	2.18	-3.37	132.7	122.7	137.3	93.6	125.6	148.1	128.0	150.7	126.3	21.4	136.7	133.4	154.4	130.7	126.1	133.9
6157.75	Fe I	4.07	-1.26	125.5	94.5	102.3	51.0	110.7	107.7	137.9	122.8	112.6	...	94.7	103.1	120.9	113.0	95.4	115.7
6159.38	Fe I	4.61	-1.97	47.8	...	...	...	...	...	...	28.9	...	...	...	...	27.8	...	...	25.2
6165.36	Fe I	4.14	-1.47	64.4	56.4	66.5	37.2	65.2	74.7	88.5	63.9	60.9	...	66.1	62.7	73.7	68.4	68.0	50.6
6173.34	Fe I	2.22	-2.85	169.3	150.5	169.6	102.5	160.9	166.9	176.6	176.2	169.7	33.9	148.4	164.9	167.7	164.6	155.9	161.5
6180.20	Fe I	2.73	-2.78	49.8	119.4	93.6	79.4	119.5	131.8	112.9	...	134.2	34.7	130.9	116.4	144.3	123.9	112.0	123.5
6187.99	Fe I	3.94	-1.58	81.4	65.1	72.7	32.1	76.7	81.8	90.9	96.2	78.7	...	77.9	71.1	76.7	87.8	67.2	79.2
6200.31	Fe I	2.61	-2.44	138.8	138.5	151.4	114.0	151.2	151.5	147.9	164.4	150.6	39.3	144.0	145.4	157.9	152.0	140.0	158.7
6213.43	Fe I	2.22	-2.66	188.6	170.0	195.5	143.4	183.2	203.7	207.2	200.8	200.5	72.5	165.1	178.5	185.4	182.4	175.7	180.6

Continued on next page

λ(Å)	elem	χ	gf	038	045	052	065	076	077	079	081	084	085	091	092	096	097	100	104
6219.29	Fe I	2.20	-2.44	199.9	185.7	209.7	135.0	187.8	199.5	203.6	210.5	206.1	68.3	190.2	195.3	205.4	191.4	179.8	190.3
6226.74	Fe I	3.88	-2.20	60.2	41.4	62.4	21.0	59.3	57.1	74.1	48.4	51.9	...	58.8	70.3	72.2	55.6	57.4	61.7
6252.57	Fe I	2.40	-1.76	217.9	193.7	200.3	154.7	207.4	218.5	203.1	214.9	203.2	115.3	187.0	198.0	216.1	205.6	190.3	205.3
6265.13	Fe I	2.18	-2.55	178.1	167.1	180.8	113.5	179.0	194.9	190.2	186.1	183.0	66.5	170.4	190.9	192.1	196.7	181.2	171.2
6271.28	Fe I	3.32	-2.96	49.7	46.8	59.8	21.5	59.2	63.2	65.5	72.3	56.8	...	53.4	49.4	67.4	65.0	44.8	49.2
6297.80	Fe I	2.22	-2.74	...	...	...	...	...	...	...	...	...	42.0	...	...	...	...	...	...
6301.50	Fe I	3.65	-0.72	...	144.9	...	...	...	...	...	...	...	40.0	...	...	...	...	...	...
6307.85	Fe I	3.64	-3.27	...	...	...	...	...	...	33.6	26.1	...	...	...	...	...	...	15.8	...
6322.69	Fe I	2.59	-2.43	163.0	140.4	158.5	116.1	160.4	174.6	169.0	170.1	155.4	36.1	146.2	146.2	150.4	159.7	153.5	165.0
6330.85	Fe I	4.73	-1.22	37.8	26.3	35.3	17.3	42.6	38.5	41.3	50.7	31.4	...	34.7	44.3	34.0	35.6	36.5	17.1
6335.33	Fe I	2.20	-2.23	214.5	198.2	250.2	151.0	224.3	209.1	234.5	220.8	206.2	83.2	197.4	191.7	207.9	213.3	201.1	212.5
6336.82	Fe I	3.69	-1.05	144.3	144.9	145.5	108.8	140.5	139.9	157.7	144.0	142.3	33.7	150.9	129.9	138.0	134.0	130.4	128.6
6344.15	Fe I	2.43	-2.92	169.6	165.4	165.2	100.0	170.3	181.3	196.6	189.3	168.3	20.7	149.4	...	180.6	170.0	143.6	165.7
6355.04	Fe I	2.84	-2.29	164.2	143.2	149.7	86.5	160.5	163.5	176.3	148.2	153.6	35.2	150.7	159.1	...	162.0	150.4	160.1
6380.75	Fe I	4.19	-1.50	79.5	49.9	74.2	30.1	76.5	79.5	88.1	87.6	73.3	...	72.3	78.5	66.7	73.8	63.3	88.9
6392.54	Fe I	2.28	-3.95	80.1	84.8	82.9	46.2	85.7	89.3	78.2	106.7	90.0	17.3	78.8	94.2	95.9	87.9	87.5	94.1
6393.61	Fe I	2.43	-1.63	236.5	228.0	221.5	194.6	241.1	248.4	249.6	260.1	236.6	120.8	240.6	204.9	240.4	251.8	221.3	251.5
6408.03	Fe I	3.69	-1.00	149.0	140.4	142.1	101.0	149.6	153.4	131.4	167.8	140.8	32.2	141.5	118.5	143.8	142.3	123.3	142.7
6419.96	Fe I	4.73	-0.24	112.8	91.1	115.3	61.7	99.9	115.5	132.5	118.3	105.1	...	96.8	76.4	115.4	110.0	109.5	97.1
6421.36	Fe I	2.28	-2.01	228.9	217.8	233.8	163.9	237.0	234.2	255.5	234.9	223.8	92.9	213.5	218.3	226.9	222.6	214.7	223.8
6430.86	Fe I	2.18	-1.95	256.5	215.3	282.6	174.9	256.8	269.1	...	272.7	244.7	111.1	222.4	241.4	276.1	263.7	235.9	242.2
6481.87	Fe I	2.27	-2.98	183.4	150.6	183.1	119.2	175.7	176.4	210.5	187.6	169.5	39.8	154.5	167.9	169.3	180.6	173.1	182.9
6498.94	Fe I	0.96	-4.69	205.1	151.9	215.6	110.2	178.6	198.4	243.4	203.5	191.3	28.5	163.7	186.0	208.9	185.0	176.6	205.9
6533.93	Fe I	4.55	-1.46	43.4	34.9	...	...	52.3	51.2	70.7	63.9	39.5	...	40.0	55.9	50.8	32.2	40.7	37.9
6556.81	Fe I	4.79	-1.72	26.7	20.3	...	...	...	...	51.0	24.6	17.7	...	...	28.9	38.5	19.3	21.4	...
6569.22	Fe I	4.73	-0.42	110.3	84.1	122.0	59.8	115.9	114.9	159.8	124.1	106.0	...	100.0	104.6	110.5	102.6	111.7	100.3
6574.23	Fe I	0.99	-5.02	191.0	151.3	...	101.1	177.6	180.7	169.8	191.4	180.5	32.7	150.5	162.1	151.7	186.5	158.2	166.9
6593.88	Fe I	2.43	-2.39	194.6	167.8	100.8	156.8	179.5	192.2	151.5	220.5	217.3	76.2	179.1	156.4	160.7	200.6	173.5	177.5
6597.56	Fe I	4.79	-1.07	45.3	44.8	53.7	...	66.1	66.7	75.1	68.7	64.2	...	60.3	43.5	56.1	54.4	58.7	48.3
6608.03	Fe I	2.28	-3.94	92.1	73.6	143.8	35.5	99.6	93.2	154.2	104.1	96.2	29.8	79.7	75.8	119.0	92.3	98.9	94.6
6609.12	Fe I	2.56	-2.66	158.0	149.2	206.9	107.1	167.1	171.1	208.3	179.3	170.5	36.6	156.9	149.4	184.9	159.7	174.4	151.7
6627.54	Fe I	4.54	-1.68	16.9	22.7	83.1	...	29.7	32.9	75.1	43.1	...	...	25.0	37.4	55.4	25.2	27.6	28.6
6633.76	Fe I	4.56	-0.82	107.4	86.2	149.8	...	112.2	94.4	155.8	115.3	85.9	...	102.2	110.4	...	107.5	95.4	88.3
6646.93	Fe I	2.60	-3.99	63.5	42.7	79.8	27.3	66.0	59.1	92.6	62.5	58.8	...	49.3	67.5	89.5	52.7	59.8	49.2
6653.85	Fe I	4.15	-2.52	26.6	23.3	69.6	15.0	24.7	24.0	62.2	34.7	36.1	...	26.0	...	37.3	28.9	16.5	24.5
5414.08	Fe II	3.22	-3.61	...	23.3	...	42.9	33.4	20.9	...	...	...	16.4	34.1	...	34.4	34.1	20.7	...
5425.25	Fe II	3.20	-3.36	56.9	50.1	45.7	64.2	44.8	36.0	35.5	38.7	45.3	29.5	53.4	43.7	39.3	37.8	57.1	54.0
6149.25	Fe II	3.89	-2.72	36.3	39.3	...	23.8	...	...	...	25.0	22.6	...	21.2	25.9	34.5	36.8	36.1	24.0
6432.68	Fe II	2.89	-3.71	37.7	57.7	72.7	41.8	68.6	64.9	75.8	51.9	48.7	16.7	65.8	51.7	...	55.3	45.5	54.4
6456.39	Fe II	3.90	-2.08	56.4	65.0	...	99.8	83.9	93.6	...	92.8	64.2	37.7	113.3	...	31.4	129.0	39.0	105.7
5578.73	Ni I	1.68	-2.67	135.0	119.9	116.0	86.8	117.7	130.9	142.9	140.0	138.5	29.0	133.0	123.0	125.5	141.0	115.4	151.5
5587.87	Ni I	1.93	-2.37	147.1	119.4	121.6	83.3	147.5	159.3	150.8	183.1	157.3	30.6	158.0	129.2	146.5	176.0	135.9	158.7
5589.37	Ni I	3.90	-1.15	25.0	19.1	26.3	...	32.4	24.6	29.2	34.7	29.1	...	18.7	31.3	26.7	18.8	23.9	27.7
5593.75	Ni I	3.90	-0.79	41.1	31.2	33.4	21.8	34.5	47.1	43.5	57.6	31.9	...	35.1	40.6	34.2	30.7	24.5	31.1
6128.97	Ni I	1.68	-3.39	94.8	61.2	93.5	48.1	87.6	76.9	99.4	90.0	82.1	...	74.3	72.9	105.7	88.8	75.0	82.8
6130.14	Ni I	4.27	-0.98	17.1	...	...	...	...	...	...	...	...	...	...	17.9	...	...	17.1	...
6177.25	Ni I	1.83	-3.60	72.6	40.2	51.7	...	55.4	57.7	76.8	73.3	65.4	...	69.5	...	52.4	72.2	45.0	61.6
6186.72	Ni I	4.11	-0.90	40.7	28.3	22.8	...	...	41.8	32.9	43.6	31.0	...	...	...	...	30.2	26.9	...
6204.61	Ni I	4.09	-1.15	...	...	...	18.7	20.8	22.3	24.5	22.4	...	...	28.9	...	...	23.0	22.4	...
6223.99	Ni I	4.10	-0.97	24.2	...	...	24.5	...	30.3	37.9	24.2	...	...	...	43.0	37.4	30.9	29.2	...
6230.10	Ni I	4.11	-1.20	45.7	23.6	24.5	...	26.5	...	42.7	...	26.7	...	25.4	...	...	32.9	...	...
6322.17	Ni I	4.15	-1.21	21.0	...	...	...	...	27.0	...	20.4	...	...	...	...	24.8	19.2	...	...
6327.60	Ni I	1.68	-3.09	110.9	94.9	100.3	70.4	109.7	106.5	127.7	116.7	107.2	...	102.2	119.9	102.0	117.2	106.6	113.6
6378.26	Ni I	4.15	-0.82	29.4	...	...	...	25.9	30.9	...	34.2	32.7	...	24.2	19.5	34.5	...	25.8	43.7
6384.67	Ni I	4.15	-1.00	22.9	...	...	...	33.3	...	50.2	35.4	30.4	...	...	...	20.9	27.6	...	36.2
6482.80	Ni I	1.94	-2.85	110.5	96.8	141.8	48.7	113.0	108.0	147.1	123.6	107.3	16.2	92.5	104.6	115.4	109.2	106.8	107.7
6586.32	Ni I	1.95	-2.79	137.0	135.4	44.1	123.9	66.9	89.8	...	134.5	144.6	45.8	128.7	57.0	51.5	148.1	66.5	94.6
6598.61	Ni I	4.24	-0.93	...	...	...	...	...	...	...	...	...	17.7	...	...	...	34.9	24.2	...
6635.14	Ni I	4.42	-0.75	...	15.1	...	...	...	...	46.9	...	...	...	18.6	24.9	...	...	...	18.2
5402.78	Y II	1.84	-0.51	52.0	...	30.7	...	...	...	67.2	35.5	26.3	...	25.0	52.1	31.9	39.3	20.5	43.3
6141.73	Ba II	0.70	-0.08	265.7	182.3	227.5	174.2	236.8	226.5	290.2	267.4	238.8	141.6	226.5	224.8	248.4	247.7	197.9	238.5
6496.91	Ba II	0.60	-0.38	259.7	204.4	278.5	161.6	257.9	244.2	...	287.1	272.3	134.5	231.4	246.9	260.8	274.8	228.3	252.4
6320.43	La II	0.17	-1.56	90.7	43.2	...	...	...	41.7	101.7	88.1	68.3	18.4	57.3	64.6	80.8	58.0	44.3	76.6
6390.46	La II	0.32	-1.40	71.4	...	57.1	...	57.3	50.9	93.8	76.1	78.6	...	57.7	65.1	...	66.8	49.1	...
5416.38	Nd II	0.86	-0.98	17.2	...	...	17.1	27.5	20.6	18.5	34.1	29.3	...	32.0	25.3	27.5	28.5	16.3	40.0
5431.54	Nd II	1.12	-0.47	65.0	...	43.7	...	47.3	42.4	73.6	62.0	58.0	35.3	42.5	45.0	72.1	48.3	39.4	52.3
5485.71	Nd II	1.26	-0.12	40.7	19.3	25.6	...	27.4	25.2	48.2	34.7	30.1	...	45.2	39.3	37.3	39.4	...	35.9
6645.13	Eu II	1.37	0.20	85.0	27.3	81.5	23.3	50.9	50.7	90.1	59.0	65.4	...	57.9	62.2	79.0	60.7	...	76.0

Table A.4. List of all the lines, their associated parameters and their measured equivalent width (EWs in mÅ, measured by DAOSPEC) for all our Fornax stars. Part 2/5.

				Equivalent witdh, one star per column, BLxxx															
λ(Å)	elem	χ	gf	113	115	123	125	132	135	138	140	141	146	147	148	149	150	151	155
6154.23	Na I	2.10	-1.56	41.3	...	...	20.5	20.4	20.9	...	...	21.9	20.2	...	46.1	...	33.3	24.7	27.3
6160.75	Na I	2.10	-1.26	59.5	...	31.9	66.9	22.8	49.0	...	33.4	19.6	26.1	18.9	81.9	41.0	42.1	43.0	58.0
5528.41	Mg I	4.35	-0.36	229.7	168.1	218.5	234.1	214.5	219.7	211.1	203.8	201.3	213.3	179.4	221.2	203.4	211.4	215.0	205.7
6318.72	Mg I	5.11	-1.97	...	16.2	34.9	49.1	34.8	...	35.6	46.7	39.3	30.9	18.4	49.4	...	48.0	35.6	...
6319.24	Mg I	5.11	-2.21	...	16.2	...	...	...	...	20.5	...	...	16.8	...	31.6	29.6	15.2	25.0	43.2
6319.49	Mg I	5.11	-2.43	...	...	...	...	17.4	...	...	29.5	...	...	30.2	...	...	...	...	...
6125.03	Si I	5.62	-1.57	...	...	...	...	20.1	20.8	...	...	...	...	...	...	31.7	...	...	...
6142.48	Si I	5.62	-1.51	...	...	...	...	...	...	...	...	...	...	...	...	...	...	...	...
6145.02	Si I	5.61	-1.37	25.9	...	19.3	15.4	...	...	...	...	21.0	16.3	...	...	21.8	25.1	...	...
6155.14	Si I	5.62	-0.80	58.8	...	42.5	46.5	38.9	40.0	50.4	35.3	30.6	52.0	24.6	59.3	47.5	52.5	31.9	49.2
6237.33	Si I	5.61	-1.02	38.7	16.0	20.6	31.0	21.7	18.8	...	20.6	...	24.1	16.8	31.6	21.1	25.6	...	24.1
6243.82	Si I	5.61	-1.27	...	...	...	37.4	...	...	...	22.8	...	22.0	18.5	59.8	...	...	29.3	...
6122.23	Ca I	1.89	-0.32	249.6	192.4	242.8	254.1	250.0	244.7	255.0	234.6	234.5	230.0	162.3	293.5	228.1	256.4	240.9	...
6156.03	Ca I	2.52	-2.39	43.4	...	...	40.5	28.5	...	24.2	34.5	...	...	...	70.9	18.7	36.6	22.4	27.6
6161.30	Ca I	2.52	-1.27	156.4	52.9	131.7	145.8	126.1	113.7	148.3	131.4	119.2	116.1	66.5	170.4	111.5	125.8	119.4	155.3
6162.17	Ca I	1.90	-0.32	264.2	204.5	262.9	284.9	261.6	266.1	279.5	254.3	247.1	265.4	194.6	...	244.5	268.6	265.7	277.2
6166.44	Ca I	2.52	-1.14	127.7	60.6	111.8	124.8	121.9	119.2	145.6	133.1	105.3	117.6	52.9	145.8	112.6	116.7	124.8	138.2
6169.04	Ca I	2.52	-0.80	145.9	87.2	141.7	139.1	135.1	129.7	153.1	148.0	149.2	139.0	59.7	143.1	116.5	155.5	148.3	147.9
6169.56	Ca I	2.52	-0.48	165.6	111.5	157.5	178.6	155.6	175.7	146.1	154.7	156.3	167.7	90.4	174.5	144.9	167.7	158.0	187.9
6439.08	Ca I	2.52	0.39	232.7	168.5	225.1	235.0	226.6	235.2	238.2	214.9	219.1	227.5	181.8	253.0	230.3	240.7	220.4	251.1
6455.60	Ca I	2.52	-1.29	155.8	85.6	106.2	92.6	172.9	192.2	134.1	135.9	159.0	155.3	...	178.6	...	194.4	177.9	149.0
6471.67	Ca I	2.52	-0.76	...	...	...	...	...	...	...	...	...	...	...	...	...	...	...	...
6493.79	Ca I	2.52	-0.32	195.3	139.0	193.3	213.1	187.8	174.8	196.5	176.7	192.2	186.3	134.8	205.0	188.9	199.2	183.4	193.1
6499.65	Ca I	2.52	-0.82	129.7	80.5	132.1	147.0	129.4	122.0	130.1	136.8	128.4	118.6	80.8	139.6	122.0	120.3	134.2	133.4
6508.84	Ca I	2.52	-2.41	42.4	...	26.8	43.2	27.7	17.6	33.6	19.8	21.9	20.8	...	46.0	22.3	33.2	29.5	51.5
5490.16	Ti I	1.46	-0.93	110.1	58.0	110.6	116.7	120.2	91.1	122.7	109.7	102.3	114.6	27.2	130.8	82.4	111.7	118.5	128.8
5503.90	Ti I	2.58	-0.19	67.9	37.5	58.1	69.5	68.6	61.1	78.3	64.8	48.9	52.4	17.1	101.7	31.1	60.6	65.1	98.4
6126.22	Ti I	1.07	-1.42	116.7	68.4	139.4	137.9	148.0	144.5	150.6	146.2	118.2	132.2	51.4	192.2	112.1	145.7	139.4	153.2
6220.50	Ti I	2.68	-0.14	...	...	...	64.9	...	76.8	...	...	...	...	27.1	...	...	...	...	91.7
6258.10	Ti I	1.44	-0.35	...	98.9	190.7	...	225.1	187.2	206.2	187.1	147.7	182.3	79.2	229.9	152.7	188.5	196.3	219.2
6303.77	Ti I	1.44	-1.57	93.2	42.4	80.8	107.9	91.6	91.4	104.1	86.3	79.1	85.1	...	137.0	61.7	102.3	91.0	106.3
6312.24	Ti I	1.46	-1.55	...	...	...	92.2	88.8	89.8	95.7	83.1	...	71.3	15.5	...	67.4	...	86.2	93.4
6336.10	Ti I	1.44	-1.74	68.1	26.4	74.0	76.7	79.4	76.6	90.5	68.3	65.0	73.7	...	104.9	...	84.8	78.0	86.6
6508.12	Ti I	1.43	-2.05	38.7	...	46.6	68.8	...	61.0	61.7	52.8	30.8	44.5	...	100.9	40.0	52.2	54.7	76.2
6556.08	Ti I	1.46	-1.07	...	63.2	143.9	...	...	...	...	...	111.7	...	...	...	...	139.5	...	...
6599.13	Ti I	0.90	-2.09	131.4	67.1	134.4	152.6	164.2	126.2	147.0	141.4	94.4	127.9	48.6	208.9	99.1	132.2	146.6	157.7
6666.53	Ti I	1.46	-1.62	...	...	16.4	34.4	...	27.9	27.4	16.3	...	...	...	39.6	...	15.5	28.1	32.9
5418.77	Ti II	1.58	-2.11	106.8	93.4	88.2	102.3	109.2	97.9	108.2	109.0	104.4	99.2	82.3	97.1	122.5	112.2	115.8	107.1
6219.94	Ti II	2.06	-2.82	...	27.4	...	...	...	...	...	...	32.2	...	...	60.9	...	...	29.2	32.8
6559.58	Ti II	2.05	-2.02	...	36.1	61.0	...	...	...	...	...	59.4	...	...	57.0	...	66.1	...	...
6606.95	Ti II	2.06	-2.79	50.9	28.4	44.2	54.1	32.3	31.4	31.2	36.8	29.3	...	61.6	37.6	50.0	33.7	35.9	28.7
6680.13	Ti II	3.09	-1.86	33.2	18.7	...	29.1	...	21.6	22.9	...	22.5	...	24.3	...	21.5	35.0	32.5	29.3
6330.09	Cr I	0.94	-2.92	127.0	63.7	141.3	127.1	146.4	127.9	141.2	141.4	127.0	132.2	36.7	169.3	116.1	143.9	140.8	146.2
5369.96	Fe I	4.37	0.54	167.3	136.9	218.7	145.2	142.3	143.1	173.4	160.3	166.5	165.7	128.4	163.3	132.5	155.5	160.1	119.1
5383.37	Fe I	4.31	0.50	185.9	150.1	150.5	171.1	157.9	160.1	188.8	162.0	157.8	161.6	114.1	182.2	161.0	174.9	159.2	170.3
5386.34	Fe I	4.16	-1.74	53.4	...	...	...	38.8	57.5	62.9	...	44.6	51.8	...	61.2	27.4	33.5	45.2	53.9
5393.17	Fe I	3.24	-0.92	199.6	180.7	198.8	217.9	209.6	233.1	216.2	200.3	218.7	212.3	176.0	239.2	187.7	207.6	221.0	214.6
5395.22	Fe I	4.45	-1.73	29.4	...	29.8	30.2	23.3	30.1	31.4	29.3	23.1	...	...	34.6	34.9	...	30.1	31.4
5405.79	Fe I	0.99	-1.85	...	...	...	...	...	...	...	...	...	...	262.0	...	...	...	...	...
5415.19	Fe I	4.39	0.51	155.8	145.2	151.4	174.2	167.5	186.8	152.5	155.3	176.2	167.1	108.5	168.1	162.7	166.5	174.0	184.9
5417.04	Fe I	4.42	-1.42	58.4	26.7	38.4	48.0	39.8	51.5	37.4	40.4	34.9	66.0	...	53.7	28.8	52.4	35.7	71.3
5434.53	Fe I	1.01	-2.12	...	299.9	...	...	...	...	...	...	...	...	245.4	...	...	...	...	...
5436.30	Fe I	4.39	-1.35	...	...	...	...	...	...	...	...	...	...	...	...	...	...	...	...
5464.29	Fe I	4.14	-1.62	82.1	...	59.5	90.4	53.5	...	51.8	70.7	52.6	60.1	27.0	...	49.2	52.6	62.9	73.5
5470.09	Fe I	4.45	-1.60	15.1	...	28.2	24.7	25.2	17.5	25.4	24.2	33.7	21.2	16.8	...	26.5	22.1	27.1	27.7
5501.48	Fe I	0.96	-3.05	251.8	238.7	266.5	267.8	275.4	254.1	274.3	260.6	257.5	270.8	185.7	274.6	242.7	273.0	251.4	286.4
5506.79	Fe I	0.99	-2.79	...	234.7	...	...	...	...	...	...	...	...	214.3	...	279.6	...	...	...
5539.29	Fe I	3.64	-2.59	68.3	33.8	49.5	67.2	59.1	...	57.5	58.8	58.1	59.5	...	78.3	59.9	63.0	55.9	76.0
5586.77	Fe I	3.37	-0.10	235.9	177.8	206.8	244.4	239.6	245.6	243.9	225.7	228.8	224.0	143.4	248.2	227.3	245.4	228.6	250.2
6120.26	Fe I	0.91	-5.94	79.1	49.5	76.0	92.1	109.1	75.3	88.9	83.4	95.8	85.6	21.9	92.5	83.9	87.7	97.7	89.8
6136.62	Fe I	2.45	-1.50	...	206.5	...	...	...	...	...	...	...	...	217.6	...	...	...	...	...
6137.00	Fe I	2.20	-2.95	...	129.5	...	...	...	...	...	...	...	...	...	...	...	...	...	...
6151.62	Fe I	2.18	-3.37	140.1	95.0	138.2	142.5	147.0	125.3	137.1	138.8	125.4	134.2	80.9	147.5	135.1	128.9	134.2	137.7
6157.75	Fe I	4.07	-1.26	133.4	50.1	105.8	125.1	100.1	104.2	113.4	110.4	104.8	115.1	82.2	151.9	86.0	104.4	104.6	126.4
6159.38	Fe I	4.61	-1.97	...	...	...	23.5	26.4	...	...	18.7	19.1	...	...	65.3	...	...	16.9	34.5
6165.36	Fe I	4.14	-1.47	83.7	32.6	67.6	64.3	64.9	67.5	58.8	65.4	74.7	68.5	24.2	92.0	63.1	72.8	71.0	75.5
6173.34	Fe I	2.22	-2.85	162.7	113.0	156.6	171.8	169.0	156.1	171.4	167.6	157.9	158.9	121.6	176.5	156.0	158.8	157.1	154.7
6180.20	Fe I	2.73	-2.78	133.2	101.8	138.6	119.5	149.9	116.9	123.1	139.7	154.7	132.3	59.3	85.7	132.5	142.0	143.8	147.3
6187.99	Fe I	3.94	-1.58	84.5	43.5	75.3	79.9	84.2	75.2	67.6	81.8	72.9	80.1	40.8	...	63.7	86.5	76.2	69.4
6200.31	Fe I	2.61	-2.44	158.0	120.6	143.2	152.2	148.0	159.7	153.8	152.7	151.5	149.3	98.8	145.4	154.9	163.4	155.3	158.0
6213.43	Fe I	2.22	-2.66	210.8	147.0	194.4	200.8	184.6	189.0	192.7	183.8	181.6	211.8	143.0	199.2	194.4	183.9	187.4	187.5

Continued on next page

λ(Å)	elem	χ	gf	113	115	123	125	132	135	138	140	141	146	147	148	149	150	151	155
6219.29	Fe I	2.20	-2.44	206.1	160.9	189.8	197.5	207.2	...	198.5	184.7	204.1	202.2	133.7	212.0	191.6	202.5	189.9	201.2
6226.74	Fe I	3.88	-2.20	68.4	32.8	52.3	65.2	55.6	57.7	52.5	57.2	64.5	53.7	29.7	110.4	46.9	70.8	60.1	67.6
6252.57	Fe I	2.40	-1.76	205.2	180.6	207.3	199.2	199.8	198.6	210.1	205.0	194.4	205.9	153.3	223.5	194.1	203.8	199.8	202.1
6265.13	Fe I	2.18	-2.55	178.4	137.1	186.1	173.1	196.7	169.8	190.6	185.0	167.5	195.1	125.9	195.1	176.7	189.2	182.5	199.8
6271.28	Fe I	3.32	-2.96	65.9	17.8	52.9	57.7	64.5	54.3	52.2	68.3	71.0	51.7	21.1	57.0	64.9	53.0	67.1	77.7
6297.80	Fe I	2.22	-2.74	...	...	...	...	...	...	...	...	...	...	...	...	...	...	...	...
6301.50	Fe I	3.65	-0.72	...	...	...	...	...	...	...	...	...	...	...	...	...	...	...	...
6307.85	Fe I	3.64	-3.27	16.1	...	...	24.0	...	...	...	...	...	...	...	...	...	...	...	23.3
6322.69	Fe I	2.59	-2.43	162.5	127.2	153.4	164.7	164.6	162.2	164.7	160.1	160.6	172.0	111.3	178.3	158.5	153.4	160.5	179.3
6330.85	Fe I	4.73	-1.22	42.9	...	31.3	48.0	34.2	41.5	37.2	43.4	31.8	27.0	18.2	48.2	39.8	42.7	39.1	37.6
6335.33	Fe I	2.20	-2.23	206.3	173.4	208.8	210.1	218.4	209.7	222.1	221.7	210.4	211.5	141.0	231.0	216.4	216.5	211.3	221.3
6336.82	Fe I	3.69	-1.05	152.0	126.2	141.9	143.0	139.4	138.7	144.1	144.5	170.1	141.9	98.9	163.1	135.3	141.4	136.1	163.9
6344.15	Fe I	2.43	-2.92	184.5	117.9	174.1	185.6	165.2	166.3	173.1	177.7	167.8	163.8	118.9	206.3	160.1	181.2	163.1	187.8
6355.04	Fe I	2.84	-2.29	165.2	116.7	170.7	164.0	159.6	157.0	165.8	163.6	154.9	168.7	87.9	172.1	143.3	172.9	166.7	174.9
6380.75	Fe I	4.19	-1.50	93.9	33.1	73.6	...	77.9	80.3	77.1	79.7	73.4	65.7	28.2	121.3	99.8	56.4	82.7	86.6
6392.54	Fe I	2.28	-3.95	88.2	51.5	97.3	93.7	90.2	83.9	86.1	82.7	94.8	92.9	31.1	108.3	89.6	80.9	90.9	...
6393.61	Fe I	2.43	-1.63	251.5	205.5	239.4	231.0	255.6	245.3	244.3	235.1	244.5	235.4	169.2	261.1	228.0	255.6	236.7	259.4
6408.03	Fe I	3.69	-1.00	172.0	122.9	152.2	143.3	141.6	153.1	158.7	137.8	143.7	146.3	94.8	157.1	123.4	166.6	154.6	...
6419.96	Fe I	4.73	-0.24	112.5	73.9	98.2	104.6	110.7	94.8	113.4	121.4	110.9	108.3	54.0	135.0	99.1	113.0	102.4	106.6
6421.36	Fe I	2.28	-2.01	234.4	182.0	214.5	244.3	233.0	214.8	244.0	221.2	211.1	223.1	175.3	243.3	224.9	230.0	216.7	228.1
6430.86	Fe I	2.18	-1.95	261.9	201.4	250.8	269.5	272.7	264.8	269.7	244.4	251.7	245.5	180.9	297.6	240.2	251.8	245.5	262.0
6481.87	Fe I	2.27	-2.98	154.2	126.2	167.0	181.5	168.9	158.4	195.0	159.7	163.0	162.9	136.6	176.4	172.4	167.1	158.1	153.1
6498.94	Fe I	0.96	-4.69	182.7	131.5	190.8	204.4	196.2	189.8	186.7	188.1	186.6	185.1	134.8	212.6	185.1	183.0	180.5	218.1
6533.93	Fe I	4.55	-1.46	47.3	24.4	39.8	60.5	55.5	41.5	46.8	36.7	55.2	45.5	25.9	55.6	50.5	46.1	46.4	49.6
6556.81	Fe I	4.79	-1.72	18.6	...	...	24.9	21.0	...	21.1	...	20.8	...	20.7	...	27.2	18.4	20.6	20.4
6569.22	Fe I	4.73	-0.42	134.3	61.1	98.3	118.4	112.2	84.9	106.9	109.0	103.9	110.9	89.4	136.6	117.0	105.7	103.6	110.4
6574.23	Fe I	0.99	-5.02	175.0	142.2	174.0	173.2	...	...	177.1	...	160.1	171.1	98.8	222.9	144.9	169.5	...	...
6593.88	Fe I	2.43	-2.39	231.2	180.8	195.1	192.9	225.9	205.3	193.8	210.1	182.7	192.4	90.7	246.4	151.8	211.4	227.0	203.7
6597.56	Fe I	4.79	-1.07	93.4	48.1	50.0	63.7	79.3	67.6	71.8	66.2	57.4	60.8	30.7	96.8	49.7	60.1	72.0	73.4
6608.03	Fe I	2.28	-3.94	94.3	58.4	107.6	116.4	104.8	85.5	99.0	91.1	96.0	97.5	60.1	101.3	98.9	97.7	112.8	97.5
6609.12	Fe I	2.56	-2.66	162.7	143.0	168.4	185.4	169.7	163.5	158.3	160.6	164.5	165.9	137.5	161.4	170.6	165.5	167.5	159.9
6627.54	Fe I	4.54	-1.68	39.8	...	27.9	31.2	25.7	22.6	25.2	22.2	31.8	20.9	34.8	27.9	47.2	39.8	18.6	22.6
6633.76	Fe I	4.56	-0.82	122.6	53.0	103.2	123.2	95.0	109.5	94.9	112.9	112.6	...	48.1	128.5	118.7	116.7	100.8	111.7
6646.93	Fe I	2.60	-3.99	56.4	34.6	63.6	69.7	55.1	49.0	52.6	56.0	59.1	50.2	...	72.2	65.1	70.3	47.5	66.6
6653.85	Fe I	4.15	-2.52	33.6	...	...	28.2	24.2	44.9	...	30.2	34.7	39.6	34.3	37.1	...	42.9	23.5	40.6
5414.08	Fe II	3.22	-3.61	29.1	...	...	...	19.6	19.0	39.2	21.9	27.3	43.1	25.4	...	24.4	...	...	25.5
5425.25	Fe II	3.20	-3.36	52.3	37.0	41.5	52.5	40.0	49.2	38.1	44.9	69.4	54.5	50.3	36.7	51.9	45.2	36.7	70.5
6149.25	Fe II	3.89	-2.72	44.7	25.4	31.8	...	25.2	...	40.8	37.5	36.1	33.3	33.6	49.8	24.7	28.9	29.1	...
6432.68	Fe II	2.89	-3.71	59.3	57.8	54.5	55.9	50.9	60.5	55.6	59.2	53.4	53.1	59.5	49.9	54.3	64.5	50.9	51.3
6456.39	Fe II	3.90	-2.08	78.7	74.6	51.0	50.9	...	44.3	46.7	123.6	78.7	65.5	...	68.0	27.9	84.7	...	...
5578.73	Ni I	1.68	-2.67	143.8	101.6	125.0	142.4	131.0	144.8	178.3	131.1	141.7	139.2	77.9	157.8	123.1	130.2	141.3	159.8
5587.87	Ni I	1.93	-2.37	178.7	110.3	160.3	167.9	174.8	168.4	160.2	154.8	155.5	164.5	77.3	168.8	146.9	165.8	164.0	161.1
5589.37	Ni I	3.90	-1.15	36.9	16.5	17.4	27.1	26.4	30.7	18.4	16.8	27.5	28.4	23.6	42.3	23.3	26.4	33.0	...
5593.75	Ni I	3.90	-0.79	39.5	24.1	32.6	32.6	30.3	36.5	50.2	40.1	38.7	47.1	21.4	56.9	22.9	30.6	34.2	57.4
6128.97	Ni I	1.68	-3.39	94.9	60.5	87.9	90.5	86.8	88.6	94.2	85.4	81.7	90.6	38.2	106.1	80.3	80.6	80.3	98.7
6130.14	Ni I	4.27	-0.98	...	...	...	15.2	16.4	...	...	27.6	19.6	...	...	28.5	...	...	...	18.3
6177.25	Ni I	1.83	-3.60	60.9	30.1	62.8	59.5	71.7	57.9	52.1	69.8	59.9	61.2	15.5	56.6	52.3	59.5	55.4	68.9
6186.72	Ni I	4.11	-0.90	33.4	...	30.8	39.1	...	18.6	28.9	20.7	20.9	18.1	...	63.2	22.5	...	24.1	46.1
6204.61	Ni I	4.09	-1.15	...	17.6	...	21.5	24.8	...	...	...	...	23.7	...	...	...	...	27.2	26.1
6223.99	Ni I	4.10	-0.97	26.4	...	28.9	33.5	34.3	39.7	37.0	...	32.9	26.1	...	61.9	...	36.7	37.2	34.1
6230.10	Ni I	4.11	-1.20	36.7	...	29.3	...	...	29.4	...	...	...	...	...	...	...	30.0	...	41.0
6322.17	Ni I	4.15	-1.21	...	...	15.2	23.0	...	...	...	...	...	15.4	...	...	23.1	...	...	40.0
6327.60	Ni I	1.68	-3.09	119.6	83.7	118.4	111.7	128.7	102.5	123.2	133.8	95.5	119.3	54.5	106.5	105.5	96.0	113.4	134.1
6378.26	Ni I	4.15	-0.82	33.2	...	27.8	44.3	33.8	...	32.9	35.4	32.5	23.6	...	66.8	...	...	27.1	...
6384.67	Ni I	4.15	-1.00	33.9	21.6	23.3	...	18.5	33.5	31.6	23.5	33.3	16.9	16.8	46.2	22.6	36.5	...	46.1
6482.80	Ni I	1.94	-2.85	101.1	66.4	107.9	114.1	126.7	119.3	111.3	116.9	98.8	108.5	62.4	97.0	95.9	105.9	114.7	115.1
6586.32	Ni I	1.95	-2.79	194.5	133.9	128.3	77.4	184.8	163.8	155.5	150.6	148.5	144.5	...	244.2	45.6	171.5	190.1	198.3
6598.61	Ni I	4.24	-0.93	...	...	...	...	...	32.1	21.3	30.7	22.5	...	...	28.0	27.6	...	...	...
6635.14	Ni I	4.42	-0.75	...	...	18.4	21.2	...	...	...	...	...	...	...	...	...	...	...	20.3
5402.78	Y II	1.84	-0.51	40.7	...	36.9	50.8	...	34.7	32.2	48.4	22.9	37.6	22.9	45.7	43.3	...	...	59.2
6141.73	Ba II	0.70	-0.08	276.9	182.4	241.5	256.1	218.8	240.3	255.0	241.1	209.2	240.3	236.5	...	236.0	230.1	243.6	265.2
6496.91	Ba II	0.60	-0.38	...	171.9	235.9	277.9	248.3	255.0	227.5	257.0	227.5	266.2	244.7	227.2	257.8	236.3	253.6	293.6
6320.43	La II	0.17	-1.56	86.9	23.0	74.1	119.7	56.6	72.0	80.4	83.5	65.2	71.8	87.8	119.3	61.4	73.2	71.9	100.7
6390.46	La II	0.32	-1.40	74.4	31.0	74.9	80.7	56.3	56.1	65.2	76.9	62.8	84.1	76.2	85.3	61.3	81.2	74.7	69.7
5416.38	Nd II	0.86	-0.98	27.2	19.7	19.3	41.2	34.4	28.6	16.4	...	27.1	38.4	16.3	50.2	...	35.8	38.9	59.2
5431.54	Nd II	1.12	-0.47	72.2	...	48.1	72.8	58.9	63.0	54.4	58.8	51.9	57.6	62.1	103.5	...	66.2	51.0	83.4
5485.71	Nd II	1.26	-0.12	44.5	...	37.1	47.6	33.0	37.2	36.3	33.1	32.1	41.4	58.7	50.5	29.4	32.4	36.1	26.9
6645.13	Eu II	1.37	0.20	71.3	15.9	53.5	78.2	49.1	55.0	69.0	79.7	56.2	52.8	99.1	73.9	53.1	68.6	59.5	61.5

Table A.4. List of all the lines, their associated parameters and their measured equivalent width (EWs in mÅ, measured by DAOSPEC) for all our Fornax stars. Part 3/5.

				Equivalent witdh, one star per column, BLxxx															
λ(Å)	elem	χ	gf	156	158	160	163	166	168	171	173	180	185	190	195	196	197	203	204
6154.23	Na I	2.10	-1.56	...	22.3	...	41.9	19.6	...	...	25.5	19.3	49.6	...	18.2	...	23.6	24.3	...
6160.75	Na I	2.10	-1.26	...	42.3	40.7	53.0	47.3	47.9	...	59.0	45.5	54.0	...	23.7	19.0	42.0	53.5	37.6
5528.41	Mg I	4.35	-0.36	202.6	214.5	206.5	221.8	216.6	205.1	214.3	225.0	209.3	228.0	209.7	196.9	208.5	209.9	212.6	217.3
6318.72	Mg I	5.11	-1.97	...	37.4	29.8	41.1	37.8	32.0	38.7	36.9	33.1	47.8	29.6	32.7	...	40.3	37.3	...
6319.24	Mg I	5.11	-2.21	20.3	35.0	...	...	25.3	...	30.1	25.5	...	25.5	...	...	...	...	28.9	...
6319.49	Mg I	5.11	-2.43	...	...	...	...	...	...	...	...	...	...	...	...	...	31.2	...	...
6125.03	Si I	5.62	-1.57	...	...	...	...	...	...	...	...	...	...	...	...	...	...	...	...
6142.48	Si I	5.62	-1.51	...	...	...	...	...	...	...	...	...	18.4	...	...	...	...	...	...
6145.02	Si I	5.61	-1.37	20.6	17.7	21.8	...	...	...	...	...	...	22.4	...	...	...	...	...	...
6155.14	Si I	5.62	-0.80	...	38.4	36.0	45.6	29.4	32.6	...	55.7	54.0	53.8	35.9	46.7	38.5	44.0	34.2	47.1
6237.33	Si I	5.61	-1.02	18.4	...	31.0	26.0	...	17.4	...	...	31.4	...	15.2	15.8	...	24.4	19.9	...
6243.82	Si I	5.61	-1.27	15.7	31.6	33.4	...	36.7	33.6	...	...	...	43.3	...	23.6	...	...	43.2	...
6122.23	Ca I	1.89	-0.32	215.2	219.7	242.5	287.1	251.3	245.5	247.3	258.7	210.9	254.2	249.5	205.9	225.2	236.6	245.0	234.6
6156.03	Ca I	2.52	-2.39	...	22.1	32.8	40.5	...	...	...	29.0	30.0	44.3	20.5	...	20.3	37.2	28.5	...
6161.30	Ca I	2.52	-1.27	82.4	117.5	119.1	152.0	138.7	132.7	115.0	143.1	128.1	146.0	122.7	93.3	111.4	140.4	143.2	114.8
6162.17	Ca I	1.90	-0.32	236.3	240.9	261.9	299.6	263.2	271.3	268.3	285.0	256.5	294.3	254.4	238.4	251.0	253.5	251.8	270.0
6166.44	Ca I	2.52	-1.14	89.8	102.1	122.8	137.7	117.9	110.2	121.7	132.9	108.8	132.6	134.0	93.0	115.0	127.3	128.5	112.0
6169.04	Ca I	2.52	-0.80	128.6	116.8	136.9	160.1	143.0	154.3	147.0	145.1	101.7	154.0	145.7	108.5	128.6	124.5	148.2	140.9
6169.56	Ca I	2.52	-0.48	131.8	148.2	162.7	181.1	174.7	173.7	177.3	156.9	127.1	165.2	155.1	130.8	156.6	145.7	161.1	156.5
6439.08	Ca I	2.52	0.39	200.2	228.1	212.2	251.3	229.0	232.1	243.3	232.7	...	236.3	246.8	202.8	216.5	...	237.1	...
6455.60	Ca I	2.52	-1.29	81.4	127.6	154.4	225.1	178.2	184.1	163.1	198.1	...	171.9	166.4	124.8	110.0	...	106.9	...
6471.67	Ca I	2.52	-0.76	...	...	...	...	...	...	...	...	...	...	...	...	...	...	...	...
6493.79	Ca I	2.52	-0.32	168.5	163.9	179.8	198.6	192.5	186.1	199.3	193.7	185.8	182.5	192.0	152.5	182.4	207.2	192.7	208.7
6499.65	Ca I	2.52	-0.82	109.3	117.4	123.9	150.4	124.5	133.7	131.7	139.9	132.3	142.3	130.2	106.8	124.4	151.7	137.3	132.1
6508.84	Ca I	2.52	-2.41	...	16.5	32.7	42.6	23.9	24.2	26.2	20.6	24.7	45.6	25.6	18.7	21.1	43.6	38.5	...
5490.16	Ti I	1.46	-0.93	70.3	99.8	124.8	133.6	109.2	111.7	104.3	130.2	84.2	114.5	118.2	68.1	88.1	108.5	126.7	111.7
5503.90	Ti I	2.58	-0.19	23.3	60.9	71.0	87.9	64.4	66.8	51.1	76.5	45.1	73.1	68.1	25.3	47.4	58.7	62.7	41.7
6126.22	Ti I	1.07	-1.42	113.8	119.7	138.8	153.9	132.6	132.0	132.4	152.3	124.4	149.9	147.5	101.3	120.6	145.1	154.4	126.1
6220.50	Ti I	2.68	-0.14	...	80.5	...	...	69.0	...	...	72.4	...	90.4	...	...	...	...	...	...
6258.10	Ti I	1.44	-0.35	138.9	157.8	186.4	219.4	176.7	206.5	...	207.7	149.3	197.1	191.4	117.3	158.3	205.0	185.6	178.4
6303.77	Ti I	1.44	-1.57	33.8	60.0	...	86.3	87.1	98.3	71.8	105.4	78.6	105.8	79.9	44.6	79.1	90.3	80.7	78.9
6312.24	Ti I	1.46	-1.55	37.9	60.4	81.1	97.8	72.4	...	68.2	88.5	...	87.9	84.4	44.5	...	89.6	89.7	75.1
6336.10	Ti I	1.44	-1.74	36.1	54.6	73.5	102.5	75.8	68.5	83.5	100.7	54.6	97.4	64.3	36.0	62.0	79.5	73.6	82.2
6508.12	Ti I	1.43	-2.05	...	24.8	62.3	...	56.1	42.3	42.8	59.6	33.9	64.9	45.2	22.9	33.8	65.3	54.9	57.5
6556.08	Ti I	1.46	-1.07	...	...	...	...	...	133.3	...	...	126.7	...	...	...	123.4	...	...	...
6599.13	Ti I	0.90	-2.09	72.4	93.8	141.2	166.2	117.3	136.8	144.5	178.2	...	154.9	138.3	75.9	119.3	...	115.4	...
6666.53	Ti I	1.46	-1.62	...	29.9	...	19.5	...	18.8	...	22.5	24.3	42.7	...	16.2	...	30.3	20.7	...
5418.77	Ti II	1.58	-2.11	95.7	108.8	110.7	113.7	102.1	112.0	124.6	113.1	89.6	101.4	107.3	94.0	94.2	104.3	100.3	97.9
6219.94	Ti II	2.06	-2.82	...	36.6	...	...	...	24.0	...	29.5	...	31.7	29.9	19.0	20.8	...	...	...
6559.58	Ti II	2.05	-2.02	...	...	...	...	...	...	...	...	66.8	...	...	...	50.8	...	...	...
6606.95	Ti II	2.06	-2.79	36.6	43.4	43.2	59.3	41.4	21.7	30.1	49.3	62.8	41.2	...	41.6	34.3	61.9	...	116.7
6680.13	Ti II	3.09	-1.86	...	30.1	...	41.2	35.1	...	33.8	46.0	27.6	18.9	24.0	27.8	23.6	42.1	29.4	41.7
6330.09	Cr I	0.94	-2.92	104.5	117.7	122.9	152.9	117.2	131.3	150.5	142.5	120.8	158.1	133.9	92.1	137.3	136.1	132.3	126.3
5369.96	Fe I	4.37	0.54	162.0	166.7	206.6	171.3	151.9	168.6	178.3	143.9	155.9	...	160.8	192.0	199.2	167.9	147.9	153.2
5383.37	Fe I	4.31	0.50	169.9	166.2	139.3	175.2	185.8	173.5	171.8	169.9	150.5	163.7	171.9	157.3	163.1	172.5	140.9	156.9
5386.34	Fe I	4.16	-1.74	53.6	53.1	54.8	47.3	38.5	...	54.9	56.4	54.0	67.3	62.0	25.5	44.7	37.7	48.4	58.9
5393.17	Fe I	3.24	-0.92	183.9	210.6	219.9	230.0	229.4	216.6	211.2	251.7	193.1	218.9	204.4	181.8	194.5	179.7	220.3	197.7
5395.22	Fe I	4.45	-1.73	20.7	...	...	34.8	35.1	22.3	16.7	24.3	...	26.4	42.7	...	19.6	21.3	...	...
5405.79	Fe I	0.99	-1.85	...	...	...	...	...	...	...	...	...	...	...	...	...	...	...	...
5415.19	Fe I	4.39	0.51	136.8	151.1	159.0	193.5	181.7	175.9	195.7	191.2	137.7	163.0	176.3	163.9	169.2	150.8	174.7	153.3
5417.04	Fe I	4.42	-1.42	47.1	40.0	70.3	49.3	52.3	53.5	43.0	57.7	...	53.1	48.2	46.1	46.2	...	19.9	33.8
5434.53	Fe I	1.01	-2.12	...	...	...	...	...	...	...	...	...	...	...	...	...	...	...	...
5436.30	Fe I	4.39	-1.35	...	101.2	...	...	...	...	...	...	...	...	...	...	...	...	...	...
5464.29	Fe I	4.14	-1.62	27.8	57.0	76.3	78.1	67.3	56.4	50.9	60.2	72.8	67.2	57.1	61.1	38.4	72.1	...	54.1
5470.09	Fe I	4.45	-1.60	...	25.4	28.3	42.6	22.5	16.5	...	40.6	38.9	32.0	21.5	21.8	19.7	30.1	18.4	17.6
5501.48	Fe I	0.96	-3.05	234.0	233.3	257.0	278.4	266.8	264.8	282.2	272.6	232.1	255.2	280.6	243.2	262.5	274.4	261.9	230.6
5506.79	Fe I	0.99	-2.79	262.4	295.6	...	...	...	...	...	...	290.0	...	...	274.6	...	...	...	295.9
5539.29	Fe I	3.64	-2.59	32.4	64.9	65.7	76.2	70.3	57.9	57.3	85.4	43.4	75.9	57.1	53.5	46.2	39.2	57.9	40.8
5586.77	Fe I	3.37	-0.10	227.9	246.8	223.8	250.6	246.9	237.1	230.5	256.1	168.4	232.4	238.7	221.8	220.4	202.2	243.4	195.1
6120.26	Fe I	0.91	-5.94	76.0	79.1	96.3	110.2	103.0	109.5	94.5	82.0	63.8	83.3	107.0	66.7	88.7	90.0	98.9	82.2
6136.62	Fe I	2.45	-1.50	...	...	...	...	...	...	...	...	...	...	...	227.1	261.7	281.1	...	...
6137.00	Fe I	2.20	-2.95	...	...	...	...	...	...	...	...	...	...	...	171.3	158.0	170.5	...	...
6151.62	Fe I	2.18	-3.37	113.5	140.1	130.2	133.1	138.0	122.9	129.2	143.7	122.6	144.0	143.0	126.9	128.2	129.0	133.4	126.1
6157.75	Fe I	4.07	-1.26	94.5	101.4	116.5	120.5	112.6	120.9	109.4	112.1	141.1	118.0	108.9	95.3	105.5	121.0	115.0	121.7
6159.38	Fe I	4.61	-1.97	20.1	...	...	28.6	...	...	...	20.8	...	38.7	17.0	...	...	24.3	20.3	18.5
6165.36	Fe I	4.14	-1.47	55.7	67.6	71.0	76.0	72.6	67.6	64.9	69.3	66.4	87.0	80.6	66.7	67.5	69.9	73.3	54.5
6173.34	Fe I	2.22	-2.85	142.5	142.6	173.1	169.8	155.6	157.9	153.4	165.3	160.6	162.6	182.1	155.7	154.8	163.1	163.9	162.8
6180.20	Fe I	2.73	-2.78	111.3	119.3	126.8	...	154.7	170.7	147.2	144.3	74.0	126.0	151.5	118.7	...	102.6	137.8	133.2
6187.99	Fe I	3.94	-1.58	64.3	64.9	82.2	85.5	83.3	79.1	68.8	82.8	73.2	81.0	79.5	64.7	77.8	81.6	74.0	71.1
6200.31	Fe I	2.61	-2.44	145.8	135.5	155.6	168.8	148.7	150.1	155.4	157.8	147.7	151.6	159.6	132.3	148.6	130.0	156.1	145.8
6213.43	Fe I	2.22	-2.66	171.7	193.8	185.5	195.0	192.3	181.1	201.0	191.1	187.4	203.5	205.5	164.8	190.2	193.6	184.3	190.5

Continued on next page

λ(Å)	elem	χ	gf	156	158	160	163	166	168	171	173	180	185	190	195	196	197	203	204
6219.29	Fe I	2.20	-2.44	187.0	207.9	201.6	214.2	204.7	187.9	193.5	211.4	192.1	223.9	205.5	183.7	193.6	202.9	198.7	201.7
6226.74	Fe I	3.88	-2.20	33.5	58.5	59.9	71.2	59.1	59.8	54.7	45.7	58.4	60.0	72.2	68.3	55.5	60.3	72.0	68.6
6252.57	Fe I	2.40	-1.76	188.6	190.2	210.8	222.0	217.8	200.5	202.5	209.8	198.5	199.5	223.8	194.3	211.5	214.7	190.6	202.6
6265.13	Fe I	2.18	-2.55	174.0	168.5	192.2	193.1	192.4	185.9	188.1	170.4	173.1	185.7	196.2	162.4	184.3	187.6	176.2	182.3
6271.28	Fe I	3.32	-2.96	47.9	52.8	55.0	66.9	60.2	61.6	53.1	72.0	61.2	62.3	61.9	44.7	51.7	61.7	55.3	70.6
6297.80	Fe I	2.22	-2.74	...	...	...	...	...	...	...	...	...	...	...	...	...	...	...	...
6301.50	Fe I	3.65	-0.72	...	...	...	...	...	...	...	...	...	...	...	...	...	...	...	...
6307.85	Fe I	3.64	-3.27	...	...	...	23.2	...	...	...	33.5	...	...	...	...	...	18.3	...	...
6322.69	Fe I	2.59	-2.43	151.4	148.5	160.4	165.2	147.5	166.0	169.9	171.5	137.3	162.4	173.7	140.8	156.4	158.7	140.2	153.5
6330.85	Fe I	4.73	-1.22	22.6	31.5	39.7	38.0	38.9	36.2	26.2	38.3	35.7	43.1	37.8	25.8	25.2	34.7	28.5	50.5
6335.33	Fe I	2.20	-2.23	198.4	198.9	207.1	227.9	206.1	194.0	209.6	229.7	201.3	223.0	226.4	188.2	220.2	221.9	213.3	212.8
6336.82	Fe I	3.69	-1.05	153.7	138.2	142.5	153.3	138.0	154.9	144.5	164.3	144.8	144.1	154.6	137.6	149.2	144.0	134.1	140.9
6344.15	Fe I	2.43	-2.92	161.7	167.4	163.1	201.9	177.3	165.8	169.7	188.9	175.8	198.2	183.3	126.5	...	163.6	168.5	160.7
6355.04	Fe I	2.84	-2.29	131.6	154.5	151.7	158.8	158.5	147.6	153.7	165.2	165.5	174.2	160.0	139.9	163.1	161.3	155.1	138.5
6380.75	Fe I	4.19	-1.50	50.2	88.4	74.7	93.3	67.6	80.9	68.7	96.5	72.3	99.7	90.6	77.2	80.1	75.6	84.5	99.0
6392.54	Fe I	2.28	-3.95	82.1	91.4	87.2	90.5	...	76.7	88.9	116.1	75.4	93.4	97.6	66.6	88.9	91.1	98.1	94.1
6393.61	Fe I	2.43	-1.63	225.5	226.0	241.8	257.2	227.9	243.4	251.5	249.0	236.4	258.3	256.2	225.2	236.9	220.9	242.8	235.4
6408.03	Fe I	3.69	-1.00	124.1	126.1	145.9	177.4	151.3	144.5	165.7	152.3	...	169.4	150.4	138.7	159.9	...	128.7	...
6419.96	Fe I	4.73	-0.24	91.4	112.4	106.4	123.4	89.2	96.0	112.2	120.5	...	113.2	115.1	104.2	103.8	...	107.7	...
6421.36	Fe I	2.28	-2.01	209.8	226.0	215.6	242.9	231.2	194.9	223.8	255.2	...	232.8	241.4	185.8	220.4	...	222.5	...
6430.86	Fe I	2.18	-1.95	230.1	248.4	236.8	275.6	260.4	255.1	265.1	282.6	...	261.4	279.5	227.1	232.2	...	256.6	...
6481.87	Fe I	2.27	-2.98	147.4	148.1	176.7	169.4	183.8	160.2	175.7	161.7	172.7	185.0	171.9	151.2	158.9	178.4	176.9	197.5
6498.94	Fe I	0.96	-4.69	170.8	182.5	181.7	205.0	205.6	168.4	196.6	196.1	188.4	207.3	199.9	160.8	175.8	210.1	185.3	209.3
6533.93	Fe I	4.55	-1.46	29.3	48.7	61.8	56.6	41.8	38.0	44.7	50.9	...	47.6	52.4	28.8	51.7	...	42.2	...
6556.81	Fe I	4.79	-1.72	...	...	...	15.9	24.1	...	...	...	15.1	...	19.7	22.0	...	27.0	...	...
6569.22	Fe I	4.73	-0.42	90.2	107.9	112.2	136.1	109.8	104.0	107.7	106.7	117.5	126.6	108.0	93.8	98.3	121.4	118.0	154.9
6574.23	Fe I	0.99	-5.02	...	...	167.7	...	188.2	182.6	180.5	...	...	187.1	197.2	...	187.4	...	168.0	...
6593.88	Fe I	2.43	-2.39	145.7	152.4	195.7	250.6	196.8	228.2	219.0	224.9	...	208.3	228.4	180.0	196.7	...	152.3	...
6597.56	Fe I	4.79	-1.07	32.5	51.8	55.0	87.4	70.8	74.9	81.6	65.7	...	57.5	77.0	52.0	57.1	...	50.1	...
6608.03	Fe I	2.28	-3.94	85.8	100.6	89.7	115.7	96.7	95.5	106.8	106.3	123.3	99.0	98.6	79.3	108.7	134.5	109.1	164.2
6609.12	Fe I	2.56	-2.66	165.1	162.7	150.2	190.8	166.6	150.6	171.3	184.7	184.2	161.9	170.8	159.1	159.7	185.0	173.3	225.5
6627.54	Fe I	4.54	-1.68	20.0	33.5	26.7	25.1	24.2	33.4	32.3	29.9	60.6	...	33.8	20.8	23.3	49.4	41.7	110.8
6633.76	Fe I	4.56	-0.82	85.7	111.2	115.3	118.6	111.0	94.5	98.3	122.9	133.9	121.4	112.9	97.3	89.6	137.6	119.3	187.1
6646.93	Fe I	2.60	-3.99	38.6	59.8	...	65.3	59.4	73.3	61.4	67.3	...	64.6	65.2	36.6	62.4	72.8	55.3	115.7
6653.85	Fe I	4.15	-2.52	...	40.3	...	38.4	31.6	...	34.8	29.7	36.2	32.1	27.3	21.9	...	33.3	33.4	...
5414.08	Fe II	3.22	-3.61	23.4	39.7	32.5	25.7	51.9	...	36.1	27.0	...	...	31.1	40.8	30.7	...	29.3	...
5425.25	Fe II	3.20	-3.36	50.8	45.4	42.3	49.5	38.5	61.4	56.9	34.6	53.4	44.7	48.6	48.0	28.5	35.0	57.8	41.7
6149.25	Fe II	3.89	-2.72	41.4	35.9	29.4	25.8	...	27.5	...	25.8	...	42.8	21.1	...	36.5	29.5	...	43.9
6432.68	Fe II	2.89	-3.71	59.9	70.8	55.4	66.9	45.2	35.2	51.1	48.7	...	54.0	54.5	66.5	45.2	...	53.5	...
6456.39	Fe II	3.90	-2.08	113.0	...	69.2	...	112.6	91.3	99.5	67.9	...	43.3	...	60.7	70.7	...	...	...
5578.73	Ni I	1.68	-2.67	112.7	147.7	142.8	145.1	147.2	142.7	128.4	156.1	130.1	150.4	143.3	115.8	132.9	135.1	136.1	121.8
5587.87	Ni I	1.93	-2.37	136.7	147.5	163.4	191.0	175.0	167.2	154.0	169.1	146.5	176.9	161.7	153.4	150.3	143.2	153.9	137.3
5589.37	Ni I	3.90	-1.15	...	...	26.9	...	19.9	23.5	31.0	36.2	25.2	45.0	19.1	22.3	21.7	35.6	23.8	32.3
5593.75	Ni I	3.90	-0.79	23.7	49.4	47.4	45.0	43.7	34.6	41.7	54.7	34.6	40.8	40.3	39.4	27.0	32.1	40.5	36.3
6128.97	Ni I	1.68	-3.39	68.1	79.7	76.2	84.7	82.6	89.9	84.1	83.6	79.3	95.2	87.8	69.8	72.5	86.7	98.0	76.8
6130.14	Ni I	4.27	-0.98	...	...	16.4	23.1	...	...	...	...	...	...	...	...	...	29.0	...	...
6177.25	Ni I	1.83	-3.60	54.1	53.2	69.2	79.8	51.3	62.1	69.6	55.4	44.1	64.2	67.1	38.7	55.5	57.8	56.6	60.8
6186.72	Ni I	4.11	-0.90	18.1	20.5	35.0	39.3	28.1	42.4	24.0	33.1	23.7	32.2	35.7	23.5	16.5	23.8	32.3	20.9
6204.61	Ni I	4.09	-1.15	...	20.4	36.3	38.5	15.0	21.8	...	25.7	...	16.3	30.5	...	...	...	...	...
6223.99	Ni I	4.10	-0.97	...	...	20.6	47.2	...	22.3	...	33.9	18.6	41.4	...	...	21.7	36.9	38.3	...
6230.10	Ni I	4.11	-1.20	...	...	29.2	...	...	...	27.6	29.1	37.6	47.3	...	...	...	...	20.5	...
6322.17	Ni I	4.15	-1.21	...	30.6	...	...	...	32.4	20.6	46.5	...	26.7	...	...	...	...	...	...
6327.60	Ni I	1.68	-3.09	106.8	117.3	114.2	132.6	112.0	106.7	105.5	130.8	109.1	123.6	114.1	99.2	116.8	122.5	93.3	107.2
6378.26	Ni I	4.15	-0.82	20.6	33.7	28.8	33.4	44.1	27.9	38.4	...	32.6	23.7	15.5	...	27.7	...	34.5	...
6384.67	Ni I	4.15	-1.00	...	...	26.3	41.4	31.7	26.6	28.4	...	...	42.2	...	...	...	22.3	...	...
6482.80	Ni I	1.94	-2.85	105.1	116.7	109.1	120.5	106.3	97.9	101.4	113.7	104.0	113.9	106.0	96.5	102.1	131.1	111.4	109.4
6586.32	Ni I	1.95	-2.79	57.5	84.8	133.6	210.7	143.3	217.8	183.8	192.6	...	176.2	185.4	109.3	179.5	...	92.3	...
6598.61	Ni I	4.24	-0.93	...	...	17.0	...	30.3	...	34.6	...	...	...	...	...	...	...	...	...
6635.14	Ni I	4.42	-0.75	29.3	...	...	...	...	...	...	...	25.1	...	...	...	...	38.8	25.7	...
5402.78	Y II	1.84	-0.51	...	34.8	40.5	51.6	43.8	27.1	28.8	35.0	58.2	47.6	21.6	...	36.3	53.9	30.6	26.6
6141.73	Ba II	0.70	-0.08	225.1	...	240.2	286.5	266.8	229.1	238.0	254.3	...	271.5	221.8	198.9	233.8	248.2	235.4	226.6
6496.91	Ba II	0.60	-0.38	244.0	250.3	248.0	...	254.1	238.6	221.7	265.0	290.5	279.9	230.2	229.5	231.6	294.5	245.7	293.4
6320.43	La II	0.17	-1.56	66.6	95.5	80.2	99.9	88.8	82.1	70.1	90.0	108.7	111.8	41.4	...	75.6	79.3	73.3	53.4
6390.46	La II	0.32	-1.40	73.9	70.9	...	92.7	61.5	76.2	63.4	84.2	93.7	81.7	59.7	37.8	58.1	98.7	76.9	77.3
5416.38	Nd II	0.86	-0.98	35.7	35.1	43.2	54.3	38.9	29.1	30.3	28.6	...	...	...	16.6	28.8	...	...	...
5431.54	Nd II	1.12	-0.47	...	80.1	52.8	76.6	60.0	47.6	45.2	77.4	66.9	68.0	54.2	31.0	34.9	49.7	65.3	46.7
5485.71	Nd II	1.26	-0.12	19.8	33.2	42.0	53.0	43.5	35.4	17.7	30.8	61.9	51.3	26.4	18.0	40.2	43.7	40.8	...
6645.13	Eu II	1.37	0.20	60.6	73.1	60.1	79.0	56.8	67.5	57.4	61.5	73.6	69.8	61.4	50.0	58.8	76.5	68.6	103.2

Table A.4. List of all the lines, their associated parameters and their measured equivalent width (EWs in mÅ, measured by DAOSPEC) for all our Fornax stars. Part 4/5.

				Equivalent witdh, one star per column, BLxxx															
λ(Å)	elem	χ	gf	205	208	210	211	213	216	218	221	227	228	229	233	239	242	247	250
6154.23	Na I	2.10	-1.56	37.4	38.0	36.5	40.5	...	42.5	27.2	...	33.8	16.6	29.5	37.6	16.8	...	24.6	44.5
6160.75	Na I	2.10	-1.26	50.6	51.6	51.1	57.3	40.1	65.8	60.3	27.5	48.6	29.5	51.5	63.1	...	28.9	54.0	88.7
5528.41	Mg I	4.35	-0.36	217.6	216.7	209.4	211.1	200.0	231.6	234.9	215.0	205.8	215.0	234.1	214.4	204.7	209.8	220.6	230.1
6318.72	Mg I	5.11	-1.97	46.5	41.8	55.4	46.9	39.1	51.1	47.3	...	...	31.8	35.8	44.6	...	41.6	...	58.6
6319.24	Mg I	5.11	-2.21	...	36.2	...	23.7	...	25.3	33.9	19.2	29.8	...	...	...	19.4	...	43.4	34.6
6319.49	Mg I	5.11	-2.43	...	...	35.7	...	...	...	...	...	...	...	...	24.0	...	36.0	...	...
6125.03	Si I	5.62	-1.57	41.7	...	...	48.4	...	...	...	...	16.4	...	...	...	...	...	...	...
6142.48	Si I	5.62	-1.51	...	...	...	...	...	...	...	...	18.5	...	21.8	...	...	...	...	...
6145.02	Si I	5.61	-1.37	...	...	...	...	27.6	19.2	...	...	...	23.1	34.5	...	...	...	...	...
6155.14	Si I	5.62	-0.80	57.4	45.8	40.5	45.3	43.8	51.5	50.1	43.2	54.9	31.3	42.5	45.8	32.7	45.0	42.3	33.1
6237.33	Si I	5.61	-1.02	32.5	28.2	18.4	23.9	21.0	24.3	18.1	23.3	25.5	...	27.3	19.1	23.2	23.2	...	37.4
6243.82	Si I	5.61	-1.27	41.7	47.4	35.3	56.3	29.1	...	...	...	29.2	26.3	46.1	33.8	23.5	...	37.5	40.2
6122.23	Ca I	1.89	-0.32	244.8	250.7	233.3	279.0	246.7	276.6	...	247.1	230.7	248.7	267.5	242.6	228.3	213.3	250.5	...
6156.03	Ca I	2.52	-2.39	...	26.0	25.6	36.6	24.6	42.3	39.8	25.7	26.1	35.5	42.9	26.5	20.7	28.5	36.9	38.6
6161.30	Ca I	2.52	-1.27	150.3	142.6	145.4	155.4	137.5	160.3	163.3	127.7	136.1	129.6	143.4	141.2	108.0	106.0	145.6	167.0
6162.17	Ca I	1.90	-0.32	261.5	273.6	274.5	...	268.1	...	...	255.5	266.5	269.6	289.8	285.5	249.2	237.1	279.7	...
6166.44	Ca I	2.52	-1.14	133.0	132.0	119.9	146.1	117.2	136.1	148.2	117.9	117.6	123.8	158.7	121.9	118.0	96.5	133.1	174.5
6169.04	Ca I	2.52	-0.80	144.1	155.5	133.2	156.5	152.7	149.2	148.9	144.0	126.5	150.0	146.1	147.2	150.0	95.7	147.2	170.9
6169.56	Ca I	2.52	-0.48	164.3	170.2	176.8	167.0	159.8	171.8	183.3	167.8	169.8	153.2	176.3	164.3	146.0	117.5	169.5	210.3
6439.08	Ca I	2.52	0.39	225.4	228.8	231.7	234.7	227.2	...	243.2	205.2	210.7	231.2	235.4	235.6	224.7	200.1	237.1	243.9
6455.60	Ca I	2.52	-1.29	192.1	161.5	184.7	113.3	117.5	...	...	57.1	102.5	133.8	175.2	185.3	175.1	123.0	163.5	222.9
6471.67	Ca I	2.52	-0.76	...	...	...	...	...	...	...	...	...	...	...	...	...	...	...	...
6493.79	Ca I	2.52	-0.32	195.2	181.3	191.7	191.3	182.7	222.4	223.7	179.6	178.8	189.8	208.7	196.6	180.4	160.4	163.1	190.3
6499.65	Ca I	2.52	-0.82	111.5	122.6	135.9	140.6	124.9	153.6	145.6	115.7	124.0	116.1	137.1	126.5	126.6	125.1	121.6	159.1
6508.84	Ca I	2.52	-2.41	31.7	36.6	32.1	50.9	25.0	67.1	58.0	36.9	24.0	18.6	41.6	33.1	22.5	16.0	25.5	67.4
5490.16	Ti I	1.46	-0.93	100.1	107.3	122.6	134.3	112.7	135.9	148.3	109.9	112.4	105.2	123.3	134.1	93.7	95.3	133.0	140.3
5503.90	Ti I	2.58	-0.19	67.3	70.1	71.8	83.0	68.6	88.7	89.3	57.4	44.5	58.7	83.7	79.9	43.2	39.5	71.4	109.5
6126.22	Ti I	1.07	-1.42	122.8	150.5	134.6	164.4	145.3	169.4	170.1	134.9	130.7	143.2	151.8	140.1	118.9	117.5	159.2	189.2
6220.50	Ti I	2.68	-0.14	...	...	...	87.8	...	...	86.3	...	...	52.1	...	...	...	...	...	65.2
6258.10	Ti I	1.44	-0.35	151.1	182.8	187.5	207.9	184.1	228.0	232.0	170.1	199.9	212.6	206.9	178.7	150.3	142.5	153.9	297.9
6303.77	Ti I	1.44	-1.57	77.5	89.4	88.6	118.9	93.1	118.0	115.2	76.7	78.8	86.2	112.3	91.1	80.3	67.8	91.0	122.5
6312.24	Ti I	1.46	-1.55	...	87.6	93.7	109.2	...	...	...	73.4	76.1	92.9	...	91.8	61.6	66.7	74.4	130.0
6336.10	Ti I	1.44	-1.74	67.5	80.4	76.9	94.4	80.4	96.4	98.4	69.0	79.1	77.2	84.1	84.7	55.2	40.0	84.6	128.3
6508.12	Ti I	1.43	-2.05	31.5	45.7	59.1	81.0	57.5	86.4	84.7	45.7	66.1	52.5	66.3	65.7	26.5	...	46.9	110.6
6556.08	Ti I	1.46	-1.07	...	...	...	...	133.0	...	...	...	...	...	...	...	...	...	...	...
6599.13	Ti I	0.90	-2.09	111.3	120.8	153.8	181.9	142.2	...	186.1	101.0	113.8	148.0	156.7	132.8	110.5	99.0	149.9	221.2
6666.53	Ti I	1.46	-1.62	19.2	34.5	34.7	36.1	...	41.7	38.9	...	...	...	35.8	18.4	15.1	...	37.9	59.0
5418.77	Ti II	1.58	-2.11	111.5	96.6	114.0	97.2	111.6	101.5	97.4	103.3	95.0	100.9	109.3	104.3	82.5	80.7	98.5	99.3
6219.94	Ti II	2.06	-2.82	36.1	...	...	...	...	...	...	...	...	...	41.7	37.2	...	28.1	40.3	...
6559.58	Ti II	2.05	-2.02	...	...	...	...	49.2	72.9	54.2	...	...	...	...	...	...	...	...	...
6606.95	Ti II	2.06	-2.79	45.7	49.4	43.0	52.7	40.4	67.7	35.3	55.5	45.0	40.3	25.8	51.0	34.4	48.0	27.7	23.8
6680.13	Ti II	3.09	-1.86	36.3	...	29.2	19.9	22.4	25.4	18.2	26.7	...	28.0	21.7	27.1	...	...	31.5	...
6330.09	Cr I	0.94	-2.92	122.0	122.3	132.8	160.3	130.2	161.8	160.6	133.3	138.7	150.4	142.5	132.2	116.1	120.3	147.0	178.8
5369.96	Fe I	4.37	0.54	167.4	163.5	164.9	168.3	147.9	175.4	146.3	201.7	148.9	217.2	...	152.5	148.5	134.5	194.3	199.0
5383.37	Fe I	4.31	0.50	181.5	162.1	170.0	164.5	169.7	172.1	204.0	171.3	166.6	166.8	165.7	169.5	145.3	155.0	182.6	177.1
5386.34	Fe I	4.16	-1.74	60.5	52.5	53.0	...	53.7	55.1	59.5	...	22.1	46.8	51.8	61.5	72.8	25.3	60.5	...
5393.17	Fe I	3.24	-0.92	221.4	227.6	200.5	209.7	222.4	226.2	211.3	211.4	210.9	209.1	231.5	230.0	224.4	201.2	222.3	246.8
5395.22	Fe I	4.45	-1.73	25.6	24.3	24.7	37.6	...	31.9	36.1	...	44.0	35.6	19.7	40.2	...	...	...	36.0
5405.79	Fe I	0.99	-1.85	...	...	...	...	...	...	...	...	...	...	...	...	...	...	...	...
5415.19	Fe I	4.39	0.51	188.5	163.3	179.9	185.6	175.6	172.9	163.6	144.5	153.8	173.8	172.0	164.7	179.3	133.7	189.9	170.1
5417.04	Fe I	4.42	-1.42	47.8	44.0	45.5	36.5	28.8	40.2	49.6	32.7	49.8	44.8	34.4	46.3	67.8	27.4	58.3	42.6
5434.53	Fe I	1.01	-2.12	...	...	...	...	...	...	...	...	...	...	...	...	...	...	...	...
5436.30	Fe I	4.39	-1.35	...	...	...	...	...	...	...	...	...	...	...	...	...	...	...	...
5464.29	Fe I	4.14	-1.62	78.2	81.2	59.0	...	56.1	88.6	89.9	62.3	61.6	54.0	81.9	85.5	55.0	61.4	52.1	...
5470.09	Fe I	4.45	-1.60	24.2	28.7	...	51.0	29.4	55.1	32.4	20.7	39.1	16.2	...	30.9	22.1	...	26.7	57.7
5501.48	Fe I	0.96	-3.05	250.9	257.7	261.3	265.2	254.2	274.4	297.6	242.7	230.1	273.8	279.0	263.5	260.7	238.4	274.6	...
5506.79	Fe I	0.99	-2.79	...	...	...	...	...	...	...	...	275.1	...	...	...	297.8	282.4	...	...
5539.29	Fe I	3.64	-2.59	75.1	72.4	73.9	82.0	61.6	74.2	95.8	58.1	60.1	54.3	78.0	71.8	56.2	36.9	78.9	86.2
5586.77	Fe I	3.37	-0.10	239.6	237.1	247.2	236.5	236.5	222.0	249.5	214.1	192.1	235.0	242.8	238.3	231.8	192.0	279.5	288.0
6120.26	Fe I	0.91	-5.94	78.6	78.7	89.7	107.2	105.7	96.8	113.2	88.6	75.8	100.8	97.2	82.1	82.5	63.2	87.8	112.1
6136.62	Fe I	2.45	-1.50	...	...	...	288.4	...	...	...	...	...	...	...	...	...	255.6	...	...
6137.00	Fe I	2.20	-2.95	...	...	...	164.4	...	...	174.1	...	...	...	...	...	...	164.9	...	...
6151.62	Fe I	2.18	-3.37	134.8	134.6	126.9	147.0	136.5	142.0	141.4	124.7	137.7	139.2	133.4	150.7	125.6	115.7	147.1	146.2
6157.75	Fe I	4.07	-1.26	122.8	123.1	115.8	127.0	118.0	124.3	132.6	108.9	116.6	102.5	125.4	134.5	109.0	103.9	121.7	109.4
6159.38	Fe I	4.61	-1.97	16.6	...	16.8	34.0	...	...	40.8	19.3	...	26.7	...	16.9	...	...	...	...
6165.36	Fe I	4.14	-1.47	65.1	72.9	73.8	76.1	68.3	70.3	74.1	68.4	64.8	78.8	77.9	80.4	58.5	52.3	68.7	97.4
6173.34	Fe I	2.22	-2.85	167.9	171.2	159.8	156.2	160.9	166.2	179.1	166.7	159.6	165.3	179.0	179.5	150.8	156.8	177.6	175.4
6180.20	Fe I	2.73	-2.78	142.3	135.5	158.9	133.2	137.1	131.0	141.5	122.1	107.0	133.3	143.2	139.8	138.4	87.1	141.0	144.5
6187.99	Fe I	3.94	-1.58	80.3	86.8	97.2	85.8	78.7	80.5	85.4	77.2	66.0	78.5	77.8	70.5	78.7	60.8	92.8	94.0
6200.31	Fe I	2.61	-2.44	157.3	150.8	157.3	150.1	148.1	152.8	147.3	154.7	129.6	156.9	159.5	155.7	159.0	141.7	175.0	138.3
6213.43	Fe I	2.22	-2.66	179.4	184.1	192.5	182.8	191.9	187.1	183.4	196.9	200.1	189.3	198.5	187.0	168.8	177.8	200.1	184.1

Continued on next page

λ(Å)	elem	χ	gf	205	208	210	211	213	216	218	221	227	228	229	233	239	242	247	250
6219.29	Fe I	2.20	-2.44	201.7	204.1	198.7	203.1	192.4	204.3	190.6	194.0	198.8	208.5	200.7	198.6	195.0	191.2	223.6	198.7
6226.74	Fe I	3.88	-2.20	71.7	72.4	49.0	70.7	75.1	69.2	70.5	49.4	53.9	59.6	76.6	69.8	53.1	47.5	51.8	87.6
6252.57	Fe I	2.40	-1.76	202.2	196.9	204.6	200.4	200.6	217.1	189.9	193.4	207.3	206.2	203.2	200.5	208.4	189.7	205.0	196.3
6265.13	Fe I	2.18	-2.55	181.0	179.9	190.6	183.7	167.1	189.0	201.1	177.6	181.4	192.7	182.8	173.4	175.5	171.9	188.3	213.4
6271.28	Fe I	3.32	-2.96	71.3	59.8	84.7	81.2	68.9	73.8	71.0	...	56.2	58.1	55.0	63.8	60.7	50.9	51.9	65.4
6297.80	Fe I	2.22	-2.74	...	...	...	...	...	...	...	...	...	...	...	...	...	...	...	...
6301.50	Fe I	3.65	-0.72	...	...	...	...	...	...	...	...	...	...	...	...	...	...	...	...
6307.85	Fe I	3.64	-3.27	...	...	26.1	26.6	...	...	...	...	...	18.2	...	21.8	...	...	...	...
6322.69	Fe I	2.59	-2.43	152.4	155.6	162.8	151.3	156.4	173.8	168.2	154.4	153.9	179.7	156.8	162.6	153.0	142.6	172.5	170.5
6330.85	Fe I	4.73	-1.22	51.9	63.2	45.0	54.3	37.3	49.6	43.7	35.7	34.3	33.5	52.2	...	39.5	29.9	52.5	26.0
6335.33	Fe I	2.20	-2.23	196.9	216.0	218.7	213.1	216.5	233.3	228.9	206.0	211.5	208.0	226.1	201.3	203.5	202.1	209.1	233.0
6336.82	Fe I	3.69	-1.05	161.6	143.0	160.9	147.3	143.2	155.8	149.3	141.8	143.2	149.9	155.6	142.5	142.7	128.4	158.8	145.1
6344.15	Fe I	2.43	-2.92	187.9	191.9	179.6	195.9	185.9	191.7	200.8	170.1	170.1	174.4	189.4	196.4	159.6	145.3	191.2	204.8
6355.04	Fe I	2.84	-2.29	162.9	164.4	151.7	171.9	170.8	178.9	171.9	152.1	150.7	163.7	139.8	169.0	146.2	136.6	158.0	168.8
6380.75	Fe I	4.19	-1.50	97.3	102.2	89.6	77.1	87.3	90.2	103.2	85.2	83.9	89.3	75.3	93.9	77.4	68.0	87.3	85.8
6392.54	Fe I	2.28	-3.95	103.5	92.9	96.2	94.8	95.1	106.7	110.1	85.6	83.0	93.5	96.7	107.3	80.2	75.7	102.6	97.7
6393.61	Fe I	2.43	-1.63	228.9	245.7	256.1	259.2	238.7	263.7	256.5	239.2	233.3	253.0	248.8	238.4	236.2	231.7	264.9	280.4
6408.03	Fe I	3.69	-1.00	159.6	144.2	161.6	160.2	152.4	...	173.0	129.1	125.9	160.8	158.2	156.8	146.4	140.1	167.5	175.0
6419.96	Fe I	4.73	-0.24	118.5	116.0	130.2	122.3	102.3	...	118.8	109.5	111.5	92.4	135.7	117.2	116.6	108.2	120.5	124.7
6421.36	Fe I	2.28	-2.01	224.1	208.2	230.2	230.3	226.3	...	228.7	222.5	209.4	229.7	235.3	226.7	221.9	212.6	233.4	272.4
6430.86	Fe I	2.18	-1.95	236.7	247.0	276.1	274.0	247.2	...	293.5	245.6	256.8	260.1	252.5	264.6	248.3	228.3	235.1	...
6481.87	Fe I	2.27	-2.98	163.5	167.5	181.6	189.0	155.5	207.5	180.3	173.3	157.6	172.0	159.7	174.4	171.4	161.4	164.2	180.8
6498.94	Fe I	0.96	-4.69	177.3	190.6	201.9	216.9	187.1	219.8	220.2	183.3	181.2	197.4	192.1	191.6	163.4	173.1	183.1	235.5
6533.93	Fe I	4.55	-1.46	46.9	54.7	54.1	42.5	43.7	...	47.6	46.8	48.5	54.7	61.4	51.9	50.7	41.8	49.1	37.1
6556.81	Fe I	4.79	-1.72	...	16.9	23.8	24.3	...	25.3	...	22.8	25.6	19.6	...	16.5	...	...	...	...
6569.22	Fe I	4.73	-0.42	126.2	122.2	124.0	117.1	109.5	139.8	124.8	98.3	111.5	96.3	128.5	130.1	100.2	88.2	101.6	128.6
6574.23	Fe I	0.99	-5.02	161.1	184.0	205.3	194.7	168.4	...	200.7	159.5	153.3	190.8	196.9	180.7	171.2	...	...	...
6593.88	Fe I	2.43	-2.39	206.4	203.9	248.3	195.4	197.4	...	238.5	162.8	128.0	215.0	220.9	202.0	196.8	171.6	231.3	249.6
6597.56	Fe I	4.79	-1.07	74.0	75.2	75.1	68.6	57.8	...	73.9	55.4	35.0	66.5	72.9	74.8	67.0	43.8	69.7	78.2
6608.03	Fe I	2.28	-3.94	98.4	104.0	97.6	114.9	88.4	133.3	112.3	103.0	92.2	103.9	98.3	106.2	105.2	76.0	94.4	115.6
6609.12	Fe I	2.56	-2.66	175.7	175.4	164.2	169.7	167.0	198.7	177.0	166.1	195.2	172.0	156.1	161.2	162.4	165.2	158.6	174.1
6627.54	Fe I	4.54	-1.68	26.7	37.4	33.3	35.7	30.9	48.2	30.0	34.7	37.8	22.6	36.9	36.5	15.9	20.4	27.0	23.8
6633.76	Fe I	4.56	-0.82	125.1	120.0	126.9	118.1	113.7	148.6	115.4	110.8	118.0	108.7	134.8	122.3	97.5	93.4	126.1	105.0
6646.93	Fe I	2.60	-3.99	54.5	61.8	61.7	64.9	48.6	80.3	71.3	55.6	69.8	54.7	70.4	70.2	45.7	42.9	63.6	53.7
6653.85	Fe I	4.15	-2.52	23.7	22.9	39.1	35.4	26.0	41.2	44.8	34.8	41.6	...	35.6	30.7	39.7	35.2	27.5	58.5
5414.08	Fe II	3.22	-3.61	34.7	...	39.0	...	22.5	...	...	25.8	30.9	...	46.9	...	44.2	...	44.3	...
5425.25	Fe II	3.20	-3.36	64.5	47.6	46.0	19.3	40.5	27.1	36.6	54.5	40.7	32.9	31.1	42.0	36.1	56.6	69.4	37.9
6149.25	Fe II	3.89	-2.72	35.3	...	30.5	29.9	36.7	30.4	...	19.7	...	29.8	...	33.1	...	...	31.3	38.3
6432.68	Fe II	2.89	-3.71	62.8	48.8	58.5	37.8	51.7	...	36.2	50.3	48.3	47.9	52.3	59.5	53.8	56.8	39.8	39.5
6456.39	Fe II	3.90	-2.08	86.2	63.5	124.5	45.8	63.8	...	78.3	22.8	...	84.1	70.7	80.2	76.2	39.9	76.7	127.7
5578.73	Ni I	1.68	-2.67	142.9	143.8	160.6	142.6	142.5	148.6	164.2	121.6	123.3	150.8	145.0	142.7	129.9	129.3	135.9	184.6
5587.87	Ni I	1.93	-2.37	171.5	168.7	191.9	154.0	154.7	177.2	172.2	131.3	166.7	165.8	184.2	168.3	163.9	121.0	180.6	177.0
5589.37	Ni I	3.90	-1.15	27.6	35.4	31.8	32.0	26.8	28.3	37.3	...	26.3	20.2	20.1	26.7	19.7	17.8	...	...
5593.75	Ni I	3.90	-0.79	51.5	56.2	59.7	43.0	35.4	39.2	43.3	32.4	45.5	35.0	38.1	51.7	29.4	38.9	45.0	49.4
6128.97	Ni I	1.68	-3.39	78.6	85.2	93.6	97.5	93.8	106.0	104.8	90.8	71.8	92.9	90.9	99.0	78.8	79.3	90.2	93.8
6130.14	Ni I	4.27	-0.98	17.0	19.7	...	19.2	...	...	33.2	...	...	...	...	...	...	...	25.6	...
6177.25	Ni I	1.83	-3.60	57.7	68.3	77.5	73.0	58.1	79.0	61.1	54.6	55.8	61.7	76.6	66.2	60.1	45.9	78.2	63.9
6186.72	Ni I	4.11	-0.90	33.5	33.6	40.0	39.3	38.9	50.3	52.2	29.5	22.0	30.9	32.3	30.2	25.1	25.5	41.4	86.0
6204.61	Ni I	4.09	-1.15	28.4	23.7	...	20.2	25.2	...	22.5	16.8	23.9	...	25.1	27.2	27.4	...	30.5	...
6223.99	Ni I	4.10	-0.97	45.0	44.0	41.2	44.4	34.7	28.8	44.0	39.0	...	25.2	40.3	32.3	26.2	31.1	48.3	61.9
6230.10	Ni I	4.11	-1.20	26.8	30.5	39.3	...	26.7	45.1	...	15.2	...	28.3	...	32.0	...	24.3	27.2	46.6
6322.17	Ni I	4.15	-1.21	23.4	26.4	16.4	29.0	21.4	...	...	...	...	...	...	...	15.2	...	...	...
6327.60	Ni I	1.68	-3.09	121.5	118.8	124.0	125.6	103.0	131.3	129.8	116.6	109.6	112.7	116.5	109.8	110.1	97.3	129.5	130.5
6378.26	Ni I	4.15	-0.82	33.2	25.4	23.3	40.5	33.4	32.9	50.0	30.1	31.3	30.8	32.5	34.2	22.8	...	38.5	47.2
6384.67	Ni I	4.15	-1.00	...	...	29.8	47.9	...	38.7	45.6	...	38.8	...	37.7	47.0	...	33.3	58.1	43.2
6482.80	Ni I	1.94	-2.85	103.8	99.7	121.0	116.2	86.2	127.1	117.2	104.6	101.6	105.6	97.7	113.8	103.5	100.4	110.0	125.8
6586.32	Ni I	1.95	-2.79	142.5	165.3	179.6	139.6	154.3	...	157.2	80.0	58.3	150.4	174.5	155.2	154.8	120.3	185.7	185.8
6598.61	Ni I	4.24	-0.93	...	30.9	...	...	...	...	33.8	17.0	...	17.8	...	...	...	...	42.1	...
6635.14	Ni I	4.42	-0.75	...	17.0	...	...	...	36.7	...	31.8	23.1	...	...	...	...	...	...	20.1
5402.78	Y II	1.84	-0.51	44.6	24.4	45.0	58.4	53.7	55.9	55.2	40.5	50.7	29.3	26.5	60.0	...	32.0	74.5	49.2
6141.73	Ba II	0.70	-0.08	267.8	259.2	265.1	271.8	252.9	282.6	...	251.0	244.0	215.3	275.9	261.5	228.5	226.7	250.1	...
6496.91	Ba II	0.60	-0.38	243.1	270.3	284.0	297.9	235.1	281.4	280.7	256.7	268.8	232.7	284.4	247.9	258.8	250.3	246.8	...
6320.43	La II	0.17	-1.56	80.1	94.6	90.4	96.5	81.2	107.2	106.3	83.2	65.3	51.3	102.2	87.0	41.0	47.9	88.7	92.9
6390.46	La II	0.32	-1.40	70.7	77.9	88.4	85.7	79.7	99.8	93.8	98.9	69.8	56.5	87.1	67.6	49.2	66.5	78.1	96.8
5416.38	Nd II	0.86	-0.98	...	38.9	50.4	43.3	36.4	40.5	40.0	...	34.3	...	21.4	22.1	22.8	...	57.5	65.4
5431.54	Nd II	1.12	-0.47	65.2	60.6	57.3	68.0	...	66.6	73.5	69.4	90.6	47.5	64.9	52.6	30.8	66.1	86.5	66.9
5485.71	Nd II	1.26	-0.12	37.2	40.6	45.4	54.2	41.9	58.1	54.4	50.7	36.4	...	53.4	51.7	25.4	34.8	...	36.7
6645.13	Eu II	1.37	0.20	57.2	52.8	72.2	74.0	68.7	86.3	68.4	83.5	76.2	50.7	80.2	65.1	40.1	47.2	66.4	62.5

Table A.4. List of all the lines, their associated parameters and their measured equivalent width (EWs in mÅ, measured by DAOSPEC) for all our Fornax stars. Part 5/5.

				Equivalent witdh, one star per column, BLxxx																
λ(Å)	elem	χ	gf	253	257	258	260	261	262	266	267	269	278	279	295	300	304	311	315	323
6154.23	Na I	2.10	-1.56	41.9	37.6	45.3	...	25.0	...	...	31.7	24.5	52.8	16.2	48.8	33.4	17.0	24.3	...	...
6160.75	Na I	2.10	-1.26	68.6	62.1	63.6	34.0	32.5	25.2	...	58.8	51.6	96.0	...	70.2	52.3	38.9	47.2	26.3	44.3
5528.41	Mg I	4.35	-0.36	227.2	223.4	220.8	205.5	219.7	217.4	169.5	216.3	221.3	234.8	164.9	225.7	240.7	208.9	208.1	207.0	220.0
6318.72	Mg I	5.11	-1.97	44.0	64.6	47.2	32.4	25.6	50.3	27.4	43.6	28.3	...	...	49.7	42.8	...	41.7	...	30.7
6319.24	Mg I	5.11	-2.21	26.0	25.8	...	...	...	20.5	...	...	26.4	38.8	...	41.9	...	...	25.7	...	...
6319.49	Mg I	5.11	-2.43	...	...	...	...	...	...	...	28.2	...	...	...	...	31.0	18.5	...	...	15.2
6125.03	Si I	5.62	-1.57	...	...	...	31.7	...	...	...	32.3	38.8	...	...	56.2	...	...	...	17.4	...
6142.48	Si I	5.62	-1.51	...	...	...	...	...	...	...	26.0	...	...	16.5	...	...	...	...	16.9	...
6145.02	Si I	5.61	-1.37	15.4	22.7	...	...	...	...	...	22.1	...	21.2	...	...	...	...	19.3	...	21.7
6155.14	Si I	5.62	-0.80	47.6	55.8	39.1	42.8	27.6	45.5	...	41.0	38.9	51.2	34.6	49.0	40.0	39.0	43.5	47.9	45.0
6237.33	Si I	5.61	-1.02	26.6	23.7	32.1	16.0	...	30.2	...	33.6	23.4	43.1	22.3	31.0	26.8	...	21.6	31.4	...
6243.82	Si I	5.61	-1.27	...	53.1	44.0	...	...	...	22.5	28.0	33.8	46.9	...	...	...	29.3	17.0	23.1	...
6122.23	Ca I	1.89	-0.32	279.3	291.0	281.2	242.9	236.3	...	182.2	223.9	258.7	...	174.8	...	275.1	271.8	247.5	201.6	252.6
6156.03	Ca I	2.52	-2.39	38.4	46.8	43.7	32.1	20.5	...	...	32.0	28.5	45.4	...	...	17.5	15.6	36.5	...	...
6161.30	Ca I	2.52	-1.27	163.2	166.7	180.6	127.1	127.9	113.3	50.6	132.8	132.2	177.4	47.0	161.4	145.4	143.2	138.3	87.7	148.1
6162.17	Ca I	1.90	-0.32	...	...	...	278.8	266.5	256.1	196.0	270.4	282.6	...	184.9	...	291.6	288.4	277.4	221.8	282.1
6166.44	Ca I	2.52	-1.14	148.6	150.4	150.5	136.3	125.4	121.0	64.0	146.7	124.0	147.9	37.8	157.0	135.9	130.7	128.6	103.2	113.8
6169.04	Ca I	2.52	-0.80	163.3	169.7	161.6	145.9	135.6	129.1	94.4	148.5	144.6	159.9	64.5	154.9	152.0	149.4	133.3	123.6	105.8
6169.56	Ca I	2.52	-0.48	170.4	196.1	182.1	165.5	140.1	154.1	112.4	168.4	151.7	177.3	86.8	196.2	176.1	171.7	171.3	156.6	146.5
6439.08	Ca I	2.52	0.39	236.5	223.4	247.4	213.6	209.2	230.1	183.4	225.8	215.5	238.4	155.1	260.0	224.0	228.4	...	207.2	235.2
6455.60	Ca I	2.52	-1.29	84.2	113.4	187.4	152.1	...	...	29.3	153.2	75.5	170.9	...	192.0	...	130.8	...	155.9	60.6
6471.67	Ca I	2.52	-0.76	...	...	...	...	...	...	...	...	...	...	...	...	...	...	...	...	...
6493.79	Ca I	2.52	-0.32	209.7	223.2	189.5	187.3	182.2	181.5	139.8	196.4	194.6	211.4	126.6	199.2	210.3	205.2	204.5	156.9	195.8
6499.65	Ca I	2.52	-0.82	144.6	159.2	138.6	118.5	121.0	133.3	77.6	106.5	138.1	151.2	45.9	141.8	127.3	131.3	152.9	105.2	126.8
6508.84	Ca I	2.52	-2.41	45.2	57.3	55.8	38.7	32.4	43.9	...	37.1	46.5	61.5	...	57.0	29.9	28.7	38.6	...	41.5
5490.16	Ti I	1.46	-0.93	132.3	158.9	148.0	98.6	116.9	97.2	50.8	87.2	113.2	143.2	32.3	152.3	123.0	132.5	106.5	92.5	117.3
5503.90	Ti I	2.58	-0.19	76.8	94.2	120.5	66.3	65.9	56.5	23.4	53.6	52.8	107.6	...	103.1	86.6	67.2	53.2	40.6	71.7
6126.22	Ti I	1.07	-1.42	167.5	167.6	172.5	130.1	130.7	127.2	56.8	138.8	148.4	182.3	32.4	172.4	162.0	159.6	138.8	119.0	160.5
6220.50	Ti I	2.68	-0.14	...	...	...	...	...	...	24.1	...	56.6	94.0	...	81.3	80.0	...	...	...	...
6258.10	Ti I	1.44	-0.35	223.9	231.1	232.3	195.2	160.5	181.7	83.5	165.8	209.4	258.2	72.4	243.1	216.5	223.1	181.3	138.1	204.8
6303.77	Ti I	1.44	-1.57	121.7	117.2	115.7	91.1	79.0	87.1	41.0	77.9	87.3	121.2	...	115.6	96.2	100.3	87.9	68.3	97.9
6312.24	Ti I	1.46	-1.55	...	114.7	107.9	...	...	79.2	20.6	78.5	91.3	113.1	...	100.9	...	...	88.7	45.6	86.3
6336.10	Ti I	1.44	-1.74	103.0	101.2	115.0	90.8	66.1	63.6	26.0	77.7	90.6	120.9	25.3	97.7	90.7	89.7	73.6	68.5	103.8
6508.12	Ti I	1.43	-2.05	69.8	90.0	72.0	56.9	45.3	53.3	...	38.1	71.5	94.2	...	90.2	58.0	54.3	63.9	31.0	63.5
6556.08	Ti I	1.46	-1.07	...	...	...	...	138.0	...	...	...	...	...	...	...	...	139.8	...	...	...
6599.13	Ti I	0.90	-2.09	153.9	186.8	181.3	147.5	111.3	136.9	46.9	109.4	167.9	173.1	24.5	194.5	159.1	174.3	...	78.9	164.2
6666.53	Ti I	1.46	-1.62	41.8	50.1	59.5	...	...	...	...	...	39.7	39.2	...	...	29.8	33.9	46.2	...	...
5418.77	Ti II	1.58	-2.11	111.2	97.0	96.3	99.6	115.3	93.2	97.6	116.2	83.3	109.4	122.1	92.7	109.8	102.2	83.0	110.0	96.5
6219.94	Ti II	2.06	-2.82	...	...	28.0	31.3	28.1	...	21.6	48.8	...	33.9	27.4	...	40.7	...	...	21.8	...
6559.58	Ti II	2.05	-2.02	67.8	...	...	...	72.9	...	...	...	...	...	...	...	57.7	61.8	...	...	...
6606.95	Ti II	2.06	-2.79	43.8	40.7	46.2	24.6	34.4	47.6	39.3	34.1	59.6	49.2	31.7	49.9	33.7	...	88.0	27.1	31.1
6680.13	Ti II	3.09	-1.86	23.1	29.5	33.0	17.5	27.9	...	26.5	41.5	29.1	21.4	26.1	36.4	25.1	17.9	36.6	30.7	19.9
6330.09	Cr I	0.94	-2.92	152.8	162.8	163.2	142.5	123.5	130.7	64.1	132.6	130.4	172.1	35.2	159.7	150.2	140.8	137.0	106.9	158.7
5369.96	Fe I	4.37	0.54	171.7	171.0	180.1	182.4	172.0	179.4	112.4	164.9	141.9	247.5	101.7	208.0	164.4	158.8	238.5	145.2	165.1
5383.37	Fe I	4.31	0.50	153.4	169.7	181.0	171.1	145.9	149.5	130.6	135.1	153.1	182.5	93.5	173.8	187.3	160.0	139.8	129.9	162.6
5386.34	Fe I	4.16	-1.74	...	65.9	...	...	45.7	33.1	...	56.6	55.8	...	17.7	57.3	...	35.6	39.6	58.9	35.8
5393.17	Fe I	3.24	-0.92	226.5	248.5	235.0	210.7	213.9	192.2	169.3	229.2	204.2	235.2	125.3	246.4	218.6	224.3	198.2	210.6	178.5
5395.22	Fe I	4.45	-1.73	37.3	39.0	43.7	...	...	17.1	...	31.1	27.5	31.5	...	36.2	...	31.6	29.1	31.2	22.2
5405.79	Fe I	0.99	-1.85	...	...	...	...	...	...	283.9	...	...	...	284.6	...	...	...	...	...	...
5415.19	Fe I	4.39	0.51	177.9	181.1	190.1	182.6	159.5	166.7	145.1	161.7	146.3	173.3	110.4	178.1	163.2	166.8	141.8	150.5	151.3
5417.04	Fe I	4.42	-1.42	65.8	47.7	43.5	36.1	39.1	43.0	19.2	77.1	23.1	33.3	...	46.4	35.3	32.4	...	40.8	23.0
5434.53	Fe I	1.01	-2.12	...	...	...	...	...	...	271.4	...	...	...	259.8	...	...	...	...	...	...
5436.30	Fe I	4.39	-1.35	...	...	...	...	...	...	...	...	...	...	...	...	...	...	...	...	...
5464.29	Fe I	4.14	-1.62	92.2	...	90.0	56.4	59.3	56.0	...	...	74.2	...	...	108.1	71.5	58.9	62.9	19.7	67.0
5470.09	Fe I	4.45	-1.60	34.5	46.1	...	28.5	33.1	23.5	...	29.9	31.6	43.6	...	35.5	33.3	29.8	40.3	...	39.2
5501.48	Fe I	0.96	-3.05	277.6	268.8	274.5	250.1	264.8	245.2	207.2	250.1	234.0	279.6	185.4	278.9	277.9	276.9	241.0	237.5	285.3
5506.79	Fe I	0.99	-2.79	...	...	...	...	...	290.9	212.0	...	...	...	204.9	...	...	...	294.6	271.7	...
5539.29	Fe I	3.64	-2.59	78.5	95.8	83.4	71.9	61.5	55.6	26.6	87.2	52.8	86.6	21.8	84.0	...	57.8	48.2	48.9	61.5
5586.77	Fe I	3.37	-0.10	252.5	248.6	278.2	246.4	225.6	213.5	171.9	224.0	199.3	243.8	149.2	274.9	225.7	221.1	190.1	212.5	211.9
6120.26	Fe I	0.91	-5.94	101.4	111.6	106.3	102.5	97.4	72.3	28.4	93.0	83.3	96.8	36.1	102.3	94.0	107.8	106.2	76.8	82.3
6136.62	Fe I	2.45	-1.50	...	...	...	...	254.6	...	237.6	274.3	282.0	...	159.6	...	...	...	...	222.3	...
6137.00	Fe I	2.20	-2.95	...	...	...	...	172.1	...	...	158.3	163.6	195.8	85.9	...	...	...	...	139.1	...
6151.62	Fe I	2.18	-3.37	148.8	136.1	144.6	122.5	127.2	128.9	90.8	124.8	122.8	137.6	76.5	149.9	124.0	140.5	128.3	119.4	134.3
6157.75	Fe I	4.07	-1.26	129.7	142.4	139.5	102.0	100.3	125.4	59.8	125.9	107.2	143.3	43.0	146.4	127.3	109.5	119.9	107.2	130.0
6159.38	Fe I	4.61	-1.97	27.0	41.7	37.7	20.1	...	29.4	...	30.5	25.2	52.9	...	45.3	...	...	22.7	...	...
6165.36	Fe I	4.14	-1.47	82.7	87.5	86.5	59.3	65.0	67.8	39.1	75.4	60.6	84.0	28.0	76.3	65.3	68.5	72.3	80.4	72.8
6173.34	Fe I	2.22	-2.85	183.2	186.7	180.4	163.0	161.3	156.7	100.5	170.7	148.2	171.0	99.7	184.4	179.6	176.4	169.7	143.7	190.2
6180.20	Fe I	2.73	-2.78	...	148.7	168.4	147.2	165.3	100.1	98.9	146.3	125.3	134.8	84.8	157.8	140.4	138.1	131.9	125.8	76.9
6187.99	Fe I	3.94	-1.58	87.3	108.2	97.1	96.2	67.7	81.1	42.9	85.6	75.3	94.7	36.8	78.5	78.1	88.2	80.3	78.4	77.8
6200.31	Fe I	2.61	-2.44	171.8	164.5	170.2	165.1	151.3	147.9	114.6	166.8	145.1	149.0	104.1	165.9	163.2	161.1	157.6	139.1	146.9
6213.43	Fe I	2.22	-2.66	196.8	195.7	192.3	193.3	161.9	200.9	140.1	184.5	185.9	204.3	134.1	197.2	188.4	201.4	183.5	151.7	206.2

Continued on next page

λ(Å)	elem	χ	gf	253	257	258	260	261	262	266	267	269	278	279	295	300	304	311	315	323
6219.29	Fe I	2.20	-2.44	215.8	211.3	206.0	214.4	173.8	206.8	154.0	197.0	189.1	201.4	132.3	200.5	189.8	202.1	192.9	179.9	213.1
6226.74	Fe I	3.88	-2.20	67.3	78.6	72.2	63.4	...	61.1	22.7	63.5	46.8	...	...	80.6	52.6	60.6	54.8	57.7	69.8
6252.57	Fe I	2.40	-1.76	217.6	211.9	205.2	197.7	197.9	202.1	168.2	189.9	202.8	213.3	135.4	221.5	196.8	218.8	205.8	173.9	217.1
6265.13	Fe I	2.18	-2.55	195.3	207.8	209.4	188.2	163.6	180.2	107.0	180.3	187.9	208.3	120.1	206.1	191.0	195.1	193.5	160.3	175.7
6271.28	Fe I	3.32	-2.96	66.5	82.4	59.1	64.5	52.9	55.9	29.5	59.5	57.6	70.0	37.0	75.4	44.6	57.2	65.8	47.7	51.9
6297.80	Fe I	2.22	-2.74	...	...	...	...	...	...	...	...	...	...	...	...	...	...	...	...	...
6301.50	Fe I	3.65	-0.72	...	...	...	...	...	...	...	...	...	...	...	...	...	...	...	...	...
6307.85	Fe I	3.64	-3.27	...	25.0	...	...	...	19.5	...	21.4	...	27.9	...	...	...	...	...	...	...
6322.69	Fe I	2.59	-2.43	176.2	160.4	163.1	176.9	148.3	153.4	124.0	153.4	155.5	167.8	99.6	169.0	144.1	158.5	165.5	142.7	166.6
6330.85	Fe I	4.73	-1.22	35.3	...	50.8	42.8	...	49.4	...	41.6	36.5	54.1	...	50.0	37.7	28.8	...	27.6	40.7
6335.33	Fe I	2.20	-2.23	235.2	224.2	214.1	221.1	207.0	213.7	161.9	201.8	201.1	225.6	151.8	230.9	213.8	237.8	206.4	180.8	234.2
6336.82	Fe I	3.69	-1.05	157.5	150.6	146.2	153.3	144.4	134.0	122.5	162.7	140.0	156.0	80.9	161.6	152.4	155.2	146.1	92.0	148.4
6344.15	Fe I	2.43	-2.92	206.9	188.4	191.4	183.1	161.7	208.7	109.9	165.4	163.5	209.6	82.6	217.8	189.7	184.2	175.9	153.5	176.2
6355.04	Fe I	2.84	-2.29	189.5	177.7	174.5	181.2	136.5	149.6	96.0	159.7	152.6	186.8	100.9	183.4	144.1	166.6	154.4	144.1	162.0
6380.75	Fe I	4.19	-1.50	106.5	99.1	89.6	81.8	94.7	77.4	38.4	99.5	76.0	98.8	34.6	93.0	78.3	83.4	93.6	59.7	87.2
6392.54	Fe I	2.28	-3.95	93.9	98.2	104.3	108.8	100.9	87.8	30.4	99.3	85.8	101.4	36.9	113.5	87.1	106.7	96.7	67.5	86.1
6393.61	Fe I	2.43	-1.63	263.2	261.0	261.7	246.0	246.5	249.8	169.9	240.0	240.2	250.0	161.7	273.4	256.6	252.2	253.5	198.7	243.8
6408.03	Fe I	3.69	-1.00	147.4	168.0	168.1	153.0	161.0	150.2	102.9	144.7	123.7	175.4	77.8	173.2	153.4	158.4	...	154.9	147.6
6419.96	Fe I	4.73	-0.24	125.2	148.8	137.2	124.9	99.9	116.3	59.9	131.9	112.6	133.6	51.8	127.7	98.9	126.0	...	99.8	110.0
6421.36	Fe I	2.28	-2.01	251.2	235.6	232.1	235.2	221.2	229.9	178.8	205.2	225.5	236.9	152.3	248.4	222.6	236.1	...	204.5	240.8
6430.86	Fe I	2.18	-1.95	278.9	292.2	274.9	270.0	255.0	274.3	195.8	250.8	263.4	294.1	165.1	269.1	240.9	279.6	...	202.8	263.7
6481.87	Fe I	2.27	-2.98	184.2	195.7	161.7	172.9	160.0	178.4	142.7	163.6	172.2	197.0	97.8	179.3	175.8	163.6	197.4	151.7	181.3
6498.94	Fe I	0.96	-4.69	215.0	211.0	213.0	200.6	186.2	192.6	137.8	180.5	203.4	239.2	97.4	219.5	202.4	190.9	228.8	152.8	211.5
6533.93	Fe I	4.55	-1.46	55.0	45.7	61.3	52.6	52.5	55.8	...	50.3	42.8	50.6	...	57.1	45.8	41.9	...	35.9	50.1
6556.81	Fe I	4.79	-1.72	24.7	26.9	28.1	...	26.3	37.4	...	19.1	31.8	23.4	...	...	17.2	15.5	58.1	...	20.5
6569.22	Fe I	4.73	-0.42	123.7	136.9	131.4	109.9	96.8	133.7	70.0	106.8	116.7	135.7	51.0	139.2	100.6	109.3	144.0	97.8	119.6
6574.23	Fe I	0.99	-5.02	188.7	190.3	208.8	185.8	165.0	...	117.7	176.4	...	189.1	83.8	...	183.9	197.3	...	143.8	193.6
6593.88	Fe I	2.43	-2.39	190.6	210.9	225.2	208.0	174.9	160.8	124.7	193.5	138.1	207.2	90.9	241.2	213.2	200.8	...	172.9	196.0
6597.56	Fe I	4.79	-1.07	51.5	73.6	85.0	62.9	46.7	62.5	19.9	66.6	75.0	56.3	19.4	74.2	64.4	55.1	...	66.1	55.2
6608.03	Fe I	2.28	-3.94	117.4	112.9	115.0	111.9	87.4	105.7	54.9	78.3	131.0	120.0	59.3	119.9	97.5	100.9	155.1	73.8	110.7
6609.12	Fe I	2.56	-2.66	157.1	176.1	163.4	166.0	128.7	166.6	120.0	152.2	196.8	176.8	76.7	166.4	158.0	162.5	223.2	122.1	190.2
6627.54	Fe I	4.54	-1.68	53.4	32.8	41.7	36.0	30.4	43.2	18.5	29.8	56.9	42.9	...	25.8	33.0	20.6	105.3	24.3	29.6
6633.76	Fe I	4.56	-0.82	128.0	130.5	131.2	111.8	107.8	127.5	49.9	136.3	141.5	134.0	44.8	133.6	98.7	103.5	149.8	98.2	114.2
6646.93	Fe I	2.60	-3.99	78.9	74.4	86.7	54.1	65.0	60.6	17.9	66.5	53.2	76.2	...	79.9	69.6	71.1	86.1	52.4	51.2
6653.85	Fe I	4.15	-2.52	...	44.4	46.5	49.4	29.9	38.5	...	31.8	42.7	40.8	16.1	50.9	21.0	37.8	...	29.9	34.4
5414.08	Fe II	3.22	-3.61	...	...	...	...	20.3	22.5	...	30.9	...	...	...	...	...	...	...	...	...
5425.25	Fe II	3.20	-3.36	35.6	...	45.5	52.5	82.1	51.8	51.2	58.9	...	30.6	56.7	30.4	40.7	29.2	20.7	70.4	22.6
6149.25	Fe II	3.89	-2.72	35.2	28.9	35.5	35.8	...	34.0	25.9	27.7	20.0	...	...	43.4	28.2	34.0	38.6	24.7	...
6432.68	Fe II	2.89	-3.71	49.8	26.0	46.2	65.1	55.5	74.1	56.4	50.3	62.1	41.8	33.7	...	47.1	45.9	...	40.4	47.1
6456.39	Fe II	3.90	-2.08	40.4	31.9	64.7	...	60.6	79.2	29.5	86.6	...	71.4	49.2	86.6	71.8	67.2	...	66.2	37.7
5578.73	Ni I	1.68	-2.67	147.4	165.4	161.2	125.8	121.5	121.0	96.1	148.4	141.2	174.5	81.1	161.9	143.0	152.3	131.7	128.5	140.8
5587.87	Ni I	1.93	-2.37	171.3	204.0	176.8	159.7	138.7	142.1	79.7	164.8	145.6	188.1	73.0	191.4	161.9	177.5	131.3	148.8	146.6
5589.37	Ni I	3.90	-1.15	37.4	25.3	25.2	38.7	28.7	22.6	...	...	40.2	39.9	...	36.7	...	24.5	31.2	28.5	25.9
5593.75	Ni I	3.90	-0.79	39.7	53.6	47.5	38.2	45.3	42.2	...	28.6	30.1	54.8	39.7	43.5	35.9	35.2	19.7	49.5	24.3
6128.97	Ni I	1.68	-3.39	105.2	96.0	99.1	93.3	86.7	94.7	48.8	92.7	86.6	108.3	34.0	99.2	99.3	95.3	77.0	42.2	93.8
6130.14	Ni I	4.27	-0.98	16.7	27.5	...	...	25.4	...	...	26.6	...	...	...	22.4	...	...	...	25.1	17.2
6177.25	Ni I	1.83	-3.60	82.2	80.4	76.0	62.4	69.3	61.0	39.8	69.0	56.1	66.7	31.7	78.2	72.8	67.1	67.9	66.2	62.4
6186.72	Ni I	4.11	-0.90	37.1	52.5	52.6	37.1	...	20.1	...	27.4	25.2	44.9	23.9	37.3	39.8	...	33.6	32.3	30.7
6204.61	Ni I	4.09	-1.15	40.7	...	...	15.4	...	17.3	16.5	16.9	...	26.0	15.8	20.8	...	...	21.7	31.3	15.0
6223.99	Ni I	4.10	-0.97	37.8	45.9	49.3	23.0	39.9	...	...	...	25.7	46.1	...	31.2	28.4	30.1	42.3	42.0	...
6230.10	Ni I	4.11	-1.20	35.0	46.7	43.8	...	...	...	...	36.6	29.1	70.0	...	44.2	31.1	31.5	...	21.9	47.8
6322.17	Ni I	4.15	-1.21	...	32.3	...	...	...	...	23.1	...	...	...	...	...	20.4	24.4	...	...	...
6327.60	Ni I	1.68	-3.09	125.6	135.2	130.8	115.7	115.6	117.1	71.5	113.1	110.2	130.9	43.0	133.5	116.1	121.3	118.2	92.1	114.8
6378.26	Ni I	4.15	-0.82	40.4	46.7	35.4	30.4	18.4	32.6	21.6	23.9	29.3	46.1	...	41.6	26.0	20.4	40.0	41.3	31.9
6384.67	Ni I	4.15	-1.00	38.5	49.3	60.2	...	...	20.0	18.8	46.5	47.6	50.0	30.6	54.0	44.0	28.1	38.4	...	34.2
6482.80	Ni I	1.94	-2.85	113.7	115.3	110.1	98.6	93.3	118.0	66.3	110.8	136.0	134.6	57.3	110.1	102.2	96.2	136.9	93.3	105.5
6586.32	Ni I	1.95	-2.79	122.2	133.4	148.7	158.1	136.6	46.1	59.8	164.4	41.4	116.8	41.1	162.2	164.2	157.8	...	150.0	135.1
6598.61	Ni I	4.24	-0.93	27.1	...	...	...	...	...	...	...	...	...	...	...	...	...	...	...	26.3
6635.14	Ni I	4.42	-0.75	25.1	...	23.9	...	...	36.9	...	...	45.6	23.9	21.6	...	...	...	68.7	...	18.4
5402.78	Y II	1.84	-0.51	43.1	62.4	64.5	33.3	44.3	...	27.9	50.5	32.5	63.1	...	61.5	41.8	27.8	64.1	...	51.8
6141.73	Ba II	0.70	-0.08	287.8	...	297.3	232.5	218.4	230.4	173.6	248.7	246.2	...	167.2	...	293.7	261.3	253.0	215.4	260.3
6496.91	Ba II	0.60	-0.38	282.5	290.1	...	228.3	202.2	266.1	185.8	237.1	273.8	...	160.6	...	265.7	244.0	...	193.9	264.9
6320.43	La II	0.17	-1.56	94.8	128.7	111.5	63.0	70.7	53.0	20.2	91.6	73.2	109.7	25.4	130.3	118.1	82.0	79.3	63.4	68.7
6390.46	La II	0.32	-1.40	108.4	109.9	98.9	68.4	64.9	69.4	30.2	72.0	80.7	95.8	24.6	108.7	93.6	...	74.5	79.4	70.4
5416.38	Nd II	0.86	-0.98	19.8	36.1	54.3	40.6	48.5	...	...	37.3	18.9	32.6	...	69.6	35.0	33.4	...	...	...
5431.54	Nd II	1.12	-0.47	70.6	75.9	121.6	50.1	40.4	59.3	...	56.7	61.9	74.7	27.7	91.0	60.1	35.5	...	38.3	58.7
5485.71	Nd II	1.26	-0.12	55.3	60.8	59.8	31.8	46.5	37.0	...	23.3	35.6	66.5	...	50.6	59.8	43.1	34.8	...	33.9
6645.13	Eu II	1.37	0.20	75.8	74.3	90.6	51.4	62.8	54.1	30.6	64.9	82.4	78.2	34.6	82.9	61.2	59.4	113.1	75.5	70.1

Table A.5. Abundance ratio of the Fornax Field stars, where we list the abundance, its associated error (σ) and the number of lines used (n). The quoted error is the error on [element/H], not [X/Fe]. Part 1

Star	[Na I/Fe] σ (n)	[Mg I/Fe] σ (n)	[Si I/Fe] σ (n)	[Ca I/Fe] σ (n)	[Ti I/Fe] σ (n)	[Ti II/Fe] σ (n)	[Cr I/Fe] σ (n)	[Fe I/H] σ (n)
BL038	-0.46 ± 0.16 (2)	0.03 ± 0.16 (2)	0.35 ± 0.15 (4)	-0.25 ± 0.10 (8)	-0.13 ± 0.09 (6)	0.18 ± 0.13 (3)	-0.11 ± 0.23 (1)	-0.88 ± 0.07 (43)
BL045	... ± ... (0)	0.02 ± 0.13 (2)	0.25 ± 0.17 (2)	-0.33 ± 0.06 (8)	-0.23 ± 0.05 (10)	0.03 ± 0.10 (4)	-0.16 ± 0.16 (1)	-1.09 ± 0.05 (48)
BL052	-0.85 ± 0.34 (1)	0.07 ± 0.24 (2)	0.16 ± 0.34 (1)	-0.42 ± 0.12 (8)	-0.37 ± 0.13 (7)	-0.12 ± 0.34 (2)	-0.31 ± 0.34 (1)	-1.02 ± 0.06 (37)
BL065	... ± ... (0)	0.00 ± 0.18 (1)	0.32 ± 0.16 (2)	-0.09 ± 0.12 (9)	-0.18 ± 0.07 (7)	0.28 ± 0.11 (4)	-0.31 ± 0.18 (1)	-1.43 ± 0.07 (42)
BL076	-0.66 ± 0.13 (2)	-0.14 ± 0.13 (2)	-0.15 ± 0.11 (3)	-0.19 ± 0.07 (8)	-0.20 ± 0.06 (9)	0.13 ± 0.16 (3)	-0.21 ± 0.19 (1)	-0.86 ± 0.06 (43)
BL077	-0.78 ± 0.14 (1)	-0.27 ± 0.08 (3)	-0.09 ± 0.10 (2)	-0.46 ± 0.06 (8)	-0.38 ± 0.06 (10)	-0.01 ± 0.11 (2)	-0.42 ± 0.14 (1)	-0.79 ± 0.06 (39)
BL079	-0.65 ± 0.31 (2)	-0.01 ± 0.31 (2)	-0.13 ± 0.31 (2)	-0.19 ± 0.17 (7)	0.00 ± 0.16 (8)	-0.09 ± 0.32 (2)	-0.05 ± 0.44 (1)	-0.57 ± 0.08 (39)
BL081	-0.70 ± 0.13 (2)	-0.32 ± 0.13 (2)	-0.45 ± 0.13 (2)	-0.34 ± 0.06 (9)	-0.19 ± 0.07 (10)	-0.05 ± 0.13 (3)	-0.32 ± 0.19 (1)	-0.62 ± 0.06 (40)
BL084	... ± ... (0)	-0.06 ± 0.18 (1)	-0.07 ± 0.17 (2)	-0.28 ± 0.06 (9)	-0.35 ± 0.06 (9)	0.25 ± 0.16 (2)	-0.36 ± 0.18 (1)	-0.86 ± 0.05 (39)
BL085	... ± ... (0)	0.40 ± 0.15 (1)	0.86 ± 0.15 (1)	0.35 ± 0.06 (9)	0.58 ± 0.15 (1)	0.54 ± 0.22 (4)	... ± ... (0)	-2.60 ± 0.05 (31)
BL091	-0.47 ± 0.11 (2)	-0.04 ± 0.11 (2)	-0.07 ± 0.14 (3)	-0.15 ± 0.07 (7)	-0.25 ± 0.05 (9)	0.27 ± 0.17 (3)	-0.14 ± 0.16 (1)	-0.96 ± 0.06 (46)
BL092	-0.95 ± 0.15 (2)	0.04 ± 0.12 (3)	-0.08 ± 0.10 (4)	-0.23 ± 0.07 (9)	-0.23 ± 0.08 (9)	0.33 ± 0.16 (3)	-0.25 ± 0.21 (1)	-0.95 ± 0.07 (44)
BL096	-0.77 ± 0.18 (2)	0.02 ± 0.14 (3)	-0.07 ± 0.18 (2)	-0.18 ± 0.10 (6)	-0.19 ± 0.09 (8)	0.10 ± 0.14 (3)	-0.33 ± 0.25 (1)	-0.75 ± 0.08 (42)
BL097	-0.63 ± 0.12 (2)	0.06 ± 0.17 (1)	-0.08 ± 0.11 (3)	-0.18 ± 0.08 (9)	-0.19 ± 0.05 (10)	0.21 ± 0.10 (3)	-0.34 ± 0.17 (1)	-0.92 ± 0.05 (43)
BL100	... ± ... (0)	-0.01 ± 0.14 (3)	-0.10 ± 0.13 (2)	-0.48 ± 0.08 (8)	-0.42 ± 0.07 (8)	0.29 ± 0.15 (2)	-0.31 ± 0.19 (1)	-0.92 ± 0.06 (48)
BL104	-0.79 ± 0.21 (1)	-0.01 ± 0.15 (2)	0.48 ± 0.18 (3)	-0.20 ± 0.07 (9)	-0.13 ± 0.07 (9)	0.21 ± 0.12 (3)	-0.55 ± 0.21 (1)	-0.96 ± 0.06 (43)
BL113	-0.36 ± 0.14 (2)	-0.03 ± 0.20 (1)	0.00 ± 0.10 (4)	-0.08 ± 0.09 (9)	-0.18 ± 0.08 (7)	0.24 ± 0.14 (3)	-0.22 ± 0.20 (1)	-0.75 ± 0.06 (42)
BL115	... ± ... (0)	0.05 ± 0.10 (3)	0.00 ± 0.16 (1)	-0.21 ± 0.06 (8)	-0.23 ± 0.08 (8)	0.04 ± 0.13 (5)	-0.33 ± 0.16 (1)	-1.48 ± 0.06 (40)
BL123	-0.74 ± 0.17 (1)	-0.04 ± 0.12 (2)	0.03 ± 0.10 (3)	-0.30 ± 0.06 (8)	-0.19 ± 0.06 (9)	-0.10 ± 0.17 (3)	-0.20 ± 0.17 (1)	-0.97 ± 0.05 (41)
BL125	-0.56 ± 0.17 (2)	0.02 ± 0.17 (2)	-0.15 ± 0.12 (4)	-0.21 ± 0.08 (8)	-0.09 ± 0.08 (9)	0.36 ± 0.16 (3)	-0.37 ± 0.24 (1)	-0.73 ± 0.07 (44)
BL132	-0.94 ± 0.13 (2)	-0.09 ± 0.11 (3)	0.00 ± 0.12 (3)	-0.41 ± 0.07 (8)	-0.38 ± 0.08 (6)	0.04 ± 0.13 (2)	-0.30 ± 0.19 (1)	-0.89 ± 0.07 (43)
BL135	-0.51 ± 0.14 (2)	-0.02 ± 0.20 (1)	0.04 ± 0.14 (3)	-0.30 ± 0.08 (7)	-0.02 ± 0.07 (9)	0.14 ± 0.12 (3)	-0.21 ± 0.20 (1)	-0.95 ± 0.07 (39)
BL138	... ± ... (0)	-0.08 ± 0.10 (3)	0.29 ± 0.17 (1)	-0.18 ± 0.08 (9)	-0.10 ± 0.06 (8)	0.15 ± 0.12 (3)	-0.27 ± 0.17 (1)	-1.01 ± 0.06 (43)
BL140	-0.81 ± 0.17 (1)	0.02 ± 0.12 (3)	-0.15 ± 0.10 (3)	-0.29 ± 0.06 (9)	-0.23 ± 0.06 (9)	0.17 ± 0.12 (2)	-0.18 ± 0.17 (1)	-0.87 ± 0.07 (40)
BL141	-0.91 ± 0.14 (2)	-0.11 ± 0.14 (2)	-0.21 ± 0.14 (2)	-0.33 ± 0.08 (7)	-0.38 ± 0.07 (9)	-0.08 ± 0.09 (5)	-0.27 ± 0.20 (1)	-0.82 ± 0.06 (46)
BL146	-0.72 ± 0.11 (2)	-0.14 ± 0.09 (3)	0.04 ± 0.08 (4)	-0.38 ± 0.06 (7)	-0.16 ± 0.05 (9)	-0.15 ± 0.16 (1)	-0.20 ± 0.16 (1)	-0.92 ± 0.06 (39)
BL147	-0.39 ± 0.32 (1)	0.44 ± 0.20 (3)	0.11 ± 0.18 (3)	-0.29 ± 0.11 (9)	-0.31 ± 0.12 (7)	0.60 ± 0.22 (3)	-0.59 ± 0.32 (1)	-1.38 ± 0.07 (47)
BL148	-0.40 ± 0.23 (2)	-0.12 ± 0.18 (3)	-0.06 ± 0.18 (3)	-0.17 ± 0.13 (8)	0.23 ± 0.13 (6)	-0.20 ± 0.18 (4)	0.11 ± 0.32 (1)	-0.63 ± 0.11 (37)
BL149	-0.55 ± 0.25 (1)	-0.06 ± 0.18 (2)	0.23 ± 0.14 (4)	-0.30 ± 0.09 (8)	-0.40 ± 0.09 (8)	0.41 ± 0.14 (3)	-0.32 ± 0.25 (1)	-0.91 ± 0.07 (45)
BL150	-0.60 ± 0.16 (2)	0.01 ± 0.16 (2)	0.04 ± 0.13 (3)	-0.18 ± 0.08 (7)	-0.15 ± 0.08 (8)	0.02 ± 0.14 (4)	-0.18 ± 0.22 (1)	-0.83 ± 0.06 (42)
BL151	-0.64 ± 0.13 (2)	-0.06 ± 0.10 (3)	-0.02 ± 0.14 (2)	-0.25 ± 0.07 (8)	-0.12 ± 0.06 (9)	0.26 ± 0.10 (4)	-0.13 ± 0.18 (1)	-0.86 ± 0.07 (45)
BL155	-0.57 ± 0.16 (2)	-0.04 ± 0.22 (2)	-0.08 ± 0.13 (3)	-0.17 ± 0.08 (9)	-0.05 ± 0.07 (9)	0.14 ± 0.11 (4)	-0.21 ± 0.22 (1)	-0.74 ± 0.07 (40)
BL156	... ± ... (0)	0.00 ± 0.13 (2)	0.05 ± 0.11 (3)	-0.27 ± 0.07 (7)	-0.42 ± 0.07 (8)	0.35 ± 0.14 (2)	-0.23 ± 0.19 (1)	-1.14 ± 0.07 (45)
BL158	-0.60 ± 0.16 (2)	0.06 ± 0.13 (3)	0.07 ± 0.12 (4)	-0.38 ± 0.08 (9)	-0.40 ± 0.08 (11)	0.35 ± 0.12 (4)	-0.30 ± 0.23 (1)	-0.87 ± 0.07 (43)
BL160	-0.61 ± 0.15 (1)	-0.16 ± 0.11 (2)	0.02 ± 0.09 (4)	-0.24 ± 0.08 (9)	-0.07 ± 0.06 (8)	0.27 ± 0.11 (2)	-0.38 ± 0.15 (1)	-0.93 ± 0.06 (37)
BL163	-0.42 ± 0.14 (2)	-0.12 ± 0.14 (2)	-0.18 ± 0.14 (2)	-0.05 ± 0.07 (8)	0.00 ± 0.14 (8)	0.41 ± 0.17 (3)	-0.03 ± 0.20 (1)	-0.78 ± 0.07 (41)
BL166	-0.57 ± 0.16 (2)	-0.07 ± 0.13 (3)	-0.08 ± 0.14 (3)	-0.23 ± 0.08 (7)	-0.11 ± 0.07 (10)	0.28 ± 0.18 (3)	-0.39 ± 0.22 (1)	-0.89 ± 0.07 (42)
BL168	-0.47 ± 0.18 (1)	-0.11 ± 0.13 (2)	-0.02 ± 0.16 (3)	-0.12 ± 0.07 (7)	0.00 ± 0.06 (8)	0.01 ± 0.10 (3)	-0.10 ± 0.18 (1)	-0.88 ± 0.08 (41)
BL171	... ± ... (0)	-0.03 ± 0.10 (3)	... ± ... (0)	-0.26 ± 0.07 (7)	-0.23 ± 0.06 (8)	0.37 ± 0.14 (3)	-0.08 ± 0.18 (1)	-0.90 ± 0.06 (40)
BL173	-0.51 ± 0.14 (2)	-0.07 ± 0.12 (3)	0.18 ± 0.20 (1)	-0.30 ± 0.08 (8)	-0.21 ± 0.07 (8)	0.34 ± 0.17 (4)	-0.33 ± 0.20 (1)	-0.86 ± 0.07 (41)
BL180	-0.51 ± 0.23 (2)	-0.09 ± 0.23 (2)	0.04 ± 0.19 (3)	-0.26 ± 0.12 (8)	-0.18 ± 0.12 (8)	0.01 ± 0.19 (4)	-0.27 ± 0.33 (1)	-0.90 ± 0.07 (38)
BL185	-0.47 ± 0.16 (2)	-0.04 ± 0.13 (3)	0.00 ± 0.11 (4)	-0.12 ± 0.08 (8)	-0.05 ± 0.08 (10)	0.05 ± 0.11 (4)	0.07 ± 0.22 (1)	-0.73 ± 0.07 (39)
BL190	... ± ... (0)	-0.32 ± 0.13 (2)	-0.22 ± 0.13 (2)	-0.43 ± 0.06 (8)	-0.40 ± 0.06 (9)	0.11 ± 0.12 (3)	-0.47 ± 0.18 (1)	-0.79 ± 0.05 (43)
BL195	-0.61 ± 0.13 (2)	-0.07 ± 0.13 (2)	-0.02 ± 0.13 (3)	-0.23 ± 0.07 (7)	-0.19 ± 0.07 (8)	0.26 ± 0.13 (4)	-0.23 ± 0.19 (1)	-0.97 ± 0.06 (48)
BL196	-0.90 ± 0.18 (1)	-0.18 ± 0.18 (1)	0.01 ± 0.18 (1)	-0.31 ± 0.06 (9)	-0.26 ± 0.06 (9)	-0.09 ± 0.13 (5)	-0.19 ± 0.18 (1)	-1.06 ± 0.06 (43)
BL197	-0.70 ± 0.17 (2)	0.05 ± 0.14 (3)	-0.03 ± 0.17 (2)	-0.42 ± 0.09 (7)	-0.30 ± 0.09 (7)	0.32 ± 0.23 (3)	-0.37 ± 0.24 (1)	-0.89 ± 0.07 (39)
BL203	-0.56 ± 0.18 (2)	-0.07 ± 0.15 (3)	-0.05 ± 0.20 (3)	-0.19 ± 0.09 (9)	-0.19 ± 0.09 (9)	0.23 ± 0.23 (2)	-0.27 ± 0.26 (1)	-0.83 ± 0.07 (43)
BL204	-0.48 ± 0.34 (1)	-0.10 ± 0.34 (1)	0.11 ± 0.34 (1)	-0.15 ± 0.15 (5)	0.01 ± 0.12 (8)	0.36 ± 0.36 (3)	-0.10 ± 0.34 (1)	-1.00 ± 0.07 (33)
BL205	-0.48 ± 0.13 (2)	-0.07 ± 0.13 (2)	-0.02 ± 0.11 (5)	-0.21 ± 0.11 (7)	-0.20 ± 0.09 (9)	0.17 ± 0.10 (4)	-0.22 ± 0.19 (1)	-0.69 ± 0.07 (43)
BL208	-0.55 ± 0.16 (2)	-0.08 ± 0.13 (3)	-0.16 ± 0.12 (4)	-0.07 ± 0.09 (9)	-0.13 ± 0.07 (9)	0.05 ± 0.21 (2)	-0.36 ± 0.22 (1)	-0.66 ± 0.06 (43)
BL210	-0.60 ± 0.14 (2)	0.06 ± 0.14 (3)	-0.20 ± 0.16 (3)	-0.32 ± 0.07 (8)	-0.14 ± 0.07 (9)	0.16 ± 0.12 (3)	-0.33 ± 0.20 (1)	-0.76 ± 0.07 (42)
BL211	-0.62 ± 0.16 (2)	-0.17 ± 0.13 (3)	0.37 ± 0.22 (4)	-0.21 ± 0.07 (9)	-0.04 ± 0.08 (8)	0.07 ± 0.16 (3)	-0.02 ± 0.22 (1)	-0.66 ± 0.07 (43)
BL213	-0.60 ± 0.20 (1)	-0.13 ± 0.14 (2)	0.00 ± 0.10 (5)	-0.27 ± 0.07 (9)	-0.10 ± 0.07 (9)	-0.07 ± 0.14 (4)	-0.29 ± 0.20 (1)	-0.94 ± 0.06 (42)
BL216	-0.47 ± 0.17 (2)	-0.01 ± 0.14 (3)	-0.09 ± 0.14 (3)	-0.13 ± 0.09 (7)	0.01 ± 0.10 (6)	-0.14 ± 0.17 (4)	-0.07 ± 0.24 (1)	-0.78 ± 0.07 (35)
BL218	-0.79 ± 0.18 (2)	-0.07 ± 0.15 (3)	-0.06 ± 0.18 (2)	-0.24 ± 0.10 (7)	-0.13 ± 0.09 (8)	-0.27 ± 0.13 (4)	-0.15 ± 0.26 (1)	-0.62 ± 0.09 (41)
BL221	-0.87 ± 0.21 (1)	-0.11 ± 0.15 (2)	-0.13 ± 0.15 (2)	-0.26 ± 0.07 (8)	-0.26 ± 0.07 (9)	0.47 ± 0.15 (3)	-0.19 ± 0.21 (1)	-0.86 ± 0.06 (43)
BL227	-0.49 ± 0.18 (2)	-0.09 ± 0.18 (2)	0.13 ± 0.10 (6)	-0.26 ± 0.08 (9)	-0.21 ± 0.09 (7)	0.19 ± 0.19 (2)	-0.05 ± 0.25 (1)	-0.87 ± 0.08 (43)
BL228	-0.86 ± 0.11 (2)	-0.16 ± 0.11 (2)	-0.05 ± 0.10 (3)	-0.45 ± 0.07 (9)	-0.19 ± 0.05 (9)	0.16 ± 0.16 (3)	-0.17 ± 0.16 (1)	-0.88 ± 0.05 (42)
BL229	-0.71 ± 0.17 (2)	-0.16 ± 0.17 (2)	-0.03 ± 0.10 (6)	-0.25 ± 0.11 (8)	-0.24 ± 0.09 (7)	0.05 ± 0.12 (4)	-0.38 ± 0.24 (1)	-0.71 ± 0.06 (39)
BL233	-0.56 ± 0.16 (2)	-0.13 ± 0.13 (3)	-0.18 ± 0.11 (4)	-0.47 ± 0.08 (8)	-0.21 ± 0.07 (9)	0.19 ± 0.11 (4)	-0.44 ± 0.22 (1)	-0.68 ± 0.07 (44)
BL239	-0.70 ± 0.22 (1)	-0.11 ± 0.16 (2)	-0.22 ± 0.13 (3)	-0.19 ± 0.08 (8)	-0.29 ± 0.07 (9)	-0.17 ± 0.19 (2)	-0.27 ± 0.22 (1)	-0.92 ± 0.07 (43)
BL242	-0.57 ± 0.20 (1)	0.24 ± 0.13 (3)	0.08 ± 0.14 (2)	-0.36 ± 0.09 (9)	-0.19 ± 0.07 (8)	0.10 ± 0.19 (3)	-0.14 ± 0.20 (1)	-1.12 ± 0.07 (43)
BL247	-0.56 ± 0.11 (2)	0.10 ± 0.16 (2)	0.15 ± 0.14 (2)	-0.30 ± 0.10 (9)	-0.23 ± 0.08 (10)	0.18 ± 0.14 (4)	-0.18 ± 0.15 (1)	-0.82 ± 0.09 (37)
BL250	-0.29 ± 0.18 (2)	-0.03 ± 0.14 (3)	0.08 ± 0.15 (3)	0.04 ± 0.10 (7)	0.12 ± 0.10 (9)	-0.31 ± 0.18 (2)	0.17 ± 0.25 (1)	-0.67 ± 0.09 (38)
BL253	-0.49 ± 0.13 (2)	-0.13 ± 0.10 (3)	-0.11 ± 0.10 (4)	-0.20 ± 0.10 (8)	-0.15 ± 0.07 (6)	-0.09 ± 0.11 (4)	-0.28 ± 0.18 (1)	-0.74 ± 0.06 (38)
BL257	-0.73 ± 0.17 (2)	-0.11 ± 0.14 (3)	-0.03 ± 0.13 (5)	-0.30 ± 0.08 (8)	-0.19 ± 0.10 (9)	0.03 ± 0.18 (3)	-0.27 ± 0.24 (1)	-0.58 ± 0.07 (41)
BL258	-0.62 ± 0.16 (2)	-0.25 ± 0.16 (2)	-0.21 ± 0.14 (3)	-0.13 ± 0.12 (9)	-0.24 ± 0.10 (9)	0.12 ± 0.15 (4)	-0.14 ± 0.22 (1)	-0.61 ± 0.08 (39)
BL260	-0.79 ± 0.19 (1)	-0.26 ± 0.13 (2)	0.30 ± 0.23 (3)	-0.23 ± 0.08 (9)	-0.18 ± 0.07 (8)	-0.06 ± 0.10 (4)	-0.29 ± 0.19 (1)	-0.87 ± 0.06 (39)
BL261	-0.65 ± 0.14 (2)	-0.03 ± 0.14 (2)	-0.46 ± 0.20 (1)	-0.24 ± 0.08 (8)	-0.09 ± 0.07 (9)	0.00 ± 0.09 (5)	-0.19 ± 0.20 (1)	-0.85 ± 0.09 (43)
BL262	-0.86 ± 0.26 (1)	0.00 ± 0.15 (3)	-0.22 ± 0.15 (3)	-0.11 ± 0.10 (7)	0.03 ± 0.09 (9)	0.04 ± 0.21 (2)	-0.04 ± 0.26 (1)	-0.76 ± 0.07 (44)
BL266	... ± ... (0)	0.04 ± 0.16 (2)	0.39 ± 0.19 (1)	-0.18 ± 0.09 (10)	-0.13 ± 0.08 (9)	0.50 ± 0.10 (4)	-0.15 ± 0.19 (1)	-1.44 ± 0.06 (43)
BL267	-0.43 ± 0.14 (2)	0.00 ± 0.12 (3)	-0.10 ± 0.10 (7)	-0.16 ± 0.10 (9)	-0.16 ± 0.07 (8)	0.31 ± 0.12 (4)	-0.12 ± 0.20 (1)	-0.72 ± 0.08 (46)
BL269	-0.62 ± 0.20 (2)	-0.06 ± 0.16 (3)	0.27 ± 0.17 (4)	-0.22 ± 0.09 (9)	-0.13 ± 0.09 (10)	0.05 ± 0.25 (3)	-0.34 ± 0.28 (1)	-0.81 ± 0.08 (44)
BL278	-0.17 ± 0.18 (2)	0.00 ± 0.18 (2)	-0.04 ± 0.12 (4)	0.04 ± 0.10 (8)	0.16 ± 0.08 (9)	0.09 ± 0.12 (4)	0.09 ± 0.25 (1)	-0.73 ± 0.07 (38)
BL279	0.05 ± 0.21 (1)	0.19 ± 0.21 (1)	0.35 ± 0.12 (3)	0.00 ± 0.10 (9)	-0.22 ± 0.11 (5)	0.68 ± 0.12 (4)	-0.31 ± 0.21 (1)	-1.52 ± 0.08 (44)
BL295	-0.49 ± 0.18 (2)	-0.03 ± 0.14 (3)	0.05 ± 0.27 (3)	-0.06 ± 0.12 (8)	-0.10 ± 0.09 (8)	0.22 ± 0.24 (3)	-0.24 ± 0.25 (1)	-0.70 ± 0.08 (38)
BL300	-0.47 ± 0.13 (2)	0.18 ± 0.10 (3)	-0.02 ± 0.10 (3)	-0.16 ± 0.09 (7)	-0.04 ± 0.06 (8)	0.09 ± 0.11 (5)	-0.08 ± 0.18 (1)	-0.92 ± 0.07 (40)
BL304	-0.72 ± 0.13 (2)	-0.02 ± 0.13 (2)	0.12 ± 0.13 (2)	-0.28 ± 0.07 (8)	-0.22 ± 0.10 (9)	-0.17 ± 0.12 (3)	-0.35 ± 0.19 (1)	-0.97 ± 0.06 (42)
BL311	-0.68 ± 0.24 (2)	-0.17 ± 0.20 (3)	-0.12 ± 0.15 (5)	-0.25 ± 0.13 (7)	-0.30 ± 0.12 (8)	0.47 ± 0.34 (3)	-0.32 ± 0.34 (1)	-0.78 ± 0.06 (34)
BL315	-0.86 ± 0.20 (1)	-0.03 ± 0.20 (1)	-0.05 ± 0.11 (6)	-0.35 ± 0.08 (6)	-0.34 ± 0.07 (9)	0.28 ± 0.12 (4)	-0.32 ± 0.20 (1)	-0.81 ± 0.10 (45)
BL323	-0.73 ± 0.25 (1)	-0.15 ± 0.14 (3)	0.12 ± 0.18 (2)	-0.64 ± 0.13 (8)	-0.32 ± 0.09 (8)	0.03 ± 0.14 (3)	-0.28 ± 0.25 (1)	-0.91 ± 0.06 (42)

Table A.5. Abundance ratio of the Fornax Field stars, where we list the abundance, its associated error (σ) and the number of lines used (n). The quoted error is the error on [element/H], not [X/Fe]. Part 2

Star	[Fe II/H] σ (n)	[Ni I/Fe] σ (n)	[Y II/Fe] σ (n)	[Ba II/Fe] σ (n)	[La II/Fe] σ (n)	[Nd II/Fe] σ (n)	[Eu II/Fe] σ (n)
BL038	-0.70 ± 0.08 (4)	-0.13 ± 0.06 (15)	0.10 ± 0.23 (1)	0.80 ± 0.16 (2)	0.51 ± 0.23 (1)	0.22 ± 0.17 (3)	0.88 ± 0.23 (1)
BL045	-0.78 ± 0.07 (5)	-0.22 ± 0.07 (11)	... ± ... (0)	-0.05 ± 0.15 (2)	0.17 ± 0.16 (1)	-0.06 ± 0.16 (1)	0.22 ± 0.16 (1)
BL052	-0.52 ± 0.17 (2)	-0.28 ± 0.10 (11)	-0.16 ± 0.34 (1)	0.57 ± 0.28 (2)	... ± ... (0)	0.22 ± 0.24 (2)	0.91 ± 0.34 (1)
BL065	-1.06 ± 0.15 (5)	-0.15 ± 0.07 (8)	... ± ... (0)	0.19 ± 0.13 (2)	... ± ... (0)	0.49 ± 0.18 (1)	0.37 ± 0.18 (1)
BL076	-0.43 ± 0.12 (4)	-0.25 ± 0.08 (13)	... ± ... (0)	0.50 ± 0.13 (2)	... ± ... (0)	0.18 ± 0.12 (3)	0.46 ± 0.19 (1)
BL077	-0.38 ± 0.21 (4)	-0.23 ± 0.06 (14)	... ± ... (0)	0.29 ± 0.11 (2)	-0.12 ± 0.14 (1)	0.23 ± 0.11 (3)	0.39 ± 0.14 (1)
BL079	-0.15 ± 0.30 (2)	-0.18 ± 0.12 (14)	0.14 ± 0.44 (1)	1.04 ± 0.44 (1)	0.52 ± 0.44 (1)	0.45 ± 0.25 (3)	0.79 ± 0.44 (1)
BL081	-0.44 ± 0.17 (4)	-0.24 ± 0.06 (14)	-0.34 ± 0.19 (1)	0.91 ± 0.13 (2)	0.40 ± 0.19 (1)	0.21 ± 0.14 (3)	0.40 ± 0.19 (1)
BL084	-0.65 ± 0.09 (4)	-0.23 ± 0.06 (13)	-0.41 ± 0.18 (1)	0.65 ± 0.16 (2)	0.19 ± 0.18 (1)	0.19 ± 0.14 (3)	0.59 ± 0.18 (1)
BL085	-2.00 ± 0.10 (4)	0.73 ± 0.22 (5)	... ± ... (0)	0.08 ± 0.11 (2)	0.72 ± 0.15 (1)	1.50 ± 0.15 (1)	... ± ... (0)
BL091	-0.60 ± 0.19 (5)	-0.09 ± 0.06 (12)	-0.31 ± 0.16 (1)	0.56 ± 0.11 (2)	0.30 ± 0.16 (1)	0.42 ± 0.09 (3)	0.65 ± 0.16 (1)
BL092	-0.57 ± 0.08 (3)	-0.20 ± 0.09 (11)	0.20 ± 0.21 (1)	0.66 ± 0.15 (2)	0.27 ± 0.21 (1)	0.30 ± 0.12 (3)	0.68 ± 0.21 (1)
BL096	-0.95 ± 0.18 (4)	-0.29 ± 0.08 (12)	-0.32 ± 0.25 (1)	0.70 ± 0.18 (2)	0.36 ± 0.25 (1)	0.27 ± 0.18 (3)	0.76 ± 0.25 (1)
BL097	-0.53 ± 0.21 (5)	-0.11 ± 0.06 (15)	-0.06 ± 0.17 (1)	0.56 ± 0.14 (2)	0.21 ± 0.17 (1)	0.30 ± 0.10 (3)	0.63 ± 0.17 (1)
BL100	-0.67 ± 0.12 (5)	-0.28 ± 0.07 (15)	-0.42 ± 0.19 (1)	0.19 ± 0.18 (2)	0.05 ± 0.19 (1)	0.29 ± 0.13 (2)	... ± ... (0)
BL104	-0.33 ± 0.20 (4)	-0.15 ± 0.07 (12)	0.05 ± 0.21 (1)	0.58 ± 0.15 (2)	0.45 ± 0.21 (1)	0.34 ± 0.12 (3)	0.86 ± 0.21 (1)
BL113	-0.65 ± 0.10 (5)	-0.24 ± 0.06 (12)	-0.19 ± 0.20 (1)	0.94 ± 0.20 (1)	0.50 ± 0.20 (1)	0.25 ± 0.15 (3)	0.64 ± 0.20 (1)
BL115	-0.94 ± 0.10 (4)	-0.13 ± 0.07 (10)	... ± ... (0)	0.03 ± 0.11 (2)	-0.04 ± 0.16 (1)	0.45 ± 0.16 (1)	0.09 ± 0.16 (1)
BL123	-0.78 ± 0.07 (4)	-0.16 ± 0.05 (16)	-0.09 ± 0.17 (1)	0.40 ± 0.12 (2)	0.37 ± 0.17 (1)	0.34 ± 0.10 (3)	0.52 ± 0.17 (1)
BL125	-0.61 ± 0.10 (3)	-0.33 ± 0.06 (15)	-0.01 ± 0.24 (1)	0.87 ± 0.17 (2)	0.92 ± 0.24 (1)	0.39 ± 0.14 (3)	0.74 ± 0.24 (1)
BL132	-0.72 ± 0.10 (4)	-0.23 ± 0.07 (12)	... ± ... (0)	0.21 ± 0.15 (2)	-0.04 ± 0.19 (1)	0.12 ± 0.13 (3)	0.31 ± 0.19 (1)
BL135	-0.69 ± 0.14 (4)	-0.05 ± 0.08 (14)	-0.10 ± 0.20 (1)	0.62 ± 0.14 (2)	0.43 ± 0.20 (1)	0.37 ± 0.14 (3)	0.59 ± 0.20 (1)
BL138	-0.58 ± 0.13 (5)	-0.10 ± 0.08 (14)	-0.15 ± 0.17 (1)	0.47 ± 0.14 (2)	0.42 ± 0.17 (1)	0.23 ± 0.14 (3)	0.73 ± 0.17 (1)
BL140	0.06 ± 0.24 (5)	-0.13 ± 0.08 (14)	0.07 ± 0.17 (1)	0.69 ± 0.12 (2)	0.48 ± 0.17 (1)	0.33 ± 0.20 (2)	0.86 ± 0.17 (1)
BL141	-0.42 ± 0.10 (5)	-0.24 ± 0.06 (15)	-0.45 ± 0.20 (1)	0.28 ± 0.14 (2)	0.27 ± 0.20 (1)	0.25 ± 0.12 (3)	0.52 ± 0.20 (1)
BL146	-0.64 ± 0.07 (5)	-0.19 ± 0.06 (13)	-0.08 ± 0.16 (1)	0.58 ± 0.13 (2)	0.39 ± 0.16 (1)	0.27 ± 0.10 (3)	0.52 ± 0.16 (1)
BL147	-0.88 ± 0.08 (4)	-0.35 ± 0.11 (9)	-0.03 ± 0.32 (1)	1.29 ± 0.23 (2)	1.15 ± 0.32 (1)	0.91 ± 0.19 (3)	1.72 ± 0.32 (1)
BL148	-0.74 ± 0.14 (4)	-0.17 ± 0.09 (14)	-0.22 ± 0.32 (1)	0.10 ± 0.32 (1)	0.76 ± 0.32 (1)	0.72 ± 0.23 (3)	0.55 ± 0.32 (1)
BL149	-0.83 ± 0.15 (5)	-0.26 ± 0.08 (13)	0.03 ± 0.25 (1)	0.57 ± 0.18 (2)	0.29 ± 0.25 (1)	0.05 ± 0.25 (1)	0.54 ± 0.25 (1)
BL150	-0.41 ± 0.13 (4)	-0.27 ± 0.08 (11)	... ± ... (0)	0.36 ± 0.16 (2)	0.32 ± 0.22 (1)	0.41 ± 0.16 (3)	0.68 ± 0.22 (1)
BL151	-0.60 ± 0.09 (3)	-0.20 ± 0.06 (11)	... ± ... (0)	0.74 ± 0.13 (2)	0.36 ± 0.18 (1)	0.31 ± 0.10 (3)	0.60 ± 0.18 (1)
BL155	-0.52 ± 0.17 (3)	-0.13 ± 0.08 (15)	0.15 ± 0.22 (1)	0.75 ± 0.16 (2)	0.63 ± 0.22 (1)	0.65 ± 0.25 (3)	0.53 ± 0.22 (1)
BL156	-0.62 ± 0.17 (5)	-0.10 ± 0.08 (11)	... ± ... (0)	0.53 ± 0.13 (2)	0.53 ± 0.19 (1)	0.39 ± 0.23 (2)	0.81 ± 0.19 (1)
BL158	-0.40 ± 0.15 (4)	-0.15 ± 0.08 (12)	-0.13 ± 0.23 (1)	0.95 ± 0.23 (1)	0.76 ± 0.23 (1)	0.51 ± 0.22 (3)	0.84 ± 0.23 (1)
BL160	-0.67 ± 0.07 (5)	-0.23 ± 0.06 (16)	-0.07 ± 0.15 (1)	0.53 ± 0.13 (2)	0.42 ± 0.15 (1)	0.43 ± 0.09 (3)	0.57 ± 0.15 (1)
BL163	-0.62 ± 0.12 (4)	-0.14 ± 0.06 (12)	-0.02 ± 0.20 (1)	0.95 ± 0.20 (1)	0.59 ± 0.20 (1)	0.47 ± 0.12 (3)	0.71 ± 0.20 (1)
BL166	-0.54 ± 0.21 (4)	-0.18 ± 0.07 (13)	0.00 ± 0.22 (1)	0.74 ± 0.16 (2)	0.58 ± 0.22 (1)	0.49 ± 0.13 (3)	0.55 ± 0.22 (1)
BL168	-0.57 ± 0.17 (4)	-0.16 ± 0.06 (13)	-0.32 ± 0.18 (1)	0.55 ± 0.13 (2)	0.54 ± 0.18 (1)	0.29 ± 0.10 (3)	0.72 ± 0.18 (1)
BL171	-0.19 ± 0.12 (4)	-0.20 ± 0.07 (14)	-0.25 ± 0.18 (1)	0.18 ± 0.13 (2)	0.34 ± 0.18 (1)	0.30 ± 0.18 (3)	0.57 ± 0.18 (1)
BL173	-0.74 ± 0.14 (5)	-0.19 ± 0.08 (13)	-0.26 ± 0.20 (1)	0.51 ± 0.14 (2)	0.41 ± 0.20 (1)	0.41 ± 0.21 (3)	0.49 ± 0.20 (1)
BL180	-0.69 ± 0.06 (1)	-0.33 ± 0.10 (11)	0.21 ± 0.33 (1)	1.21 ± 0.33 (1)	0.84 ± 0.33 (1)	0.64 ± 0.23 (2)	0.77 ± 0.33 (1)
BL185	-0.77 ± 0.12 (4)	-0.22 ± 0.09 (16)	-0.10 ± 0.22 (1)	0.99 ± 0.16 (2)	0.76 ± 0.22 (1)	0.43 ± 0.16 (2)	0.59 ± 0.22 (1)
BL190	-0.60 ± 0.10 (4)	-0.31 ± 0.07 (11)	-0.50 ± 0.23 (1)	0.06 ± 0.13 (2)	-0.14 ± 0.18 (1)	0.27 ± 0.22 (2)	0.54 ± 0.18 (1)
BL195	-0.77 ± 0.08 (4)	-0.21 ± 0.07 (8)	... ± ... (0)	0.18 ± 0.18 (2)	... ± ... (0)	0.04 ± 0.11 (3)	0.54 ± 0.19 (1)
BL196	-0.89 ± 0.08 (5)	-0.29 ± 0.06 (11)	-0.09 ± 0.18 (1)	0.17 ± 0.13 (2)	0.39 ± 0.18 (1)	0.27 ± 0.10 (3)	0.59 ± 0.18 (1)
BL197	-0.79 ± 0.13 (2)	-0.16 ± 0.07 (13)	0.13 ± 0.24 (1)	0.79 ± 0.21 (2)	0.35 ± 0.24 (1)	0.24 ± 0.17 (2)	0.76 ± 0.24 (1)
BL203	-0.55 ± 0.10 (3)	-0.21 ± 0.08 (14)	-0.28 ± 0.26 (1)	0.58 ± 0.18 (2)	0.35 ± 0.26 (1)	0.30 ± 0.19 (2)	0.69 ± 0.26 (1)
BL204	-0.74 ± 0.11 (2)	-0.24 ± 0.11 (9)	-0.20 ± 0.34 (1)	0.46 ± 0.34 (2)	0.29 ± 0.34 (1)	0.60 ± 0.34 (1)	1.26 ± 0.34 (1)
BL205	-0.63 ± 0.08 (5)	-0.23 ± 0.06 (14)	-0.14 ± 0.19 (1)	0.76 ± 0.13 (2)	0.44 ± 0.19 (1)	0.42 ± 0.21 (2)	0.44 ± 0.19 (1)
BL208	-0.73 ± 0.06 (3)	-0.31 ± 0.06 (16)	-0.54 ± 0.22 (1)	0.86 ± 0.16 (2)	0.58 ± 0.22 (1)	0.36 ± 0.13 (3)	0.35 ± 0.22 (1)
BL210	-0.37 ± 0.20 (5)	-0.12 ± 0.07 (13)	-0.08 ± 0.20 (1)	0.90 ± 0.14 (2)	0.51 ± 0.20 (1)	0.50 ± 0.12 (3)	0.67 ± 0.20 (1)
BL211	-0.96 ± 0.14 (4)	-0.19 ± 0.07 (16)	0.03 ± 0.22 (1)	0.96 ± 0.16 (2)	0.48 ± 0.22 (1)	0.27 ± 0.13 (3)	0.59 ± 0.22 (1)
BL213	-0.78 ± 0.10 (5)	-0.27 ± 0.06 (15)	0.11 ± 0.20 (1)	0.63 ± 0.14 (2)	0.40 ± 0.20 (1)	0.33 ± 0.14 (2)	0.65 ± 0.20 (1)
BL216	-1.04 ± 0.17 (2)	-0.11 ± 0.08 (14)	0.03 ± 0.24 (1)	0.97 ± 0.17 (2)	0.60 ± 0.24 (1)	0.33 ± 0.14 (3)	0.77 ± 0.24 (1)
BL218	-0.57 ± 0.18 (3)	-0.18 ± 0.08 (16)	-0.02 ± 0.26 (1)	1.05 ± 0.26 (1)	0.57 ± 0.26 (1)	0.27 ± 0.15 (3)	0.50 ± 0.26 (1)
BL221	-0.75 ± 0.18 (5)	-0.25 ± 0.07 (15)	-0.06 ± 0.21 (1)	0.80 ± 0.15 (2)	0.52 ± 0.21 (1)	0.51 ± 0.15 (2)	0.93 ± 0.21 (1)
BL227	-0.66 ± 0.14 (3)	-0.24 ± 0.07 (12)	0.14 ± 0.25 (1)	0.88 ± 0.18 (2)	0.31 ± 0.25 (1)	0.39 ± 0.25 (3)	0.87 ± 0.25 (1)
BL228	-0.49 ± 0.14 (4)	-0.25 ± 0.07 (14)	-0.30 ± 0.17 (1)	-0.05 ± 0.11 (2)	0.02 ± 0.16 (1)	0.41 ± 0.16 (1)	0.41 ± 0.16 (1)
BL229	-0.48 ± 0.12 (4)	-0.27 ± 0.09 (14)	-0.46 ± 0.24 (1)	0.79 ± 0.17 (2)	0.56 ± 0.24 (1)	0.40 ± 0.14 (3)	0.72 ± 0.24 (1)
BL233	-0.46 ± 0.10 (4)	-0.24 ± 0.08 (15)	0.11 ± 0.22 (1)	0.66 ± 0.16 (2)	0.40 ± 0.22 (1)	0.25 ± 0.13 (3)	0.52 ± 0.22 (1)
BL239	-0.79 ± 0.10 (4)	-0.26 ± 0.08 (14)	... ± ... (0)	0.66 ± 0.16 (2)	-0.05 ± 0.22 (1)	0.10 ± 0.13 (3)	0.27 ± 0.22 (1)
BL242	-0.92 ± 0.18 (3)	-0.15 ± 0.06 (13)	-0.12 ± 0.20 (1)	0.60 ± 0.14 (2)	0.13 ± 0.20 (1)	0.27 ± 0.23 (2)	0.50 ± 0.20 (1)
BL247	-0.61 ± 0.12 (5)	-0.07 ± 0.08 (15)	0.43 ± 0.15 (1)	0.49 ± 0.11 (2)	0.51 ± 0.15 (1)	0.94 ± 0.11 (2)	0.64 ± 0.15 (1)
BL250	-0.67 ± 0.28 (4)	-0.14 ± 0.10 (14)	-0.14 ± 0.25 (1)	... ± ... (0)	0.39 ± 0.25 (1)	0.40 ± 0.18 (3)	0.40 ± 0.25 (1)
BL253	-0.77 ± 0.10 (4)	-0.21 ± 0.07 (17)	-0.21 ± 0.18 (1)	0.90 ± 0.14 (2)	0.40 ± 0.18 (1)	0.31 ± 0.17 (3)	0.60 ± 0.18 (1)
BL257	-1.09 ± 0.12 (3)	-0.20 ± 0.07 (15)	0.04 ± 0.24 (1)	0.91 ± 0.24 (1)	0.78 ± 0.24 (1)	0.31 ± 0.14 (3)	0.53 ± 0.24 (1)
BL258	-0.64 ± 0.08 (4)	-0.21 ± 0.07 (15)	0.07 ± 0.22 (1)	1.03 ± 0.22 (1)	0.60 ± 0.22 (1)	0.48 ± 0.27 (3)	0.75 ± 0.22 (1)
BL260	-0.39 ± 0.11 (3)	-0.28 ± 0.07 (12)	-0.22 ± 0.19 (1)	0.07 ± 0.13 (2)	0.17 ± 0.19 (1)	0.36 ± 0.12 (3)	0.42 ± 0.19 (1)
BL261	-0.71 ± 0.20 (4)	-0.33 ± 0.09 (12)	-0.12 ± 0.20 (1)	0.36 ± 0.15 (2)	0.28 ± 0.20 (1)	0.37 ± 0.12 (3)	0.53 ± 0.20 (1)
BL262	-0.56 ± 0.15 (5)	-0.27 ± 0.08 (13)	... ± ... (0)	0.58 ± 0.18 (2)	0.10 ± 0.26 (1)	0.21 ± 0.18 (2)	0.41 ± 0.26 (1)
BL266	-1.16 ± 0.18 (4)	-0.18 ± 0.07 (10)	0.07 ± 0.19 (1)	0.18 ± 0.13 (2)	-0.03 ± 0.19 (1)	... ± ... (0)	0.49 ± 0.19 (1)
BL267	-0.64 ± 0.11 (5)	-0.19 ± 0.09 (14)	-0.06 ± 0.20 (1)	0.65 ± 0.14 (2)	0.56 ± 0.20 (1)	0.12 ± 0.19 (3)	0.53 ± 0.20 (1)
BL269	-0.47 ± 0.28 (2)	-0.22 ± 0.10 (15)	-0.25 ± 0.28 (1)	0.89 ± 0.20 (2)	0.32 ± 0.28 (1)	0.27 ± 0.17 (3)	0.89 ± 0.28 (1)
BL278	-0.85 ± 0.13 (3)	-0.18 ± 0.07 (13)	0.09 ± 0.25 (1)	... ± ... (0)	0.62 ± 0.25 (1)	0.51 ± 0.14 (3)	0.63 ± 0.25 (1)
BL279	-1.33 ± 0.16 (3)	-0.01 ± 0.10 (12)	... ± ... (0)	0.47 ± 0.15 (2)	0.24 ± 0.21 (1)	0.67 ± 0.21 (1)	0.71 ± 0.21 (1)
BL295	-0.25 ± 0.21 (3)	-0.17 ± 0.07 (15)	0.09 ± 0.25 (1)	... ± ... (0)	0.85 ± 0.25 (1)	0.33 ± 0.17 (3)	0.70 ± 0.25 (1)
BL300	-0.60 ± 0.09 (4)	-0.22 ± 0.07 (14)	-0.03 ± 0.18 (1)	1.08 ± 0.13 (2)	0.91 ± 0.18 (1)	0.49 ± 0.10 (3)	0.61 ± 0.18 (1)
BL304	-0.84 ± 0.10 (4)	-0.19 ± 0.07 (14)	-0.36 ± 0.19 (1)	0.55 ± 0.14 (2)	0.31 ± 0.19 (1)	0.19 ± 0.11 (3)	0.48 ± 0.19 (1)
BL311	-1.00 ± 0.28 (2)	-0.16 ± 0.10 (12)	0.24 ± 0.34 (1)	0.63 ± 0.34 (1)	0.36 ± 0.34 (1)	0.02 ± 0.34 (1)	1.24 ± 0.34 (1)
BL315	-0.60 ± 0.16 (4)	-0.34 ± 0.11 (15)	... ± ... (0)	0.65 ± 0.14 (2)	0.32 ± 0.20 (1)	0.33 ± 0.20 (1)	0.88 ± 0.20 (1)
BL323	-0.78 ± 0.16 (3)	-0.23 ± 0.07 (15)	0.03 ± 0.25 (1)	0.51 ± 0.18 (2)	0.08 ± 0.25 (1)	0.13 ± 0.19 (2)	0.58 ± 0.25 (1)